The Aerodynamics of the Knuckleball Pitch: An Experimental Investigation into the Effects that the Seam and Slow Rotation have on a Baseball

Michael Patrick Morrissey
Marquette University

THE AERODYNAMICS OF THE KNUCKLEBALL PITCH: AN EXPERIMENTAL INVESTIGATION INTO THE EFFECTS THAT THE SEAM AND SLOW ROTATION HAVE ON A BASEBALL

by

Michael P. Morrissey, B.S.

A Thesis submitted to the Faculty of the Graduate School,
Marquette University,
in Partial Fulfillment of the Requirements for
the Degree of Master of Science

Milwaukee, Wisconsin

December 2009

ABSTRACT

THE AERODYNAMICS OF THE KNUCKLEBALL PITCH: AN EXPERIMENTAL INVESTIGATION INTO THE EFFECTS THAT THE SEAM AND SLOW ROTATION HAVE ON A BASEBALL

Michael P. Morrissey, B.S.

Marquette University, 2009

There has been plenty of research on the fluid dynamic effects on different spheres, including sports balls, such as baseballs. Baseball pitches have different velocities, rotation rates and orientations which will cause the baseball to move in different directions. There has also been plenty of research on the aerodynamics of curveballs, but not nearly as much on knuckleballs. The difference between the two is that the knuckleball has a much slower rotation rate and a different initial orientation. This causes the baseball to "knuckle," or moving erratically. This pitch in baseball is one of the hardest to pitch, hit, catch, and umpire. So through various wind tunnel experiments, an attempt will be made that would predict the movement of the pitch under these given conditions.

The experimental data includes force balance dynamometry, flow visualization, and hot film anemometry. The force balance data includes the lift and lateral forces acting on a two-seam baseball rotating at 50 rpm. The flow visualization presents how separation on a rotating, two-seam baseball changes position along the surface of the ball due to rotation and the seams. Lastly, hot film anemometry illustrates how the seams effect separation during a rotation of the baseball. Together, these experiments illuminate the complicated interactions the presence of the seam induces, namely for formation of the turbulent boundary layer juxtaposed against the variations in the location of separated region.

ACKNOWLEDGEMENTS

Michael P. Morrissey, B.S.

I would love to say the credit for this thesis was all mine. However, that would be a lie. So, in no particular order, I would like to thank the following persons whose collaboration, support, and participation have developed this piece of work:

A huge thanks goes to family. Without their support and direction, I wouldn't be where I am today. That includes the ability to laugh at everything that I inherited.

Thanks to Shans. Her patience and light-hearted spirit was needed when the weeks went by too long and the weekends were too short. We have gained more than I had imagined before I began graduate school. I look forward to reap the rewards from the past two years in the future.

Thanks to my advisor, Dr. John Borg. First off, thanks for the awesome thesis topic. I never would have thought that I would be able to study something that I love so much. Also, before I attended Marquette University, I didn't take a single fluid mechanics class. However, through all the courses and cheerful help he provided, I have gained a strong interest in fluid dynamics that I would like to carry into my future. I learned that you can be smart and still be a cool guy with a great sense of humor.

Thanks to my committee members Dr. Jon Koch and Dr. Philip Voglewede. Their input and help during the crucial parts of my thesis was well appreciated.

Thanks to Ray Hamilton, Tom Silman, and Dave Gibas for all of their help and input for a major part of my apparatuses.

Thanks to the graduate students I have become close with. That includes: Drew, who supposedly should take most of the credit of my thesis due to the sheer luck of everything working in his presence. Abby, for cutting weeks off of my lab time for taking time out to teach me how to build a hot wire. Johnson, for the distractions needed when the workload was tough. Aaron, for being my office mate. Sure it may not have been something that you wanted, but you have to admit…you had fun. Dan, for taking an effort to understand baseball even though you knew nothing about the game. However, you did own a Yankees and Brewers hat. Hopefully you will start following them so you can understand the players I am talking about.

Thanks to Dr. Nelson from the University of Notre Dame for lending me the helium bubble generator.

Thanks to Marquette University for the opportunity and financial support over the past two years.

And lastly, thanks to the Chicago Cubs. Even though you have broken my heart more times than I wanted in a lifetime, and probably will in the future, you provided me with a great hobby that I will enjoy the rest of my life. After all, you did give me the chance to watch a no hitter in a city that you should not have been in. Maybe that was the reason I went to Marquette. But please, instead of next year, can you do it this year?

TABLE OF CONTENTS

LIST OF SYMBOLS

English Symbols

A	cross-sectional area
C	circumference of the baseball
C_L	lift coefficient
C_n	constant, n is an integer
D	diameter
E	voltage
L	lift force
P_U	velocity pressure
P_B	barometric pressure
R	resistance
Re	Reynolds number
S	spin parameter
St	Strouhal number
T	temperature
U_o	free stream velocity; velocity of the baseball
W	weight
d	displacement from straight line
f	frequency
g	gravity
n	constant
r	radius

s arc length

t time for delivery

u local velocity

Greek Symbols

Γ circulation of air generated by friction when the ball is spinning

θ angle

ε electrical resistance

μ viscosity

ν kinematic viscosity

ρ air density

τ_w shear stress at the wall

ω rate of rotation

LIST OF TABLES

LIST OF FIGURES

CHAPTER 1. INTRODUCTION

1.1. Background of the Knuckleball

Baseball is a sport full of aerodynamics, especially pitching. There are a lot of different pitches a pitcher can have in his arsenal, which include the fastball, slider, curveball, change-up, or the ever confusing knuckleball. Each pitch is different in the way the pitcher throws the ball. That includes the axis of rotation, the orientation of the ball, the speed, and the direction and magnitude of the angular velocity. For instance, a two-seam and four-seam fastball has the exact same axis of rotation, velocity, and angular velocity. However, the orientation of the baseball is slightly different. The resulting effect of the pitch is a slight movement with the two-seam fastball rather than the straight path of the four-seam fastball. So changing any one of these conditions can change the path of the baseball.

The knuckleball is so perplexing because it can be pitched the same way each throw, yet moves a different way each and every time. Thus, the pitch is very hard to control. There have been many theories on why this happens, but after some time, the scientific community seems to agree that it has to do with the stitches of the ball disturbing the symmetry of the boundary layer separation. So, is there a way to predict the path of a knuckleball when certain conditions are known? Those conditions include the speed, the axis of rotation, the orientation, and the angular velocity.

The knuckleball pitch is believed to begin around the early 20^{th} century. Credit was given to pitcher Eddie "Knuckles" Cicotte [1]. When Cicotte gripped the ball, he only used his knuckles, hence the name. However, the grip of the knuckleball has

changed through the years. The most prolific knuckleballer was five time all-star, Hall of Famer, Phil Niekro. He currently has the most wins at 318 than any other knuckleballer in history, which ranks him 16th all time for all Major League pitchers. Bob Uecker, a catcher for both the Milwaukee and Atlanta Braves once quipped the easiest way to catch a Phil Niekro knuckleball was to "wait'll it stops rolling, then go to the backstop and pick it up." The most known knuckleballer currently is Tim Wakefield of the Boston Red Sox. Wakefield's grip of the knuckleball is most used grip for knuckleballers today.

The characteristic of the knuckleball is how much the ball unpredictably "dances" or "knuckles." The path of the baseball does not only move up or down, but also side to side. In fact, many major league teams would employ a specific catcher just for the knuckleball pitcher. This would allow for one catcher to focus on how to catch the knuckleball. It is not uncommon for the catcher to be charged with more passed balls, or the pitcher to be charged with more wild pitches than other pitchers. This is in spite of the catcher himself having a different, oversized mitt to be able to catch the baseball.

Since the knuckleball has been used, there have been many modifications of how the pitch is thrown. However, there are common characteristics of the pitch. Therefore, it is important to note that the speed of a knuckleball ranges from 65 to 80 mph (95 to 117 ft/sec), with a Reynolds number ranging from about 1.4×10^5 to 1.8×10^5, the orientation most common is the two-seamer, where only two seams are seen by the catcher during one rotation, where the axis of rotation horizontal and normal to the direction of the pitch, and it is best if the baseball rotates a half of a rotation during the full flight to home plate. This would make the rotation rate approximately 50 rpm.

1.2. Baseball Terminology

In this paper, the reader may come across some terms that are unfamiliar to a non-baseball follower. To assist in the definition of these terms, this section is dedicated to clarify these words.

A baseball is made up of 4 layers. The center is made of a rubber core, around the rubber is cork, surrounding the cork is twine, and the twine is covered with two, figure eight pieces of white cowhide that are stitched together with 108 stitches [2]. Those stitches and cowhide make the surface of the baseball. The surface has three areas that will be considered in this paper, as shown in figure 1-1.

Fig. 1-1: Terms on the surface of the baseball.

The red stitches make up the seams on the baseball. These seams are slightly elevated above the cowhide. They assist with a player's grip.

Inside the curve of the seams is the area of the horseshoe. This area is crucial for a knuckleball pitch. The most common grip of the modern knuckleball is with the index and middle fingernails to be pressed into the horseshoe, along the seams. When the baseball is released as a knuckleball, a slight amount of torque is applied to the baseball to make it rotate forward (the top of the baseball rotating towards the catcher), with the axis of rotation to be horizontal in figure 1-1.

Between the two horseshoe areas, where the seams are closest to each other, is the landing strip. This area is in the middle of each piece of cowhide and runs longwise between the seams.

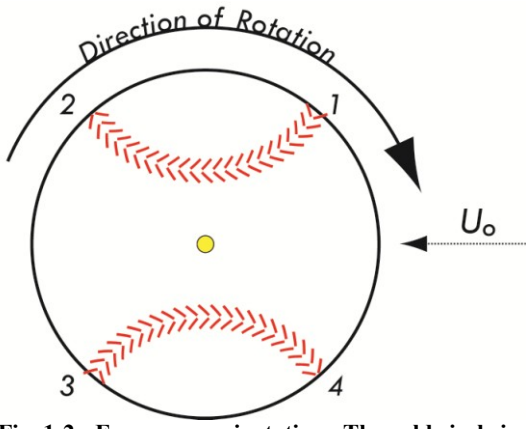

Fig. 1-2: Four-seam orientation. The gold circle is the axis of rotation going into the paper.

A baseball pitch is rotated in one of two common ways, the four-seam and two-seam orientation. As figure 1-2 illustrates, the four-seam orientation has four seams crossing the stagnation point for one complete rotation. The stagnation point is an aerodynamic term which describes the location on the surface of ball where the streamline comes in contact with the ball; in this instance, the furthermost upstream location on the ball.

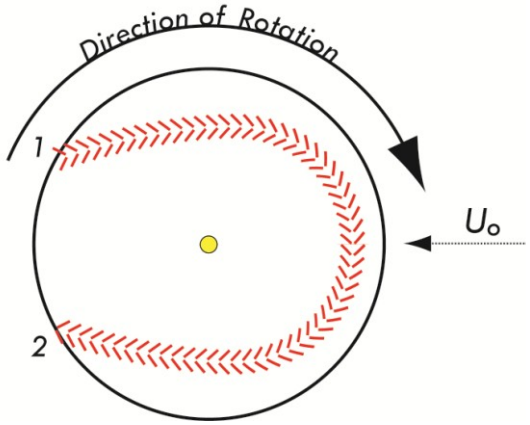

Fig. 1-3: Two-seam orientation. The gold circle is the axis of rotation going into the paper.

As figure 1-3 presents, the two-seam orientation has two seams crossing stagnation per revolution. In each figure, the gold circle represents the axis of rotation. During the pitch, the catcher would be on the right and the pitcher would be on the left. The direction of rotation is insignificant for the four and two-seam orientation.

1.3. Literature Review

1.3.1. Aerodynamics

One of the first recorded studies of sport ball aerodynamics was in 1672 when Sir Isaac Newton discovered how the flight of a tennis ball was affected by the spin [3]. He stated that for a sphere in motion and under a spin, there will be a force pressing against the side rotating against the fluid which would affect the sphere to curve. This was the foundation of the Magnus effect, described by Gustav Magnus in 1852 [4]. This quantified the lateral deflection of a spinning sphere. In his experiment, Magnus had a smooth, vertical, spinning cylinder, which was free to move laterally (normal to the flow direction) in a horizontal wind stream, but confined to not move downstream. He was able to spin the cylinder by wrapping a string around it, and quickly pulling it off. Magnus then noticed that due to the spin, the cylinder moved laterally. The explanation for this effect is related to an increase in the relative wind velocity on one side of the ball versus the other. When a sphere is rotating in the same direction as the wind, the relative velocity is increased. In opposition, when the sphere is rotating in the opposite direction of the wind, the relative velocity is decreased. According to Bernoulli's principle, the pressure is less where the velocity is greater, and the pressure is greater where the velocity is less. Consequently, this pressure

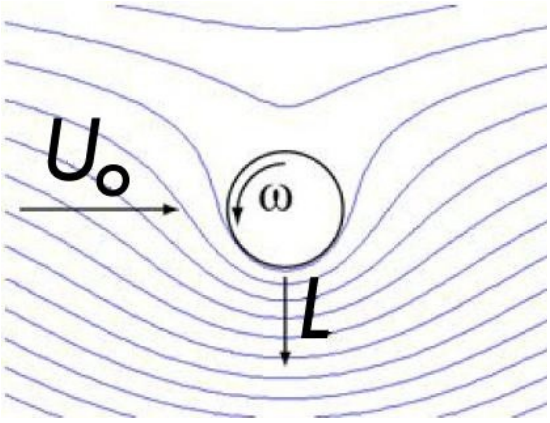

Fig. 1-4: The Magnus Effect on a cylinder. Due to the cylinder rotating, the stream functions wrap around the cylinder.

difference causes the ball to curve in the direction of the lower pressure. Figure 1-4 is an illustration of how the spin results in a pressure gradient which can force the ball to have lateral motion. This is one of the reasons why the curve ball curves; the rotation rate is so high that the pressure gradient can move the baseball. This effect also works on other objects, as spheres. However, on smooth spheres, there is an opposite effect. It is important to realize that most sport balls are considered rough spheres.

In 1904, Ludwig Prandtl championed the idea of the boundary layer concept [5]. The boundary layer results from the no-slip condition and affects the fluid flow in region where viscosity dominates. Accordingly, it is responsible for drag and the shear stress. Any asymmetry of the boundary layer would result in the asymmetry of the forces. The asymmetry of the forces would cause the object to move erratically. However, not researched in respect to any baseballs, this can cause the movement of a knuckleball.

1.3.2. Baseball Aerodynamics

The oldest study found of the aerodynamics of a baseball was published by Lyman Briggs, in 1959 [6]. His study was a nice beginning, but had some drawbacks. His first experiment with baseballs was with an air gun. Figure 1-5 illustrates the configuration of his first experiment. Briggs modified an air gun from the National Bureau of Standards, which was used to measure the coefficient of restitution. He took a baseball, and rotated it using a spinning tee, and placed it at the end of the barrel. A wooden sphere was then projected fast enough to impact the baseball off the tee at a marked target 60 feet away. The rotation of the baseball was measured with a Strobotac, as most of the future experiments would do. Unfortunately, this technique resulted in

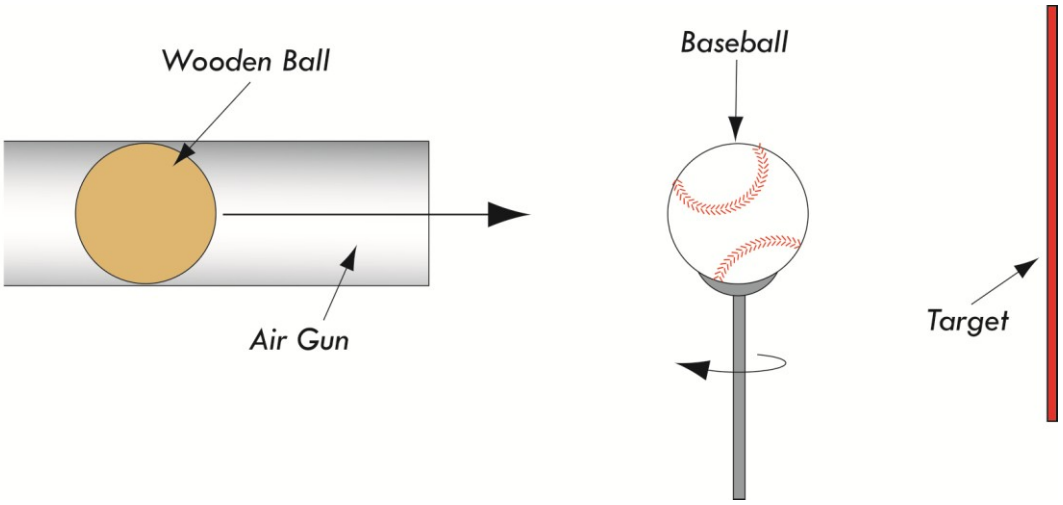

Fig. 1-5: Briggs' air gun experiment.

irregular data that is mostly attributed to the collision of the two spheres. When the wooden sphere impacted the baseball, it disrupted the spin of the baseball and resulted in a reduced spin. Therefore, this data is better for a batted baseball than a pitched baseball. Briggs then progressed to wind tunnel experiments without the impact of another ball which are more widely accepted today. Figure 1-6 shows how this experiment appeared.

As the illustration shows, the bottom of the baseball was first covered by a lamp-black lubricant. It was then spun by a vertical shaft, powered by a DC electric motor and controlled by a potentiometer, and was released by suction. The baseball, rotating at the same rpm as the shaft, descended down a short tube into a horizontal wind. The baseball then hit a target at the bottom that was marked by the lubricant. This only measured the effect of spin in a single direction, i.e., half of the deflection. The experiment was repeated, but rotated in the opposite direction. The distance between the two marks gave the total deflection. Briggs, worried about the center of mass of the baseball, knew that it was not the same as the geometrical center of the sphere. So, through trial and error, the

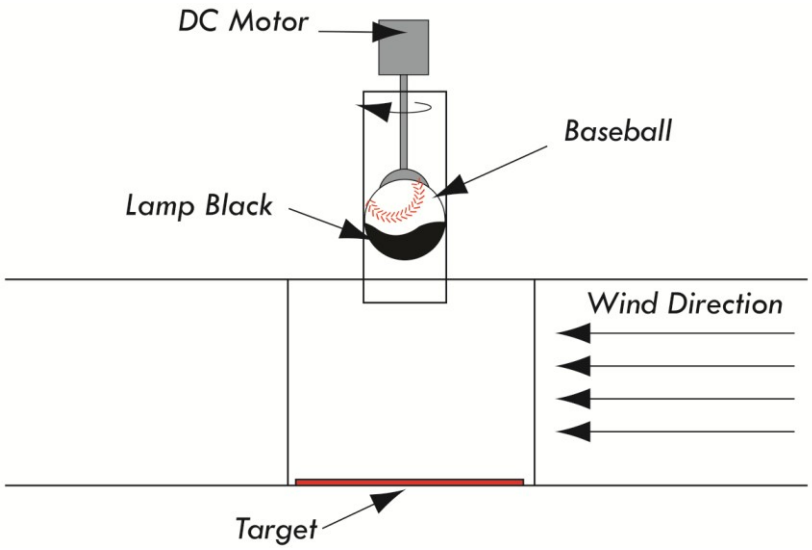

Fig. 1-6: Briggs' wind tunnel experiment.

baseball's center of mass was found. Professional American League baseballs were used throughout this experiment, considering the strict restrictions of weight and shape of the balls. Figures 1-7 and 1-8 shows the results of the experiments.

Figure 1-7 shows that the lateral deflection is linearly proportional to the spin. It is important to note that almost all of the rotation rates pass through the origin. This also explains that the greater the speed, the greater the deflection. Briggs concluded from figure 1-8 that for speeds up to 150 ft/sec (102 mph) and spins up to 1800 rpm, the ratio of the deflection is directly proportional to the ratio of the square of the wind speed. Briggs then moves on to how this would affect a baseball in an actual game. The experiment used a ball that spins on a vertical axis. In a game, the axis is mostly inclined. Briggs also includes that if the spin axis were horizontal and normal to the path of the pitch, there will be no lateral deflection. However, it would affect how much a ball will drop. It is important to notice this, because many pitchers, hitters, catchers, and umpires notice that a knuckleball, thrown in the two-seam orientation, *will* move

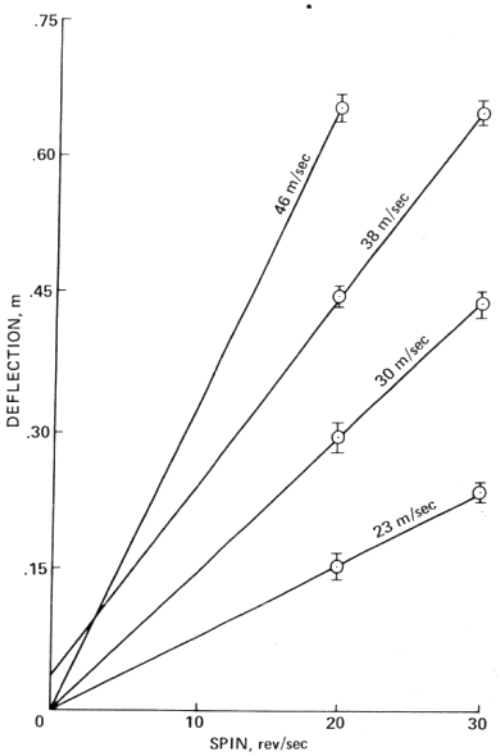

Fig. 1-7: Briggs' wind tunnel experiment; lateral deflection of a baseball with a time interval of 0.6 seconds. (Briggs, 1959)

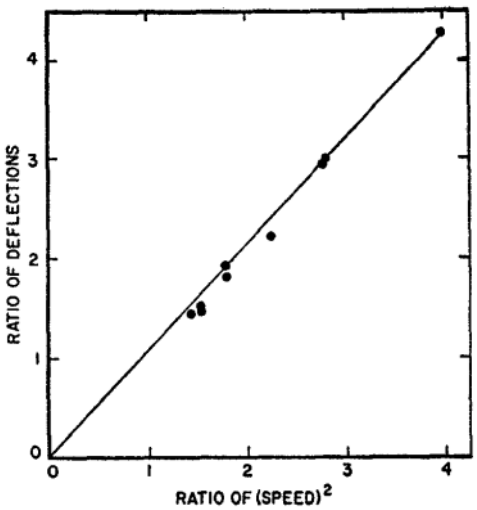

Fig. 1-8: Briggs' wind tunnel experiment; graph of the ratio of the lateral deflections against the ratio of the square of the speeds. (Briggs, 1959)

laterally. Also, Briggs never comments on the actual orientation of the ball when spun. This article is focused on a curve ball; however, the ball's movement will depend on how the stitches are positioned. That is what makes a two-seam fastball move more than a four-seam fastball.

In 1971, Dr. Brown produced outstanding photos of a different assortment of objects in a wind tunnel [7]. This includes a stationary and rotating ball with a smoke rake. Figures 1-9 and 1-10 are a couple of pictures taken from the book.

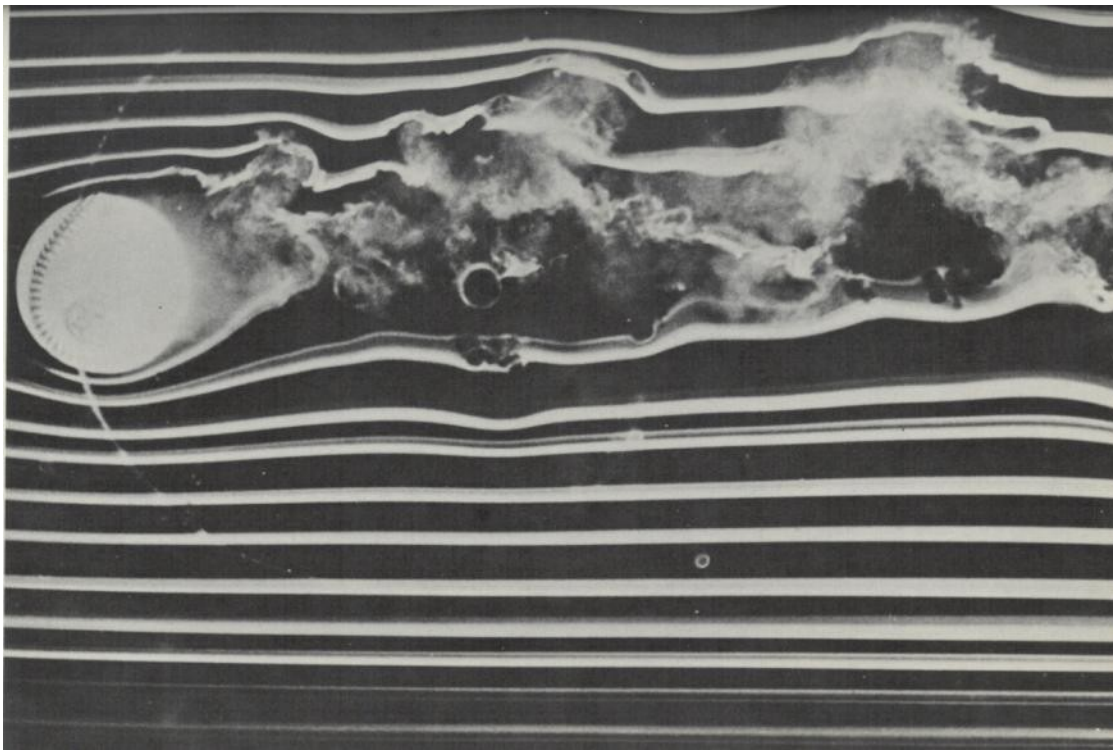

Fig. 1-9: Brown's photo of a spinning baseball with a rate of 900 rpm, counter-clockwise, and a speed of 70 ft/sec (47 mph). Seams and rotation provide a downward trajectory. (Brown, 1971)

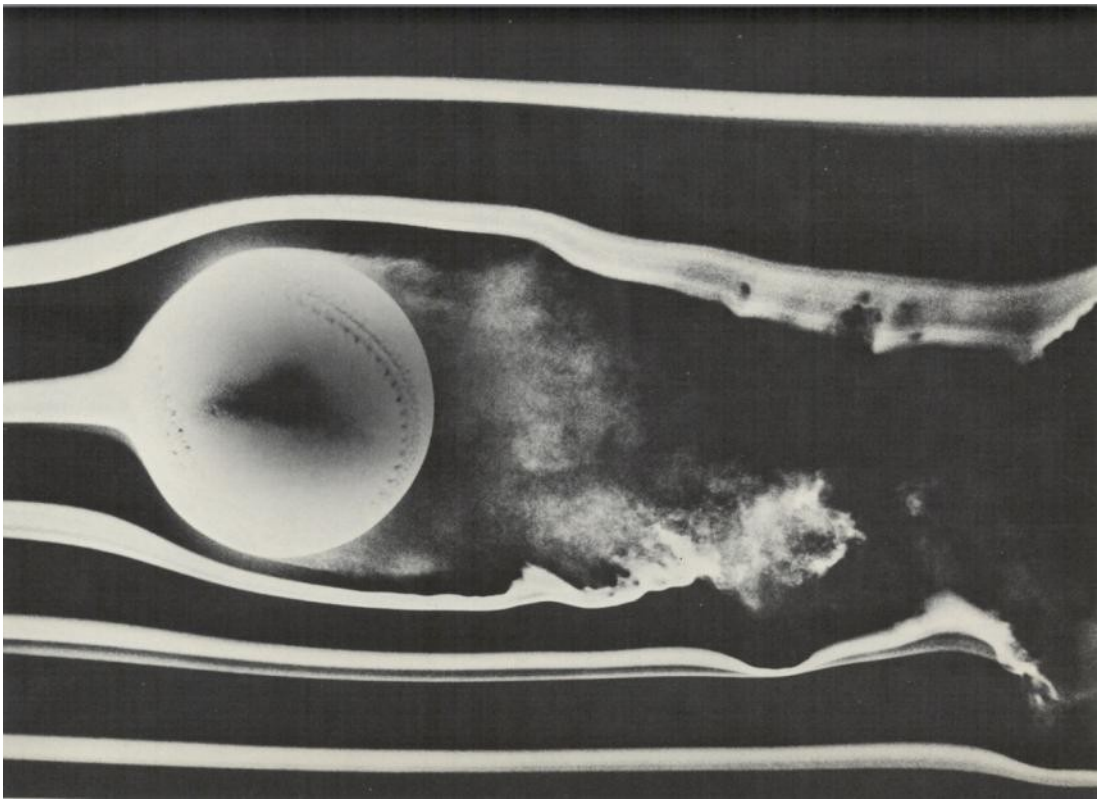

Fig. 1-10: Brown's photo of a stationary baseball. Seams, alone, produce lift. (Brown, 1971)

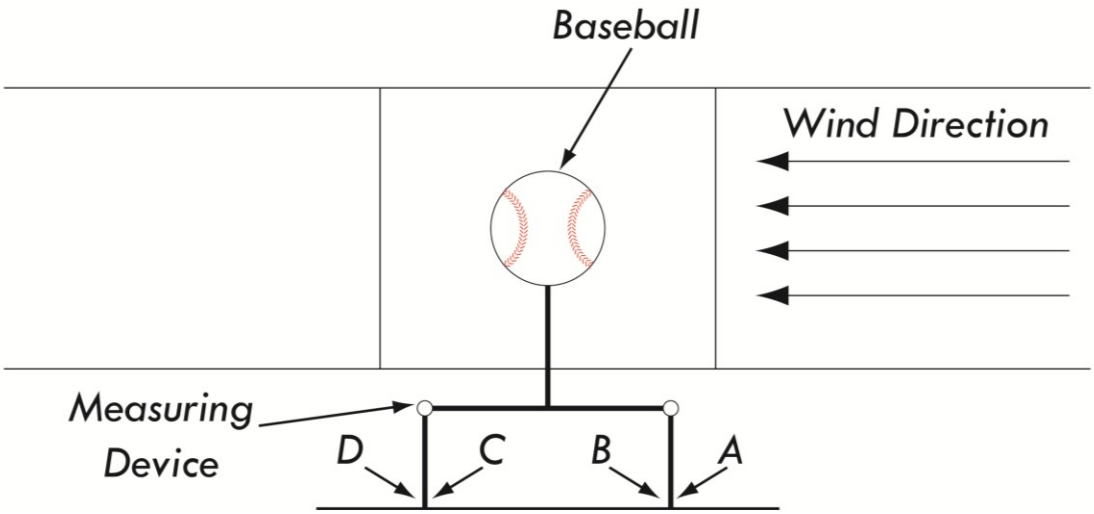

Fig. 1-11: Watts' and Sawyer's apparatus illustration. Measuring device is in the position to measure drag.

These photographs helped to understand the different wakes that result under different conditions. Figure 1-9 is visual evidence what Briggs and Magnus discovered. Both images show how the stitches of the baseball disturb the boundary layer, which can cause asymmetrical separation. The ball's trajectory curves in the direction opposite of the wake, thanks to Newton's third law. Brown states that if someone could throw a ball on an axis parallel to the ground, with a half rotation, the ball would act like a rollercoaster, moving up and down, left and right. The movement also depends on the orientation of the ball.

The next advancement in the aerodynamics of the knuckleball was done by Robert Watts and Eric Sawyer in 1975 [8]. They continued from Briggs work with the wind tunnel, and used it to measure the lift and drag forces. Figure 1-11 shows the apparatus used in their experiment.

Instead of the ball moving, as in Briggs' experiment, Watts and Sawyer put a stationary ball on a force balance in a wind tunnel. The measuring device consisted of two beams, outside of the wind tunnel, that were firmly attached to the bottom, and

pinned at the top. Foil strain gauges were located at the A, B, C, and D on each side of the beams and connected to a Baldwin-Lima-Hamilton micro strain indicator so the total output force was four times the applied force. The force balance apparatus was calibrated by applying known weights. The velocity of the wind tunnel was found by a Pitot tube. The gradient of the wind tunnel was so small that three inches from the center line was only one percent different from the center. The wind tunnel's speed was set at 68 ft/sec (46 mph). They repeated this procedure with the baseball at different azimuth angles. Figure 1-12 shows how they varied the azimuth angle, θ, in relation to the free stream wind direction. This orientation is considered a four-seam, because the stagnation point will cross over four different seams in one rotation.

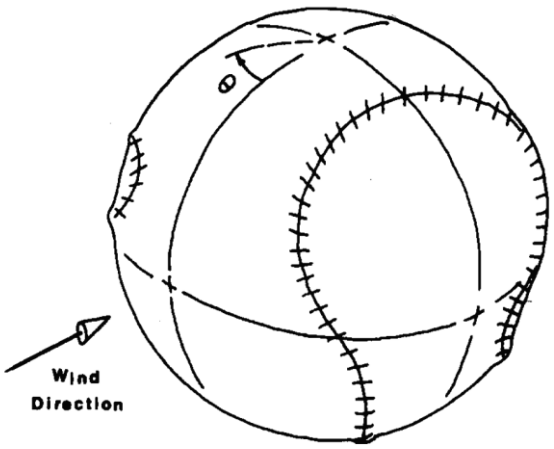

Fig. 1-12: Watts and Sawyer's orientation of the baseball in the wind tunnel. (Watts and Sawyer, 1975)

Watts and Sawyer concluded that if the ball was perfectly still, with no spin from the release of the pitcher's hand to home plate, there will be a lateral curved trajectory, but not the erratic movement of the knuckleball at some of the azimuth angles. They also found that drag can vary by as much as 50 percent as a function of the azimuth angle of the ball, and would cause the lateral force sign to change. They then plotted the results in a graph as shown in Figure 1-13.

Watts and Sawyer found that there is an oscillatory force taking place 105 to 110 degrees measured from the stagnation point, where there is a large boundary layer separation due to the jump from the front to the back of the stitches. They confirmed the separation with fine, wool threads, glued to the back of the stitches. It was found that there was a large, lateral, discontinuous force at the angles of 52, 140, 220 and 310 degrees. The magnitudes of both of these forces vary with the speed of wind tunnel. The lateral force increases approximately the square of the velocity. Unfortunately, the top speed Watts and Sawyer went to, 68 ft/sec (46 mph), is too low for a knuckleball pitcher today. Also, the orientation of the ball is incorrect for the two-seam knuckleball. The most common orientation is two-seams, not four-seams. So the axis of rotation is off by 90 degrees. It is also important to note that due to the asymmetry of the fluidic shear stress, the ball experiences a natural torque [9]. The ball would have a different torque for each different azimuth angle. Unfortunately, it is very difficult indeed to throw a pitch with zero rotation. This is important when calculating the trajectory of a slow,

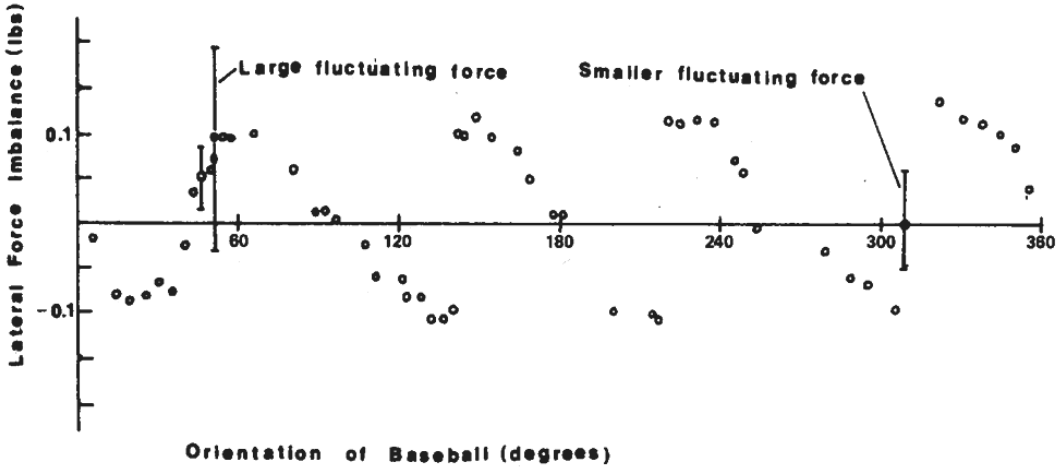

Fig. 1-13: Watts and Sawyer's results of the lateral force imbalance of a four-seam baseball as the angle changes. (Watts and Sawyer, 1975)

spinning baseball.

The question then, is there a difference of lift when comparing a two-seam pitch to a four-seam pitch? Igor Sikorsky found that there most definitely is a difference [10]. Joseph Drury published Sikorsky's unpublished work in 1956 which shed light on the aerodynamics of the curveball. In the late 1800's, baseball fans could not believe that a baseball could curve, but rather it was an optical illusion. This argument went on for decades, until Sikorsky proved that it was an aerodynamic effect. Sikorsky took common pitcher's velocity and rotation rates of the day, 98 mph and 600 rpm, respectively, and applied them to his tests. Sikorsky spun a ball on a shaft ranging from zero to 1,200 rpm at 80 to 110 mph in the two-seam and four-seam orientation. He collected the lift for all of these combinations and found that the four-seam orientation produced greater lift than the two-seam. Consequently, Sikorsky proved that a curveball does actually curve, however there still is an effect of an optical illusion. He also states that the ball travels in a uniform curved path. The curveball appears to "break" because of the batter's line of vision.

To calculate the displacement of the baseball, Sikorsky developed this formula:

$$d = \frac{\Gamma \rho {U_o}^2 t^2 g C^2}{7230\, W} \tag{1.1}$$

where d is the displacement from a straight line, Γ is the circulation of air generated by friction when the ball is spinning, ρ is the air density, U_o is the velocity of the ball, t is the time for delivery, g is gravity, C is the circumference of the ball, W is the ball's weight, and 7230 are assumed units.

With all of the information done at this time, Watts and Ricardo Ferrer found that there was a conflict, especially with Briggs and Joseph Drury conclusions [11]. Drury wrote about the findings of Igor Sikorsky, an aerodynamicist, of who never published his work. Earlier, Briggs reported that the lateral force is proportional to the rotation rate of the ball and the square of the velocity. Drury also reported the same findings. However, according to Drury, Igor Sikorsky found that the deflection of a baseball spinning *does* depend on the orientation of the baseball, something Briggs did not account for and stated there is no significance. When Drury plotted this data, he came up with a graph shown in figure 1-14.

As shown, Briggs data is out of the zone of Sikorsky's data. Sikorsky has an area of data because he used the maximum and minimum amount of force the baseball would be under. This brought up the idea that there could be some dependence on the initial orientation of the baseball. Watts and Ferrer also found that according to the Kutta-Zhuskovskii theorem [12], when a two-dimensional object is moving in an inviscid fluid, and there is a net circulation of the

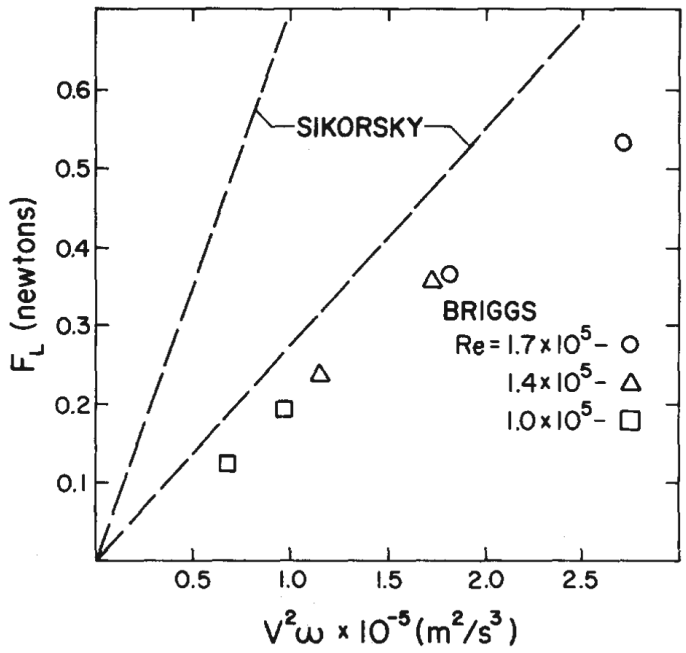

Fig. 1-14: The data of Briggs and Sikorsky, described by Drury. Sikorsky's data is bounded by the dotted lines. (Watts and Ferrer, 1987)

fluid about the object, there results a force perpendicular to the velocity and vorticity vector associated with the circulation.

This brings up the case that the lift force would also depend on the rotation and velocity, as opposed to the square of the velocity.

$$L = \frac{1}{2}\rho\omega r U_o A C_L \tag{1.2}$$

This was proven with golf balls experimented by Bearman and Harvey. Watts and Ferrer then came to the conclusion to the importance on the orientation of the baseball, as well as if the lift force is more dependent on the velocity or square of the velocity. Remember that Watts and Ferrer were studying the curveball, as opposed to the knuckleball. Watts and Ferrer used three orientations of the ball, as shown in figure 1-15.

Specifically, orientations one and three are mostly used in knuckleballs today. Orientation two is mainly used for a curveball. Figure 1-16 illustrates the schematics of the apparatus. The baseball is mounted on a shaft with an impeller attached to the end so the baseball is rotated by an air nozzle. The air nozzle system was controlled in order to

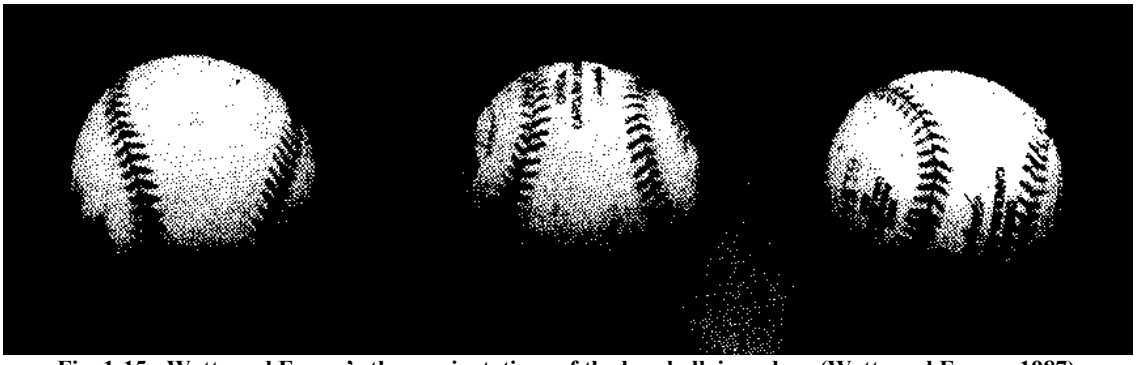

Fig. 1-15: Watts and Ferrer's three orientations of the baseball, in order. (Watts and Ferrer, 1987)

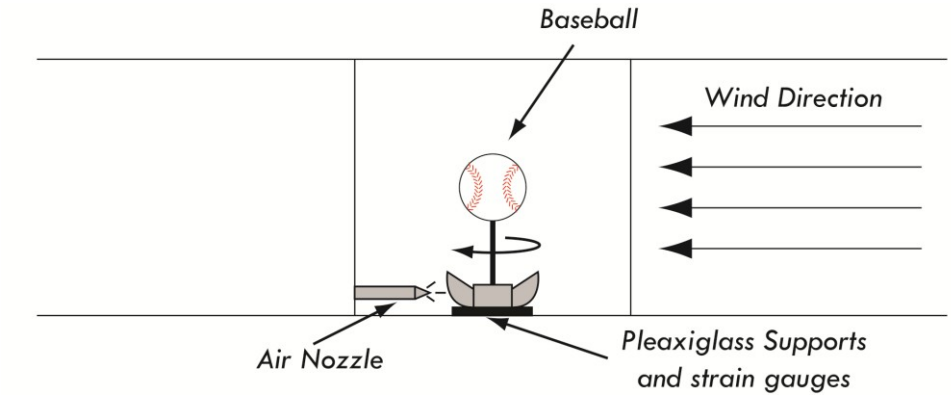

Fig. 1-16: Watts and Ferrer's apparatus.

prescribe the ball's rotation, which was measured by a photo tachometer. This whole unit was then mounted in a wind tunnel. The lift and drag forces were found through the bending stresses of the Plexiglas supports, which was measured by strain gauges attached to each side of the supports. This apparatus was calibrated just as Watts and Sawyer did, by applying known weights. Watts and Ferrer measured data at each wind speed, rotation speed, and direction of the spin. They also used a dimpled ball, which is a type of baseball used in pitching machines, as a control of a rough sphere. They were the size of baseballs, but with dimples like a golf ball. The data was then collected and plotted in the same graph as figure 1-14. Figure 1-17 demonstrates their conclusion.

As shown, their data clearly fits within Sikorsky's limits. The limits includes that the dimpled ball acts like a baseball. This implies that the roughness of the sphere can affect the lift. Most importantly, the orientation of the baseball has no effect on the lift of the ball. Also from the graph, the Watts and Ferrer data is not linear as shown by Sikorsky and Briggs. However, this does agree with the Bearman and Harvey golf ball data. To check this, they went on to dimensional analysis. What they found was that their Reynolds number did not match up with Briggs, which was a larger Reynolds

number, or Davies in Watts and Ferrer's article, who studied smooth spheres, which used a single Reynolds number. This was due to the limitations Watts and Ferrer had with their wind tunnel. When they check their data with the others, they found that when the Reynolds number is greater than 0.6×10^5, the lift coefficient is largely independent of the Reynolds number, and more of a function of $\pi D\omega/V$, where D is the diameter of the ball, ω is the rotation rate, and V is the velocity. This proves Briggs idea that the lift force is a function of the square of the velocity is incorrect, but agrees with the Kutta-Zhukovsky theorem, which applies to two-dimensional inviscid flow.

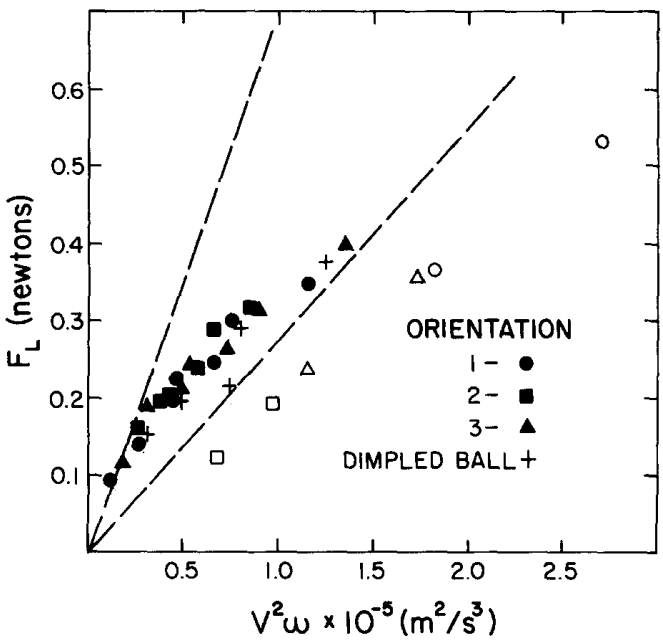

Fig. 1-17: Watts and Ferrer's data along with Briggs and Sikorsky. (Watts and Ferrer, 1987)

Overall, Watts and Ferrer comes to a conclusion that the lift coefficient is not dependent on the Reynolds number but is a function of $\pi D\omega/V$, and that the orientation of the curveball does *not* matter. Watts and Ferrer were smart to state that pitchers strongly disagree with this. However, it could be because the orientation they spin the ball may allow greater rotation rate than any other orientation. An argument one can make is that Watts and Ferrer could not reach the Reynolds numbers of the other's data.

This would make this variable uncontrolled, and may be difficult to assume that the lift coefficient is not dependent on the Reynolds number.

There have been some more realistic conditions to study the knuckleball, like using it in an actual pitching machine, which will be discussed below. However, pitching machines are not reliable. That is because they are mainly used for universal pitches, like a curveball, fastball, etc. Most pitching machines consist of two small rotating tires. The baseball is dropped between these tires and is propelled forwards. By adjusting the rotation rates of the tires, one can control the initial velocity and spin axis of the baseball. Nonetheless, the spin of these tires, as well as the variability in contact time and spin imparted, result in initial conditions where they are not reliable enough to use for actual scientific data. That is because to make a ball curve, only one wheel has to spin faster than the other wheel. To make a baseball act like a knuckleball, both wheels has to spin at nearly the exact same rate, except one tire rotating just barely fast enough to had about a half spin as the ball travels about 60 feet. That is why it is important to check the schematics of the machine itself. Mizota created a pitching machine through the theoretical knowledge known thus far [13]. Yet, nothing was mentioned of how the

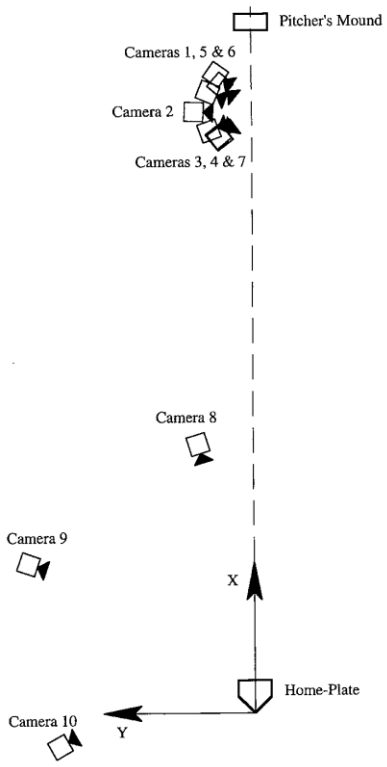

Fig. 1-18: Alaways and Hubbard's experimental setup. (Alaways and Hubbard, 2001)

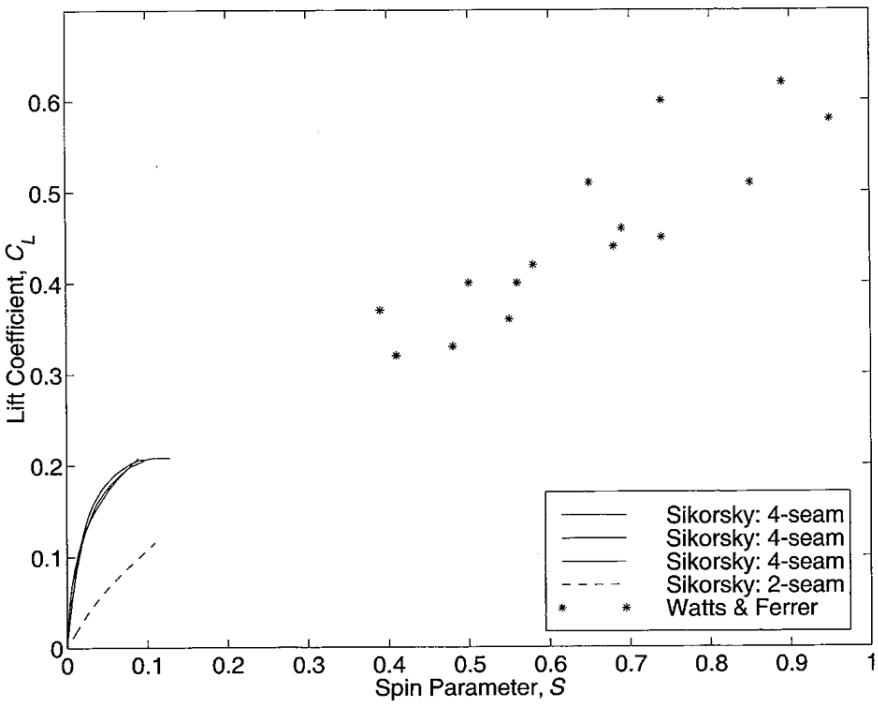

Fig. 1-19: Coefficient of lift versus spin parameter of spinning baseballs. This includes Sikorsky's, Watts', and Ferrer's data. (Alaways and Hubbard, 2001)

machine propelled the baseball, and the accuracy of the rate of rotation set on the baseball. This is what makes actual measurements so difficult. A knuckleball pitching machine has to be more precise than the universal machines, because a knuckleball's rotation rate is so crucial and small.

In 2001, Leroy Alaways and Mont Hubbard's experiment used an ATEC pitching machine to correlate the spin of a baseball to the flight trajectory [14]. The objective of their experiments was not specifically focused on knuckleballs. However, they measured the spin of the baseball actively in flight with 10 cameras as opposed to relying on the rotational rate of the tires. The illustration of the setup is shown in figure 1-18.

They put four retro-reflective tape circles on the baseballs in the shape of 'λ' to measure rotation rate and position of the baseball. The purpose of this experiment was to

check if there is a difference in two-seam or four-seam spin. As mentioned before, Sikorsky's unpublished work stated that there is a difference, and Watts and Ferrer's data did not seem to be connected to Sikorsky's data even though they used three different orientations. Figure 1-19 shows how the two pairs of data appear on the same plot. Sikorsky used three different speeds for the four seam orientation, 80, 90, and 100 mph. As shown, there is not enough of a difference to mention that speed of the pitch has a difference on the lift coefficient. The lift coefficient was plotted as a function of spin parameter, as shown in equation 1.3. It is important to note that r is the radius of the

$$S=\frac{r\omega}{U_o} \tag{1.3}$$

sphere, ω is the rotational rate, and U_o is the velocity. Alaways and Hubbard wanted to study if there was a correlation between the two, since there is a slight gap between the spin parameters between 0.1 and 0.4, which would conclude if there was continuity. They went on to measure the lift coefficient and path experimentally with a pitching machine and cameras, as well as analytically with a series of equations. Their data ended up clearing up much of the confusion between the two experiments, as figure 1-20 shows. This points out that the orientation of the baseball does have a strong effect on the lift coefficient. However, at larger spin parameters, the orientation of the baseball has less of an effect on the induced lift. This is *very* important with a knuckleball, considering a knuckleball's spin parameter is only about 0.0026. Alaways and Hubbard helped put together some of the pieces missing from all the work done thus far, and now the bigger

picture is falling into place. However, this is still assuming that there is no lift when the ball is not spinning, and Brown's photo shows that there is some lift at zero spin.

There has also been an experiment in Japan with the comparisons of Major League Baseballs to the rubber baseballs used in the schools, and the smooth sphere, which was studied by Berman and Harvey earlier. This information is not useful to the aspects at study, but their procedures are interesting. Katsumi Aoki, Yasuhiro Kinoshita, Jiro Nagase, and Yasuki Nakayama rotated six different spheres in the wind tunnel with a DC motor at the rotational speeds of a curveball [15]. Each ball differed from the smooth sphere, with an increasing amount of dimples (i.e., roughness) where the final sphere investigated was a Major League Baseball. They would vary the rotation of the ball by increasing or decreasing the voltage to the DC motor. However, to retrieve photographs

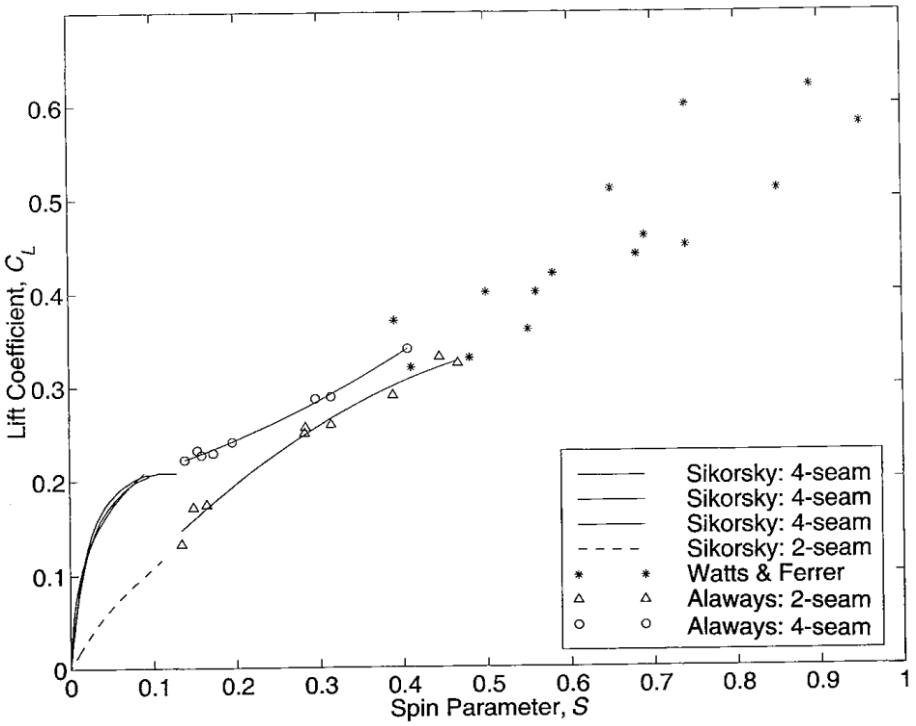

Fig. 1-20: The combination of all three data sets, showing the relationship between all three. (Alaways and Hubbard, 2001)

of the sphere in the wind tunnel, they attached the motor to a piano wire with a diameter of 2.38 mm, to minimize any effect of the wire in the wind tunnel. There was then a series of pulses at an interval of 250 μs which was supplied by a high-voltage, high-frequency pulse generator, and the spark trains were recorded on a photographic film. This was done multiple times by changing the rotation rate of the test balls from 1000 rpm to 3500 rpm at 250 rpm intervals. Once again, it is important to note that this seems to be directed to the study of a curveball, not a knuckleball, due to the rotational rate and the orientation of the ball suitable of four-seam. Figure 1-21 shows the effect made by this spark tracing method.

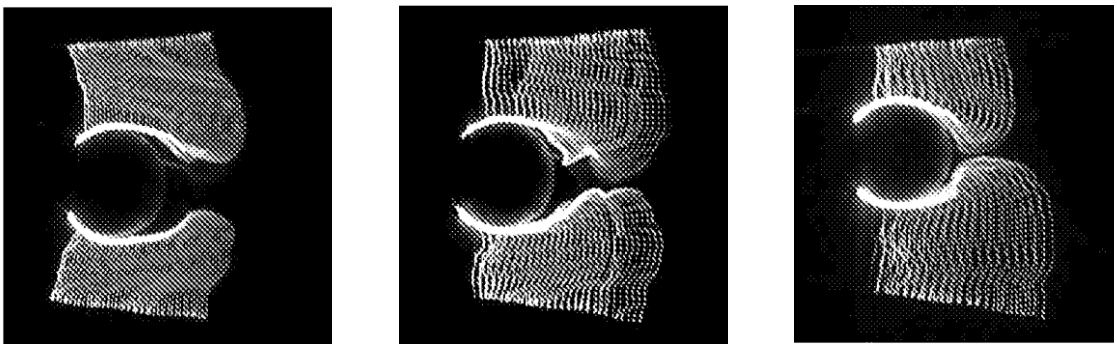

a) Re = $0.5x10^5$ **b) Re = $0.9x10^5$** **c) Re = $1.4x10^5$**

Fig. 1-21: Aoki, Kinoshita, Nagase, and Nakayama photographs of the spark tracing method with rubber ball with seams. (Aoki, Kinoshita, Nagase, and Nakayama, 2003)

A wake and separation can slightly be seen in figure 1-21. This method can be used in wind tunnels where a smoke stream is not available or would be too messy.

The most recent and up to date study was done by Alan Nathan in 2008 [16]. He wanted to continue Briggs' data and make some corrections. He exceeded the velocity to over 100 mph and investigated the dependence of the velocity on the lift coefficient for a fixed rotational speed. He repeated Alaways and Hubbard's work except there were three

main differences [16]. One difference was a single set of cameras to record the baseball for about 5 meters instead of multiple sets for the full distance from the pitcher's mound to home plate. The cameras were spaced equally to allow for the best possible way to record the initial conditions and the acceleration, over the larger distance. He made sure that the ball rotated at least once during on recording sequence. However, the second difference was that Nathan was only able to use one reflective marker as opposed to four that Alaways and Hubbard had. This was because the software he used was not able to distinguish multiple reflective markers. Therefore, he was not able to record the spin axis. He assumed the axis was parallel to the horizontal and orthogonal to the direction of the velocity because there was no deflection on that horizontal plane. He did place the reflective marker 15 millimeters apart from the assumed axis. The third difference was the ability to record almost three times more of a frame rate than Alaways and Hubbard. This allowed a larger variation of the Reynolds Number and the spin coefficient. Some of his data was plotted in figure 1-22. His coordinate system was z in the direction of the pitch, y was upward, and x was the lateral deflection. A strong, parabolic curve can be shown for the y. There is also a small, oscillatory motion in the z, but was too difficult to

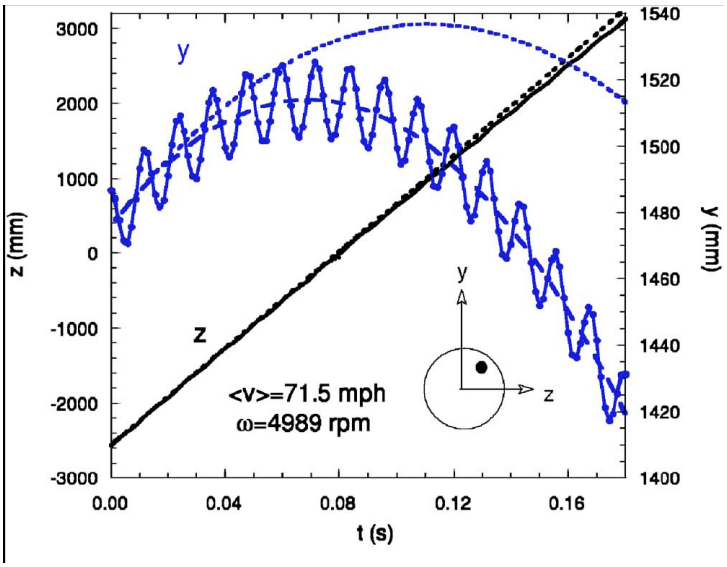

Fig. 1-22: Nathan's trajectory data. The pitch was slightly angled upward. The dotted, oscillatory line is the plot of the dot with a least-square fit. (Nathan, 2008)

view because of the larger distance of z. Nathan also concluded, as others have before, that speed of the pitch did not have an effect on the lift coefficient, when observed for the conditions for a curveball in a baseball game.

Now with all of this scientific data, one has to realize how much of it is actually useful towards a knuckleball. As commented before, most of these experiments are for curveballs, *not* knuckleballs. There was a book published to help understand how a knuckleball is thrown, and what the orientation should be. As Dave Clark writes in his book, *The Knucklebook*, there are many ways to throw a knuckleball [1]. Overall, some conditions will have to be made to convert the pitch from a curveball to a knuckleball. First off, instead of a high rotational rate to make the ball curve, a knuckleballer wants achieve a slow rotation rate. On average, a half of a rotation by the time the ball gets to home plate is ideal. Also, most of the pitches are two-seamers with rotation over the top toward home plate, as shown in figure 1-23. Past knuckleballers have also thrown the ball as a four-seam, but are less popular.

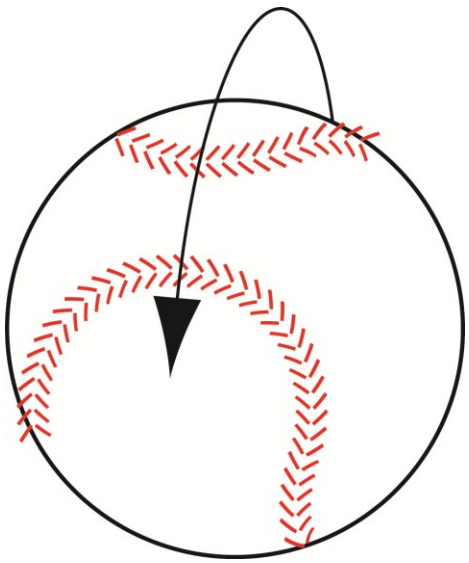

Fig. 1-23: Orientation and rotation of a knuckleball.

The grip of the baseball is as different as each pitcher. Clark did a great job finding the history of the grips of the knuckleball as shown in figure 1-24. As shown, there are many grips to the knuckleball. However, no one knows if these grips have any difference in the knuckleball's movement, since they are so few and far between. The grip depends on the pitcher and his abilities. Also, the

a) Eddie Cocotte b) Hoyt Wilhelm c) Phil Niekro e) Steve Sparks f) Tim Wakefield
Fig. 1-24: Clark's illustrations of past grips of the knuckleball. (Clark, 2006)

orientation of the baseball is a two-seamer. One possible reason could be because during a half rotation to the plate, a pitcher throwing a two-seamer will have a greater chance of the two seams disrupting the boundary layer than a four seam, since the two seams are closer together than any of the seams in the four seam. In addition, the four-seam ball presents a somewhat more symmetric configuration to the wind with respect to the location of seams than does the two-seam orientation. The average speed of the knuckleball has varied through time, but the most common is about 67 mph. There are pitchers that threw the knuckleball faster and slower, but it is up to the pitcher to find what is most effective for. According to R.A. Dickey, he throws a fast knuckleball (over 70 mph) where as Tim Wakefield throws a slower knuckleball (closer to 65 mph). The effect is much different. The Dickey pitch tends to hold a more deterministic trajectory with a hard break as it nears the batter, where as the Wakefield pitch tends to move more over the entire flight. As past experiments have shown, the speed does not have as much of an effect as the rotational speed does, however, in the game of baseball, a pitcher's unpredictability is the knuckleballer's best friend.

There has been plenty of work done to find the aerodynamics of a baseball, spinning in motion. Nevertheless, not enough work has been done to find what makes a knuckleball knuckle in the different varieties. There have been plenty of studies on the

curveball, but there is a large difference of the lift coefficient as commented by Sikorsky when the spin coefficient is low. Also, the difference of the two-seam and four-seam knuckleball is debatable. Pitchers and later scientists found that there is a difference; however, earlier work says there is not. Lastly, which may end up becoming the most important part, it was mentioned that there was no movement of the baseball when no spin was applied. However, Brown showed through his photos that there is an asymmetrical wake behind a stationary baseball. Weaver later stated that natural torque must spin the stationary baseball. So, is there a way to balance out both forces to make the ball travel with no spin? And is there movement? If so, some of the graphs shown above would be incorrect, due to the assumption that there is no lift or lateral force when there is no spin. This is what has to be done to fully understand the knuckleball, and to transition the theoretical work to actual, on game performance of a knuckleball pitcher. Can a knuckleballer pitch a knuckleball with the same movement constantly over an arbitrary amount of pitches?

1.4. Interview with R.A. Dickey

During the course of this research one can find themselves asking a question which all research scientists are faced: To what degree do our experiments matter in practice? With regard to aerodynamics we might be experts but with regard to playing the game of baseball we are amateurs and fans. Thus we sought the help of a professional in order to guide our research efforts. We were very lucky in that knuckleball pitcher Robert A. Dickey had spent the 2007 season with the Triple-A Nashville Sounds. He finished the season with a 12-6 record and a 3.80 ERA and was

named the Pacific Coast League Pitcher of the Year. After multiple calls to the Brewers organization they agreed to give us RA Dickey's cell phone number. Thus we were able to call him and ask some interesting questions to get a pitcher's view of the knuckleball rather than the scientists view.

As expected, Dickey noted that domes and places with high humidity are good environments for his knuckleball. Domes are good because of the lack of wind. High humidity is good because "the seams grip the air better." Dickey stated that Boston and Pittsburgh are two good places to pitch a knuckleball. Ironically, those are also two cities that his mentor, Tim Wakefield, played for. Two bad places to pitch are Arizona and Colorado Springs. He says the heat creates sweat on his hand that would transfer to the ball, which would make the release of the ball with no spin more difficult. The heat also makes the fingernails softer, which is crucial for the feel of the release.

R. A. Dickey grips the ball with his fingernails placed behind the seams in the horseshoe of the baseball. Dickey commented that this grip is endorsed by Tim Wakefield, Charlie Haas, and Phil and Joe Niekro. There was a difference in how much pressure was placed on each fingertip. Some other knuckleball pitchers placed their fingernails behind the seam on the landing strip of the baseball.

R. A. Dickey pitches his knuckleball at 65 to 82 mph, which is considered a "hard knuckle." Dickey states that his ball goes straight for 57 feet and then breaks down and left 60 percent of the time. Wakefield's knuckleball travels at 61 to 68 mph and believes the ideal speed is at 68 mph. His knuckleball breaks three to four times before the baseball reaches home plate.

Dickey continued to say that the rotation of the knuckleball should be one-quarter to three-quarters of a forward rotation, with the ideal rotation to be one-half. Any backwards rotation exposes the landing strip and is a "home run" because of the lack of motion the baseball would experience.

Using Dickey's pitcher mentality in a scientific manner, a series of test will be done to find how the knuckleball moves.

1.5. Purpose and Methodology

The goal of the research was to find why the knuckleball moves the way it does. This includes the aerodynamic forces the baseball experiences and the reasons why. It was presumed that the stitches of the baseball effect the boundary layer separation, which effects the movement of the baseball. Three techniques were applied: force balance dynamometry, flow visualization, and hot film anemometry.

The force balance was used to find the aerodynamic forces the baseball experiences while in flight. The apparatus found the lift and lateral forces acting on the baseball at different degree intervals. The dynamometer was initially used to match Watts and Sawyer's data as shown in figure 1-13. Once completed, the apparatus was considered to be suitable for other force balance data collection.

Flow visualization was used as visual evidence to locate boundary layer separation on the surface of the baseball. A photo of a still baseball at a critical angle can determine where separation occurs. The flow visualization was used as supporting evidence to assess if the stitches act as a tripping wire effectively delaying separation, or as a perturbation which induces separation. A movie of the baseball rotating would show if

separation changes as the ball spins. If so, a correlation of separation at different angles and the lift force would be created. The correlation would determine if the forces on the baseball is due to separation.

Hot film anemometry was used in two conditions: one hot film was placed on the landing strip part of the baseball, and two hot films were placed on each side of a stitch. The hot film on the landing strip of the baseball was used to find the shear stress and the boundary layer separation as the baseball rotates. The landing strip would act as if a sphere was covered with the cowhide that is used to cover the baseball, without any stitches. The two hot films on each side of the stitch were to evaluate the magnitude of the shear stress and separation before and after the stitch. The comparison between the shear stresses on the landing strip and the seams will show how much of an effect the stitch has on the surface of the baseball.

With all of these techniques combined, a conclusion was made on why a knuckleball pitch moves so erratically.

CHAPTER 2. EXPERIMENTAL SETUP

2.1. Baseball/Sphere

As stated before, published data will be matched to confirm the validity of the apparatus. Watts' and Sawyer's data was in a four-seam orientation. In order to find the axis of rotation for a four-seam orientation, or any sort of orientation, a geometry problem was instituted. Unfortunately, a baseball is not a simple sphere, the existence of the seams complicate the discovery of the axis of rotation. Therefore, a technique was found to best find the axis of rotation.

The four-seam position is quite clear and simple. A baseball consists of two pieces of cowhide, shaped like a figure "8," and stitched together to cover the surface of the baseball. The distance of the two nearest seams were found with a vernier caliper. This was done by placing one of the outside jaws of the caliper on a seam, and rotating the other jaw until a minimal distance was achieved. The positions were marked and the distance between the two points was recorded. The outside jaws were then moved to another position on the seams and the process was repeated until the distance begins to diverge. The position with the lowest distance was found and divided by two. That length was set into the vernier caliper and locked. One of the outside jaws was placed on the position marked on the seam, and the other outside jaw was pivoted, while marking the surface of the baseball. The process was repeated

Fig. 2-1: A picture of a Major League Baseball where the two opposite seams

on the other seam. The point where each mark intersected was the axes of rotation for the four-seam orientation. Figure 2-1 is an image of the baseball where the seams are the closest with axis of rotation marked.

Fig. 2-2: A picture of a Major League Baseball where the two-seam axis of rotation is found. The "+" is the final, corrected point where the other mark is the initial point.

In order to find the axis of rotation for a two-seam orientation, the four-seam process was first completed twice, one on each side of the baseball. A flexible, plastic tape measure was wrapped around half of the ball to find the distance between each mark from the four-seam orientation. The distance was recorded and was divided by two. The baseball was then marked where the midpoint between each point was found. To check the location, the plastic tape measure found the midpoint between the two seams where the first midpoint mark was found. Figure 2-2 is the image of the final position for the axis of rotation for the two-seam orientation.

The smooth sphere does not need any specific geometry to find the axis of rotation. However, the three inch wooden sphere was sanded down to allow for a smooth finish.

To drill the hole into the baseball or smooth sphere, it was placed in the spindle of a lathe in a position where the point desired was to be drilled. Pieces of cardboard were placed between the spindle and the baseball so no indentations are created on the surface of the baseball. A #3 center drill bit was locked into the tailstock and was guided along the bed of the lathe to make contact with the surface of the baseball to confirm the drill bit lies upon the mark on the baseball. The lathe was set to rotate at 180 rpm, slow

enough to not have the baseball move in the spindle, and fast enough to quickly cut the leather, string, and cork inside the baseball. A center hole was drilled through the leather. The center drill bit was replaced with a #25 drill bit. A 1.25 inch deep hole was drilled into the baseball. This allowed for a snug fit on the shaft and sting of the force balance that will be discussed later. The lathe was used so the hole was along the radius of the ball, or perpendicular to the surface. The position was checked by using a dial indicator placed on the tool rest. A shaft was pressed into the hole and tightened in spindle. The spindle was then rotated by hand to find the minimum and maximum of the displacement of the ball, which was 0.002", not including the stitches. The baseball was also spun on the lathe to ensure the axis of rotation was true to the radius by noticing if the baseball appeared to wobble at a high rotation rate.

2.2. Force Balance

To help understand the aerodynamic forces acting on the baseball, a force balance was used. This piece of equipment measures linear displacement of a model with the use of several cantilever beams; the linear displacement of the beams is found through a linear voltage displacement transducer (LVDT). The LVDT changes its output voltage proportionally to the displacement of the model. This voltage is sent to a circuit board that amplifies the signal to be recorded. These displacements/voltages can be calibrated to any force units. These signals can then be recorded to observe the change of forces acting on the baseball in different scenarios.

2.2.1. Apparatus

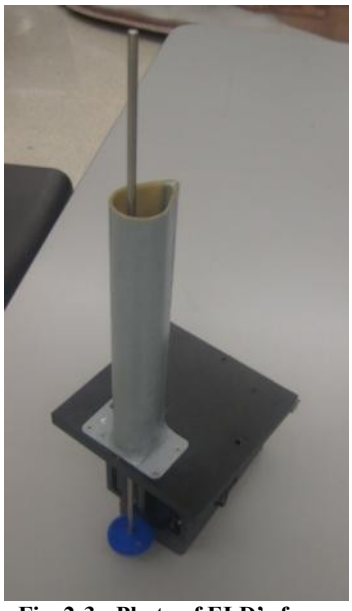

Fig. 2-3: Photo of ELD's force balance.

The force balance used in this experiment was Engineering Laboratory Design, Incorporated's (ELD) lift/drag force balance and model set, as shown in figure 2-3. This was a dynamometer that measures aerodynamic lift and drag forces. This apparatus consists of two pairs of restrained, cantilevered beams, separated by spacer blocks, for each axis. Each force that was generated to the model under test conditions was conveyed to the dynamometer via a stiff strut and results in a small deflection of the beam assemblies. Each deflection actuates a LVDT that was surrounding a fixed armature core. As the LVDT moves along its axis, the deflection was found to be proportional to the change in output voltages, which in part are proportional to the magnitude of the applied forces. This armature core was adjustable for "zeroing out" the DC voltage output to account for any applied static forces before the wind tunnel was turned on. The output voltage signals from the LVDT are demodulated and amplified by a Schaevitz LVDT Voltage Module. The resulting DC voltages represent the direction and magnitude of

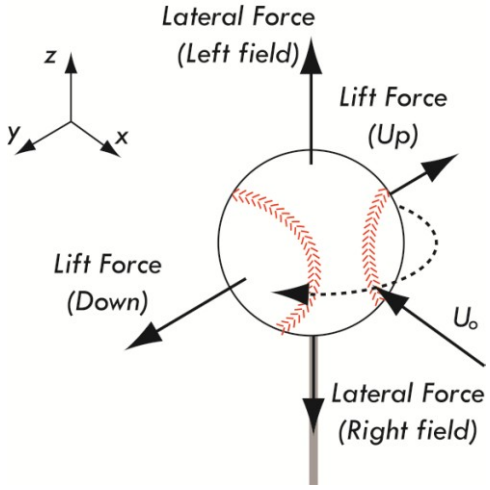

Fig. 2-4: Illustration of the force vectors in the wind tunnel.

the applied forces. This can be calibrated to any desired engineering units.

ELD's model set includes a 16.375 inch strut that allows a model to be attached in a horizontal fashion, with respect to the wind tunnel. This would place the bluff model upstream of the strut. Unfortunately, this only allows the axis of rotation to be parallel with the free stream velocity. It was desired to have the axis of rotation perpendicular to the free stream velocity (i.e., vertical with respect to the laboratory frame of reference) in order to better simulate actual pitch conditions. Therefore, two modifications will be made to the strut to allow the axis of rotation to be vertical, as well as to accommodate spinning and non-spinning baseballs. There will also be a modification to the orientation of the force balance position in the wind tunnel. If used in this original fashion, only lift and drag forces can be recorded. However, the point of interest in the knuckleball was the lift and lateral forces; this requires that the force balance to be rotated 90 degrees in the wind tunnel. Figure 2-4 is an illustration of what the force vectors are in the wind tunnel.

Fig. 2-5: Rigid strut.

The rigid strut was modeled after ELD's design, with two differences: first, the strut was modified such that the bluff body sting would be screwed to the top of the strut, instead of the side. This will allow for a vertical axis of rotation. Secondly, the length of the strut was shortened so the baseball would be centered in the wind tunnel. Stock 1018 steel was used with the same dimensions from ELD's strut, excluding the descriptions above. Figure 2-5 is a rendering of the part.

For the modified strut, a different design was implemented. A shorter strut was constructed with the same dimensions as ELD's design. Two miniature, precise, ball-bearings were attached via Bondo, screws, and an aluminum casing. A miniature, stainless steel shaft was pressed through the two ball-bearings. It is important to note that the shaft was pressed through the ball-bearings before attaching the bearings to the strut, or the bearings can be deformed when screwed to the strut. A gear was attached on the bottom of the shaft so it can be driven. Figure 2-6 is a rendering of the constructed spinning strut.

Since the whole force balance was rotated 90 degrees to record the lift and lateral forces, a new nacelle to cover the strut had to be constructed. The existing nacelle was too tall and not wide enough to house the struts in their 90 degree orientation. The new nacelle was constructed of fiberglass, canvas, and aluminum. A 1.1875 inch outside diameter pipe was attached to a 0.5 inch aluminum fin, with Bondo to smooth out the gap between the two, as a mold of the nacelle. Fiberglass was then laid over the mold and was allowed to dry. Canvas was then glued over the fiberglass and allowed to dry. A piece of aluminum was modeled after ELD's nacelle base. The base was then attached to the nacelle with Bondo and painted.

Fig. 2-6: Picture of the spinning strut without the case over the bearings.

Once all the modifications had been made to the force balance, it was placed into the wind tunnel. However, the position and rotation rate still had to be measured. In order to easily obtain a view looking down the axis of rotation, a mirror was placed on top of the wind

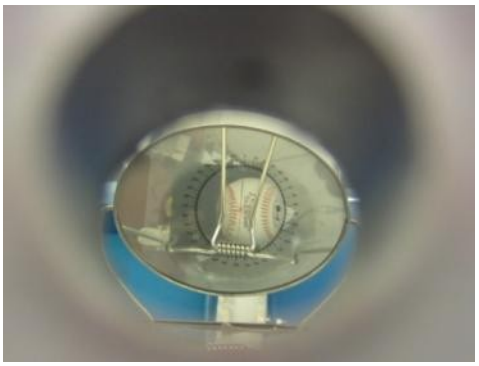

Fig. 2-7: View of the baseball from the viewing port.

tunnel test section. This was placed on top of the wind tunnel so the top view of the baseball can be shown. A protractor design was printed on a piece of 3 inch by 3 inch Mylar, so the position of the baseball could be found. The zero degree mark was found by measuring and squaring it with respect to the wind tunnel. Accordingly, this was centered above the baseball. Figure 2-7 shows the view of the baseball via the viewing port. The baseball can now be rotated to any position for data collection.

In order to measure the angular position and rotation rate of the baseball, a motor and a laser diode system was built. Before any of these were implemented, a frame had to be erected, which was constructed with aluminum angle. The frame was supported by the two hex screws that also support the force balance to the wind tunnel floor. The motor was supported by designing the aluminum in a shape of an "L." The motor was attached to the aluminum via a worm drive tube clamp. The tube clamp was used in case any other size motor would like to be attached. A gear was also attached to the shaft of the motor with superglue. The laser diode system was built and attached to the lower end of the

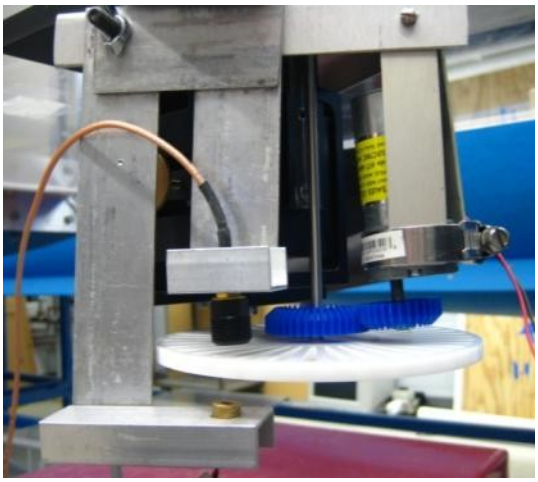

Fig. 2-8: Photograph of the motor and laser diode system.

shaft in the similar fashion. Angle aluminum and a flat plate of aluminum were used. Figure 2-8 is a photograph of the motor and laser diode system. A hole was drilled through the bottom of the frame to fit the laser through the framing. Gum putty was used as an adhesive for the laser to be held to the frame. A photodiode was screwed facing down, above the laser for the maximum light input. The photodiode was placed facing down so less ambient light would interfere with the signal. The whole laser and photodiode system was also blocked from any other light. Two different chopper plates were pressed fitted on the shaft of the spinning strut. One chopper plate has a hole every ten degrees for data collection at every ten degrees. Another one only has one hole, for data collection per each rotation.

A circuit box was made to control the rotation rate of the motor. Figure 2-9 is the design of the circuit. The motor used was DC electric gear motor, with a 120 to 60 rpm at 24-12 volt DC, respectively. The power source used was a 12 volt DC, 100 milliamp AC to DC converter. The power control switches between on, off, and temporarily on, for a quick rotation. One switch controls the high or low speed of the motor, while the potentiometer controls the speed of rotation. Another switch controls the direction, clockwise or counter-clockwise. This control box was used to set the rotation rate and

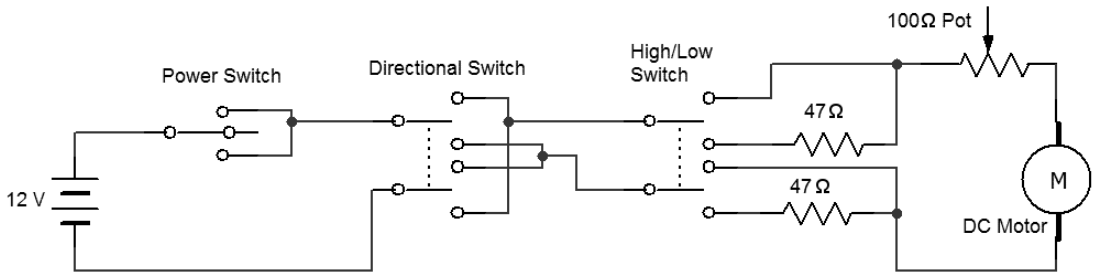

Fig. 2-9: Schematic design of the motor circuit.

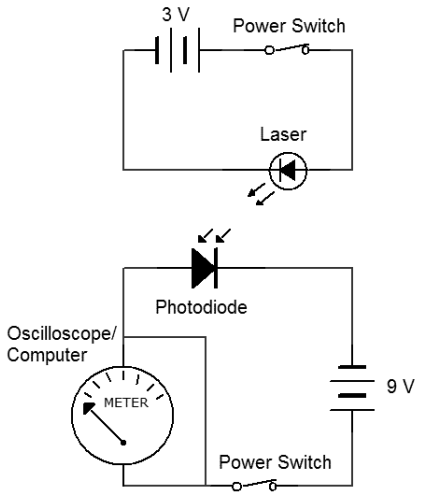

Fig. 2-10: Laser diode circuit.

position of the ball.

The circuit for the laser diode system was quite simple. Figure 2-10 is a schematic drawing of the circuit. This circuit consists of a transmitter and a receiver. The laser acted as the transmitter and the photodiode acted as the receiver. The receiver part of the circuit was connected to an oscilloscope, or computer, and then a photodiode. This part of the circuit measured the offset of light entering the photodiode. The transmitter part of the circuit, or the laser circuit, consists of two AA batteries and a 650 nm wavelength laser. The laser was aimed at the photodiode. Whenever the laser hit the photodiode with no interference, the oscilloscope would show 9 volts. However, when there was no light entering the photodiode, the oscilloscope would show zero volts. Two different chopper plates were used to break the light signal from the laser to the photodiode as the baseball spins. In doing so, the rotation rate and angular position of the ball can be determined by measuring the pulse rate on the meter. If the single slit chopper plate was installed, then the motor speed would be set until a frequency of 833 mHz was met, or 50 rpm. When the 36 slit chopper plate was installed, the angular position of the ball was found at every ten degrees. The frequency was found through the oscilloscope.

The data was recorded with either a computer with National Instrument's LabVIEW. The speed of the computer was 2.67 GHz with an Intel® Core2 CPU, along

with 1.98 GB of RAM. LabVIEW version 8.0 software was installed on the computer, with National Instrument's BNC-2110 terminal block installed. A couple different programs were written for data collection. One included real time data observation, which integrated the voltage from the LVDT, free stream velocity calculation from a pitot tube, calibration tools, and hot wire data.

Before data collection can occur, the sampling frequency must be determined. The goal was to resolve any frequencies that are of interest. The dominant frequency in this experiment was the shedding frequency. The shedding frequency can be estimated by knowing the Strouhal number, i.e., a non-dimensional shedding frequency, given in equation 2.1.

$$St = \frac{fD}{U_o} \tag{2.1}$$

If the Strouhal number for a right circular cylinder (St = 0.2) is assumed for a sphere, the shedding frequency would be about 83 Hz. This will be verified with hot wire data, which will be discussed in section 2.4.1. To fully resolve that frequency, data must be collected at least double the dominant frequency. This is called the Nyquist frequency, and thus 166 Hz for this experiment. Therefore, any frequency greater than 166 Hz was valid for a sampling rate. Considering that the Nyquist frequency was low, the rate chosen for all data recording was 2000 Hz. This was selected because that would allow for 2400 data points per rotation, which was only 1.2 seconds. That would result in only about 67 kilobytes per file, which was relatively a good size for multiple sets of data and could easily be stored in computer memory.

2.2.2. Calibration

To determine the forces acting on the baseball, the force balance must be calibrated. This was done with a variety of masses ranging from 0 to 200 grams and recording the output voltage. The maximum amount of lift on the baseball was not expected to be over 150 grams, so calibrating the force balance to 200 grams was applicable. To calibrate the lateral force on the baseball, each weight was placed on top of the ball. It was important to make sure the weights are centered on top of the baseball. This was completed by using the view port located on the side of the wind tunnel test section. The real time LabVIEW program was then used to find the mean and standard deviation of the output voltage from the force balance with 100 data points. The real time program was used as opposed to the data collection program because of ease of use. The mean and standard deviation was checked with respect to the data collection program, and the differences were negligible. A graph was then compiled of voltage versus mass. Due to the design of the force balance and range of operation, the resulting voltage versus force calibration curve was linear, so the slope and y-intercept can found, as shown in figure 2-11. The slope and y-intercept was then entered into the LabVIEW program.

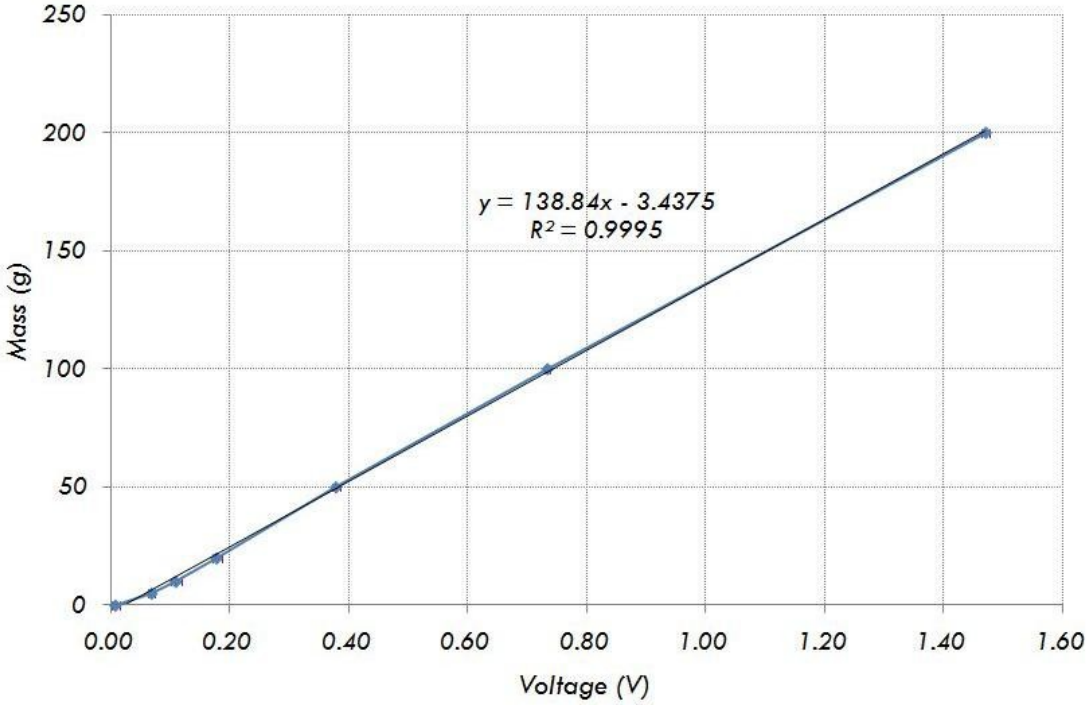

Fig. 2-11: Sample plot of calibration of lift forces.

To calibrate the lift force on the baseball, or lateral force in the wind tunnel, the same procedure was used, except a pulley system was devised. The weights are hung by a string that was hung by a pulley, and tied around the baseball. The pulley was attached to the wind tunnel wall with a suction cup. The top of the pulley was centered with the side of the baseball with measuring the wind tunnel wall, as shown in figure 2-12. A graph

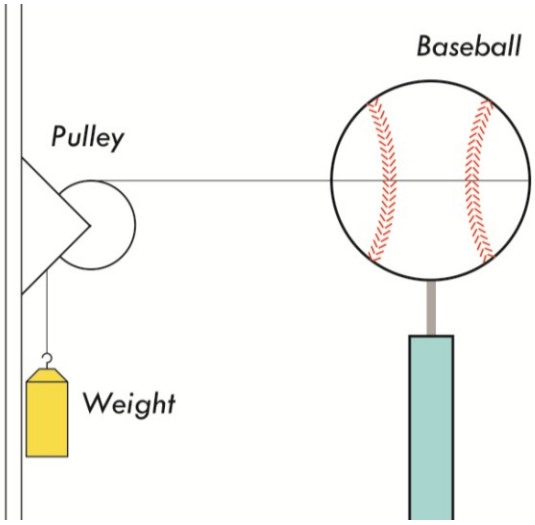

Fig. 2-12: Schematic drawing of the lift force calibration with suction cup.

of the voltage and mass was plotted, and the slope and y-intercept was found and entered into the LabVIEW program.

2.2.3. Data Collection

Before any data can be collected, the spinning or non-spinning weight must be considered. Install which the rigid strut for the static data and spinning strut for the dynamic data. The baseball was placed on the sting. The LVDT was zeroed out, and then the force balance was calibrated. The free stream velocity was calculated from the real time LabVIEW program in appendix A-1.1. The temperature and pressure of the air was entered into the program in order to accurately calculate the air density. The wind tunnel velocity, and the subsequent total pressure change measured with a manometer, was varied until the desired velocity obtained from equation 2.2 was obtained.

$$U_o = 1096.2\sqrt{\frac{P_U}{\rho}} \tag{2.2}$$

This equation finds the free stream velocity, where P_U is the velocity pressure in inches of water. To find the air density, ρ, the equation below was applied.

$$\rho = \frac{1.325P_b}{T} \tag{2.3}$$

All of the variables are in English units, where P_b is the barometric pressure in inches of mercury, and T is temperature in Rankine.

When recording the non-spinning baseball data, the single data collection program was used (see appendix A-1.2). Starting from 0 to 360 degrees at 10 degree increments, 2400 data points were collected at 2000 Hz per increment for five seconds to record the full vibration until the strut was still. This was done by rotating the baseball by hand, while matching up the orientation in the view port. Nine trials were performed. This test was only done in the four-seam orientation.

For all the other tests, the spinning strut was used. The spinning strut was used in two different conditions: in ten degree increments and as the baseball rotates. For the incremented data, the 36 slit chopper plate was installed. Data was recorded at every ten degrees in a static fashion. However, instead of the viewing port, the laser diode system was implemented. Nine trials were performed as well. For the rotating baseball data collection, the multiple data collection program was used (see appendix A-1.3). First, the one slit chopper plate was installed and the rotation rate was set via the oscilloscope at 833 mHz. Data was then recorded, per rotation. Three-hundred rotations were recorded and later processed. Results were then drawn and discussed in Chapter 3.

2.3. Flow Visualization

To observe the flow of the fluid around any model, flow visualization was used. There are many techniques of flow visualization in air available, including fog or smoke rakes, mist rakes, smoke wires, or even particle dispersion. To determine which technique was suitable, the application must be considered. In the case of Marquette University's Wind Tunnel Lab and testing conditions, helium bubble visualization was best. This was because the lab includes a closed-circuit wind tunnel and the velocities

tested were at 70 mph (31 m/s). Fog and smoke generators usually use oil based working fluids which can leave an oily build up on the wind tunnel walls and fans. Considering it was a closed-circuit wind tunnel, these pollutants would circulate in the wind tunnel until they stick to a surface. Smoke wires, which use considerably less oil, could not be used because the smoke was only visible at low velocities, 6-22 mph (3-10 m/s), which was much too slow for the velocity required. Therefore, helium bubbles were sufficient for flow visualization. The objective of the helium bubble technique was to determine the dynamic separation of the baseball, which can help explain why the baseball moves erratically.

2.3.1. Apparatus

The helium bubble generator used was manufactured by Sage Action, Incorporated, and was on loan to us by the University of Notre Dame. The machine produces helium-filled, neutrally buoyant bubbles of uniform size. The bubble could be inserted into the free stream, upstream of the test section, and illuminated for visualizing the resulting flow patterns around the baseball. These bubbles were roughly 1/8 of an inch in diameter and very durable. They can be used to view laminar, unsteady, and turbulent flows. The bubbles are made from a bubble film solution (BFS), a proprietary solution sold through Sage Action. The bubbles are created by a concentric

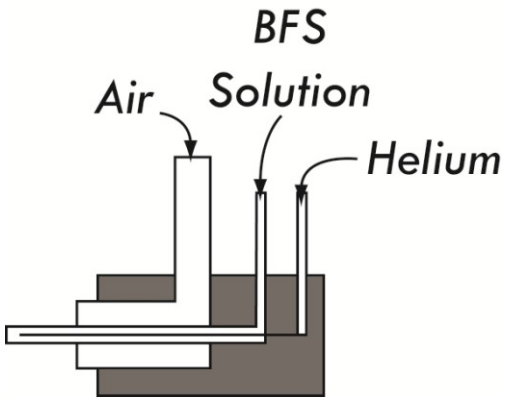

Fig. 2-13: Schematic cross section of the plug-in head for helium bubble generator.

arrangement of two stainless steel hypodermic tubes in the plug-in head, as shown in figure 2-13. The BFS solution was extruded by the pressured helium, gravity and surface friction, and blown out by the air pressure. The neutrally-buoyant bubbles were separated from the non-neutrally-buoyant bubbles via a mini-vortex canister, which swirls bubbles in a large open container. Only those bubbles which were neutrally-buoyant can enter the exit orifice located in the center of the vortex canister. The heavy bubbles sunk and the light bubbles floated; the neutrally buoyant bubbles were drawn up in the outlet tube. The outlet tube was then connected to a firmer tube, and placed into the wind tunnel.

The camera used to capture the flow visualization images was the Photron Fastcam-APX RS CMOS high speed camera. This camera, which was a digital CMOS design, has a maximum resolution of 1024 by 1024 pixels with recording up to 3,000 frames per second (fps), with a maximum fps of 250,000 at greatly reduced resolution. It has 2.6 GB of memory built into the camera, which can be partitioned for recording multiple instances. The size of memory allows for 2,048 recorded images with a 1024 by 1024 pixel resolution. For easy playback and operation, the camera can be connected via an IEEE 1394 interface connector to a PC. To record specific, time sensitive instances, an internal and external trigger system can be applied. With all of these options, still photos and a movie were created.

In order to capture the bubbles at such high wind tunnel air speeds, strong lighting was needed. Two halogen lamps were used with a Fresnel lens for each. The Fresnel lens was used to focus the light on a specific area of the test section, namely a vertical plane on the center of the ball. The schematic setup is shown in figures 2-14 and 2-15,

with the height of the lamps at four feet and 3 inches. An intense amount of light was needed to illuminate the bubbles considering the bubble velocity. Therefore, it was best to focus the light with the halogen lamps and Fresnel lens to observe what was most interesting. Unfortunately, the bubbles were emitted in a volumetric cone shape. However, only a plane of bubbles was needed. Consequently, two shields were placed to block all the light, except for 5/8" on the top of baseball. Blocking the light also discarded all of the bubbles not traveling in the plane over the ball. Unfortunately, only a few bubbles at a given time were observed to flow over the ball. Therefore, a series of Matlab programs were written to superimpose the images on top of each other.

2.3.2. Image Recording and Processing

A post-processing algorithm was implemented to record the separation on the baseball and smooth sphere as still images and a movie. For the still images, the process was quite simple. The camera was set at 500 fps, with a 105 mm focal length lens at an f-stop of *f*/5.6. All of the lights were turned off in the lab, except for the two halogen

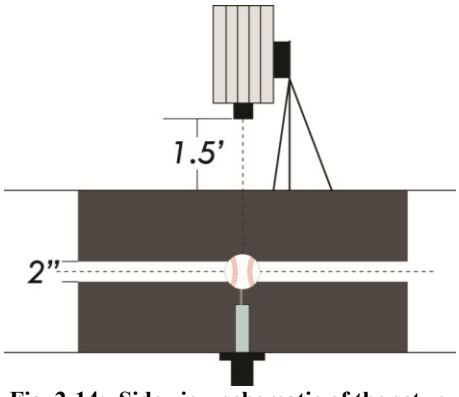

Fig. 2-14: Side view schematic of the setup for the camera.

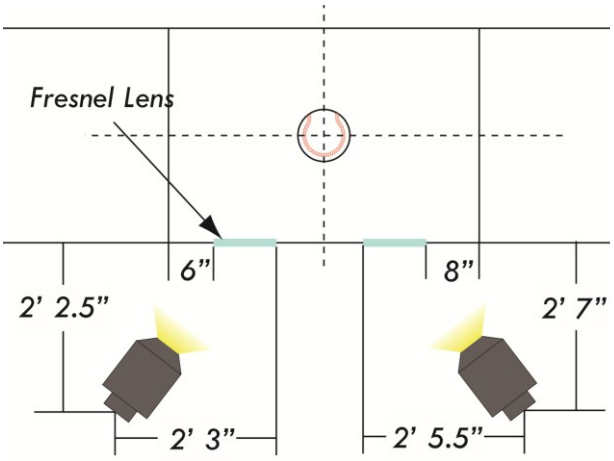

Fig. 2-15: Top view schematic of the setup for the lighting.

lamps. The wind tunnel was then set to the desired velocity. Once done, the helium bubble generator was turned on. The output tube was placed a foot in front of the ball. The high speed camera was triggered on, and the images were recorded. The images were then post processed.

When the baseball was spinning, only two modifications were applied. The single slit chopper plate was installed on the force balance shaft. The camera's memory was then partitioned to three parts, with 682 frames in each partition. Once one partition was finished recording, the camera would automatically go to the next partition for recording. The partition would be triggered for recording by the oscilloscope. The oscilloscope was connected to the "trigger sw in" on the camera's input component cable. As the laser diode system was plugged into the oscilloscope, a trigger level was set to send a trigger to the camera. Every time the trigger was sent, the camera would record one rotation of the baseball. Three rotations were saved on each trial, with 600 frames per rotation. There were 57 total rotations recorded. These images were then post processed with a Matlab program.

The Matlab programs operate just as a camera with a multiple exposure operates. A series of images were recorded and layered on top of each other. Since only a few bubbles were captured by each image, multiple superimposed images allowed multiple bubbles to be observed. The more bubbles captured; the easier it was to locate separation. For the still images, the multiple exposure photo program (shown in appendix A-2.1) was used. This program superimposed all of the images together by converting the images to matrices and overwriting the higher element. For creating a movie, the movie compiler program (shown in appendix A-2.5 was used). This did the

same as the multiple exposure photo program but at all 600 angles. Once all of the images at each angle were superimposed, a movie was created. This allowed for the observation of separation moving along the surface of the ball as the baseball rotated. To make the study straightforward, a tracer was placed on each frame where separation occurred. The tracer was placed on each image via a photo editing freeware program, Gimp [17]. To help determine the angle of separation, a protractor was placed on top of each frame. A plot was then constructed of the angle of separation in respect to the azimuth angle of the baseball.

2.4. Hot Film Anemometry

Hot film anemometry is used to measure the shear stress of a fluid acting on a surface. A hot film acts just as a hot wire. This design was based on the fact that the resistance over the wire changes as temperature changes due to the flow of the fluid. In this case, a Constant Temperature Anemometer (CTA) was utilized, but this approach requires the fluid temperature to remain constant. As fluid flows past a thin wire in a constant fluid temperature, the wire cools, therefore, the resistance changes. The material of the wire was mostly tungsten or platinum-coated tungsten with a diameter of approximately 0.0002 inches to 0.0008 inches (5 to 20 microns), depending upon the resistance. A bridge was needed to convert the change in voltage to a signal that can be calibrated. Depending upon the restrictions of the probe resistance on the bridge, equation 2.4 was employed.

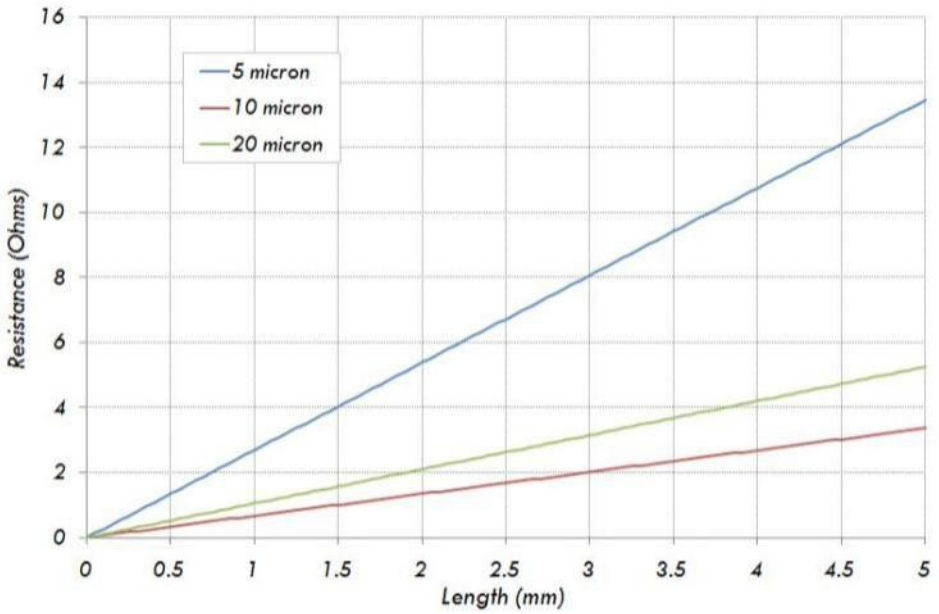

Fig. 2-16: Graph of theoretical pure tungsten wire resistances as a function of length at various diameters.

$$R=\frac{l\varepsilon}{A} \tag{2.4}$$

This equation aided to calculate the resistance of the tungsten wire over a certain length and thickness. R is the resistance, l is the length of the exposed tungsten wire, ε is the electrical resistivity, and A is the cross-sectional area. Considering that pure tungsten wire was used, the electrical resistivity of tungsten is 52.8 nΩ·m at 20° C. The correct combination of length and diameter of the tungsten wire permitted a resistance between 4 to 16 Ohms required for the bridge. Figure 2-16 is a plot of various diameters of pure tungsten. The hot wire or hot film responds to King's Law:

$$E^2=C_1+C_2U_o{}^n \tag{2.5}$$

where E is the voltage in volts, C_1, C_2, and n are constants, and U_o is the free stream velocity. In a hot wire lab, n is about 0.5. In a hot film lab, n is about one-third. Once the hot wire or hot film was calibrated, the velocity or shear stress can be found. To theoretically find the shear stress, King's Law and the following equation was applied.

$$\tau_w = \frac{\mu U_o f''(0)}{\sqrt{\frac{2vx}{U_o}}} \tag{2.6}$$

Equation 2.6 is the equation for shear stress on a flat plate, where τ_w is the shear stress at the wall, μ is the viscosity, U_o is the free stream velocity, $f''(0)$ is the constant found from the Blasius profile, which is 0.46960, v is the kinematic viscosity, and x is the distance from the leading edge of the flat plate. This equation calibrated the hot film from the flat plate which was then inserted into the baseball.

However, it was later decided that it would be better to calibrate the hot films using a smooth sphere because the flat plate calibration was found to be unsatisfactory. Therefore, previously published data of shear stress was found on the smooth sphere via Achenbach [18]. Achenbach measured the shear stress on a smooth sphere using pressure taps. Figure 2-17 is a plot of his results. The Reynolds number that the baseball data was recorded was 1.6×10^5. Fortunately, Achenbach recorded one of his data sets at 1.62×10^5. This data set was used to re-calibrate the hot films.

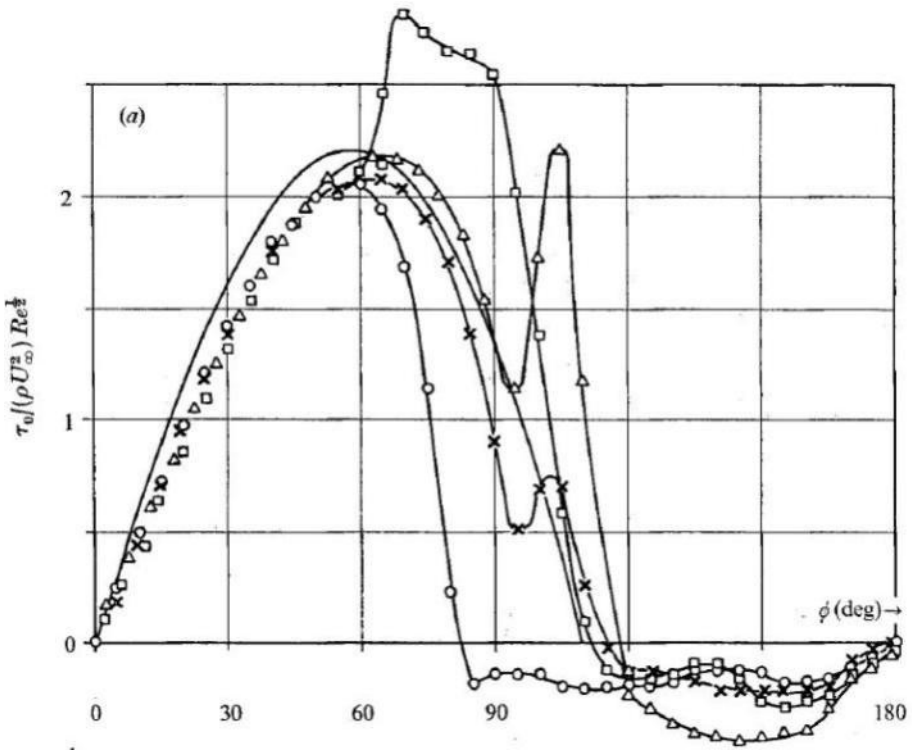

Fig. 2-17: Shear stress recorded by Achenbach on a smooth sphere at variable Reynolds numbers. —, theory. Experiment: ○, Re = 1.62x10^5; ×, Re =3.18x10^5; △, Re = 1.14x10^6; □, Re = 5.00x10^6 (Achenbach, 1972).

2.4.1. Apparatus

There were three main parts in the hot film system: the hot film plug, a flat plate for calibration, and the model to be studied. Dantec Dynamic's Miniature Constant Temperature Anemometer (CTA) 54T30 was used with the hot film to process the voltage. The following discusses how each part was made and used.

2.4.1.1. Hot Film Assembly

The hot film was constructed via Dr. John F. Foss's instructions with some modifications [19]. First, the plug was made out of acrylic. A quarter inch diameter,

right circular cylinder rod of acrylic was found at a local plastic shop.. Two slots were then cut along the side to allow for copper wires to be inserted. A piece of aluminum tubing of 0.2533" inner diameter was cut to a one inch length to act as a cover for the copper wires and acrylic plug. To check if the grooves along the side of the acrylic were to the appropriate size, the copper wires were placed into the grooves and the aluminum tubing was slid over. If the tube was not able to slide over easily, the grooves were then cut wider or deeper. This was done repeatedly until the acrylic plug and copper wires were able to fit inside the aluminum tube. Figure 2-18 is a photo of the aluminum tube sliding over the plug and wires. The top surface of the plug and top edge of the tube were made flush as much as possible. Together, the plug and tube were sanded to have the tops of each perfectly flush with each other. The tube was then removed and the copper wires were stripped on each end and glued with super glue to the acrylic plug, with the top of the copper wire just a bit above the top surface of the plug. Once dry, the copper wires were checked to be rigid with the plug by moving and sliding the wires as much as it would allow. This was done to confirm that the copper did not slide from the sleeve of the wire. It was important to super glue not just the sleeve, but also the copper of the wire to the acrylic plug. The aluminum tube was then slid to the top surface of the plug. The copper wires were then sanded down with the plug and tube to have all three materials to be flush with

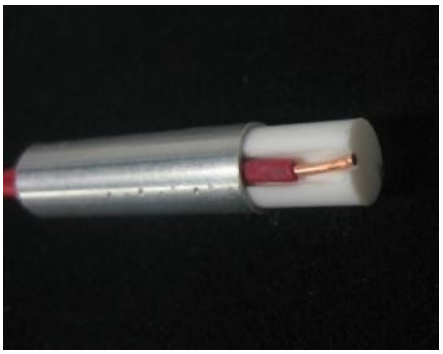

Fig. 2-18: Photo of the aluminum tube sliding over the acrylic plug and copper wires with the grooves on the side of the acrylic.

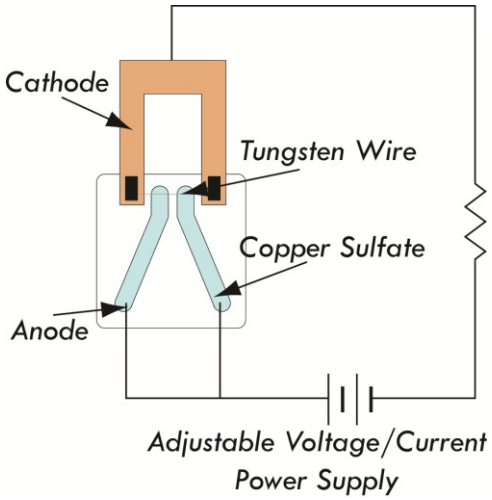

Fig. 2-19: Schematic of the copper plating circuit.

each other. The tube was then slid back down on the plug to expose the copper along the sides. Now that the plug was ready, the tungsten wire had to be prepared.

Five micron thick tungsten wire was taped to a copper fixture. The fixture was then attached to a vertical micrometer driven translation system using an alligator clip. The tungsten wire was then slowly lowered into two wells filled with copper sulfate. The gap between the wells was 0.0625 inches. A circuit was then completed as shown in figure 2-19. Figure 2-20 is a photo of the tungsten wire in the copper sulfate solution. A current of 0.8 mA was then applied across the tungsten. In about 6 to 8 minutes, the tungsten was then copper coated. The fixture was then slowly raised from the copper sulfate and removed from the alligator clip. It was noticeable that there was a gap of pure tungsten wire between the coats of copper due to the gap between the wells. The fixture was then placed on a horizontal micrometer driven translation system. Solder paste was applied to the ends of the copper wires on the plug and aligned with the bare tungsten part of the wire. The fixture was moved slowly towards the surface of the plug. Once the wire was taut on the surface of the plug, the arms of the fixture were rotated

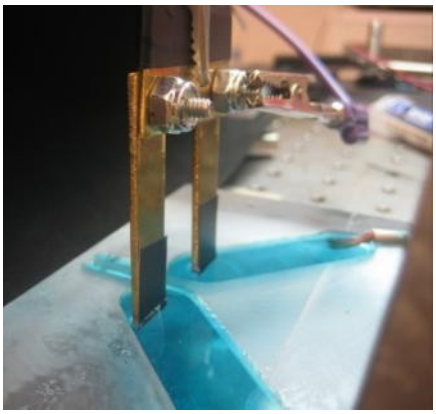

Fig. 2-20: Photo of the tungsten wire taped to the fixture that was lowered into the copper sulfate.

inward to allow for more slack so the fixture can be moved closer. This was repeated until the smallest angle between the tungsten wire and the edge of the plug was achieved. A soldering gun with narrowest point was used on the soldering paste until the solder was shiny. This was repeated on the other side as well. The fixture was then moved away from the plug to check if there was a connection between the tungsten wire and the copper wire. It was then checked for continuity.

It was important to have the total resistance of the copper and tungsten wire system at about 6 to 16 Ohms; otherwise the MiniCTA Anemometer will not operate correctly. If the resistance does not fall within this range, repeat. Otherwise, carefully cut the ends of the tungsten wire. Remove the plug from the alligator clip. The excess tungsten wire was removed by carefully bending the tungsten wire back and forth until the wire breaks off. Continuity was checked again. The plug was then swirled around in a small beaker of acid flux neutralizer for 25 to 30 seconds and then in distilled water for 25 to 30 seconds and allowed to dry. Continuity was confirmed once again. The aluminum tube was then slid over the plug to the top of the surface, as shown in figure 2-21. A straight edge was used to confirm the acrylic plug was flush with the aluminum tube. Continuity was verified once again. The gap at the bottom of the tube was filled with epoxy so the tube, plug, and copper wires were all fixed together. The epoxy was allowed to dry. If there was still continuity, the hot film plug was available for use. Two hot film

Fig. 2-21: Photo of the aluminum tubing slide over the side of the acrylic plug. The surface of the plug and tubing are flush with each other.

plugs were made. Figures 2-22 and 2-23 are a photomicrograph of each hot film made. The length of tungsten wire exposed of hot film 1 and hot film 2 was 1.88 mm and 1.97 mm, respectively. This was confirmed by calibrating the microscope with a ruler. Any sort of disturbance on the surface of the plug was sure to be free of the exposed tungsten wire and upstream during testing.

Fig. 2-22: Photomicrograph of 14.3 Ohm hot film in baseball. (Hot film 1)

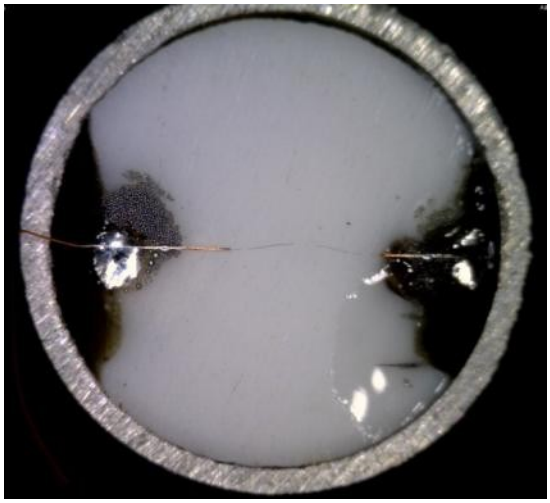

Fig. 2-23: Photomicrograph of 10.3 Ohm hot film in baseball. (Hot film 2)

2.4.1.2. Flat Plate Assembly

A flat plate was constructed to calibrate the hot films. The flat plate was made of acrylic, polycarbonate, and aluminum. The most crucial property of a flat plate was that the leading edge was "razor sharp." The leading edge was made

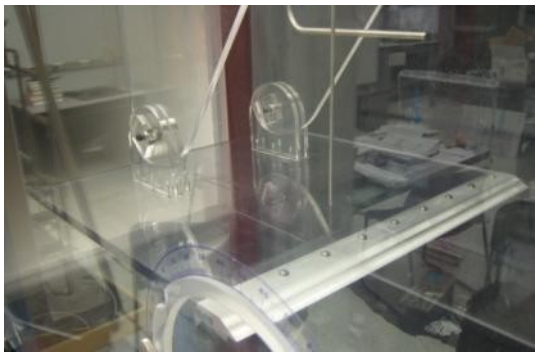

Fig. 2-24: Photo of the flat plate in the wind tunnel.

of aluminum. The aluminum was milled using an angle vice. It was sharp enough to slice a wad of paper towels during cleaning. The leading edge was screwed to the polycarbonate plate. The joint between the aluminum and polycarbonate was smoothed down using very fine sandpaper to allow for a smooth surface. The flat plate was hung in the wind tunnel using a set of hinges and screws.

A threaded rod was inserted into the flat plate and allowed the flat plate to pivot up and down. Figure 2-24 is a photo of the flat plate in the wind tunnel. The flat plate experienced no visible vibrations or movements in the wind tunnel at velocities exceeding 80 mph.

2.4.1.3. Baseball Taps for Hot Films

Holes had to be drilled into the baseballs in three different locations; one hole on the landing strip of the baseball, and another hole before and after the stitch of the baseball. The holes drilled into the baseball for the hot film plugs were performed the same as described in section 2.1, especially for the hole on the landing strip. Coincidently, the landing strip hole was in the same position as the four-seam orientation hole for the shaft. The same procedure was applied, except a through hole was drilled. The hole was started using a #3 center drill bit. The through hole was then started with a #9 drill bit. This gave enough clearance for the wires of the hot film to exit the baseball. A 0.3125 inch drill bit was used to drill the hole for the hot plug. The hole was drilled only 1.25 inches deep. The holes drilled before and after the stitch were measured to be perpendicular to the axis of rotation and as close to the stitch as possible. The holes were

drilled the same way as stated above. The baseball was then prepared to be used for hot film data collection.

2.4.1.4. Constant Temperature Anemometer

The hot film was plugged into Dantec Dynamic's Miniature CTA 54T30. The CTA is designed for measurement of velocity and turbulence in subsonic flows. This is suitable for hot wire and hot film probes. The anemometer accepts probes with cold resistances typically up to about 16 ohms. The anemometer can offset, amplify, and filter the voltages. To avoid overheating, the CTA comes with an Excel spreadsheet with different inputs, which include the sensor resistance, temperature of flow, and desired wire temperature. Once the values are inputted, the spreadsheet displays which DIP switches should be turned on or off. Figure 2-25 is a schematic drawing of the circuit in the CTA [20]. The probe is the adjustable resistance. The top resistances are equal to each other. The servo amplifier makes sure that the overheat and probe resistances are the same. Once the probe resistance is set in the ambient temperature, the bridge voltage adjusts the current through the probe's resistance so it's resistance and overheat resistance is the same. Therefore, when the probe

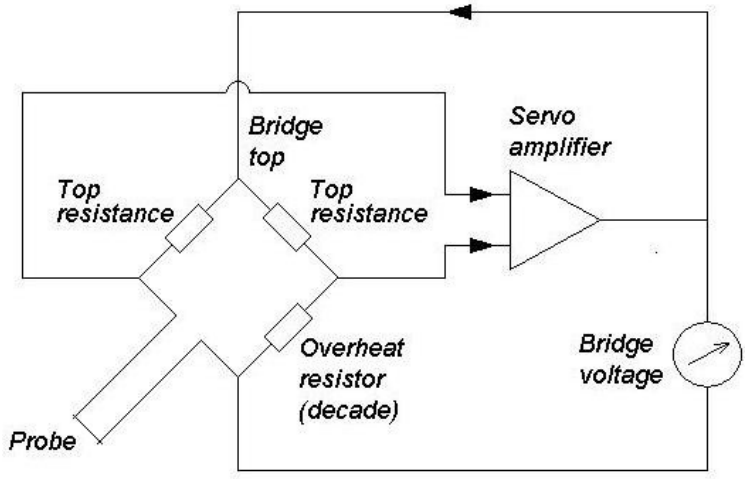

Fig. 2-25: Bridge inside the CTA. (Dantec Dynamics, 2002)

is inserted into a flow, the wire cools down and its resistance increases. So, the greater the velocity of the flow, the more the wire cools down, the higher the resistance, and greater the voltage. The CTA was plugged into the LabVIEW computer and the data was collected as shown in section 2.2.2.

2.4.2. Calibration

The calibration of the hot films began with the flat plate. The known was the shear stress from the Blasius profile. The Blasius profile is based on no pressure gradient over the flat plate. Therefore, the flat plate was angled to tolerate no change in pressure. This was confirmed by placing pressure taps on the surface of the flat plate at three inches and twelve inches from the leading edge of the flat plate. Once the angle for constant pressure on the flat plate was achieved, a hot plug was placed into a hole that was three inches away from the leading edge. The wind tunnel was set a variable amount of velocities. The voltages were recorded at 2000 Hz for five seconds using the program in appendix A-1.2. The data was then matched to the shear stress expected at that Reynolds number and location. King's law was implemented and used as equation 2.7. This equation included E as the voltage from the CTA box, C_1 and C_2 as constants, and τ_w is

$$E^2 = C_1 {\tau_w}^{1/3} + {C_2}^2 \tag{2.7}$$

the shear stress at the wall. This equation fits a linear line. Figure 2-26 is the graph of the voltage squared and shear stress to the one-third at wind speeds ranging from 25 to 76 mph. Once calibrated, data can be collected from the baseball.

However, as stated above, the calibration for the flat plate was not sufficient to measure the shear stress on the baseball. Hence, a smooth sphere was used. Unfortunately, the calibration was after the data on the baseball was collected. Regardless, the shear stress was recorded on the 3 inch, wooden smooth sphere. The shear stress was found at a known location on the sphere. The smooth sphere was drilled to allow for the hot films to fit inside. Figure 2-27 is the calibration of the 10.3 Ohm hot film on the smooth sphere. The shear stress was found using Achenbach's data in figure 2-17. This calibration allowed for other tests that will be discussed in section 3.3.1.

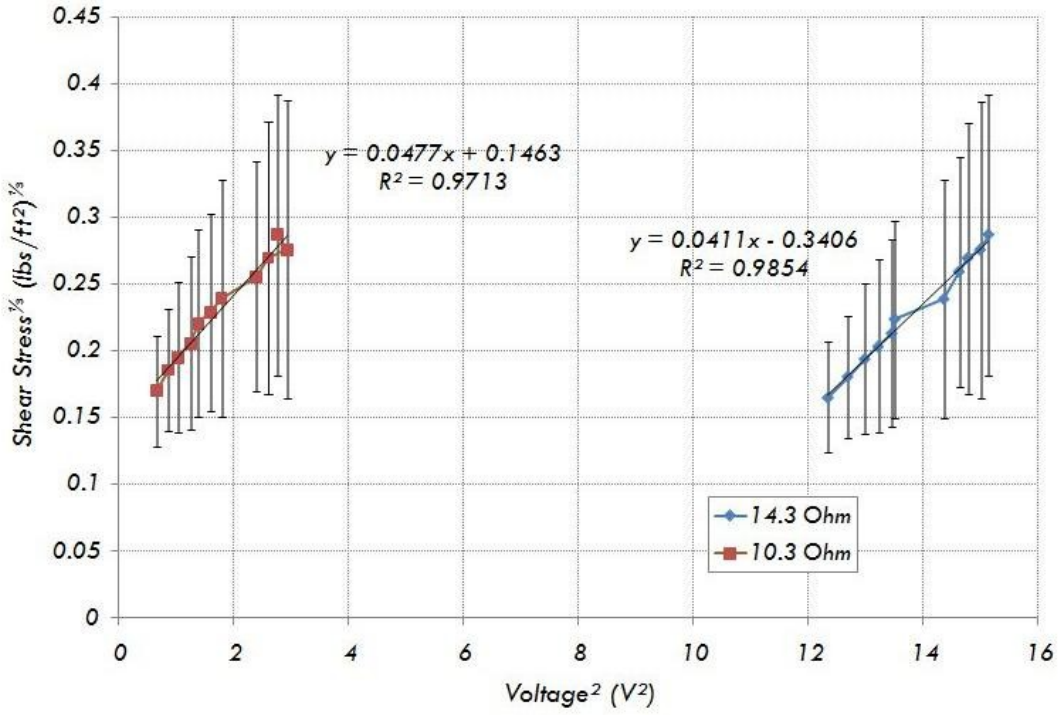

Fig. 2-26: Calibration graph of both hot films from the flat plate. The calibration curve is linear. The error bars are the standard deviation of the ensemble average.

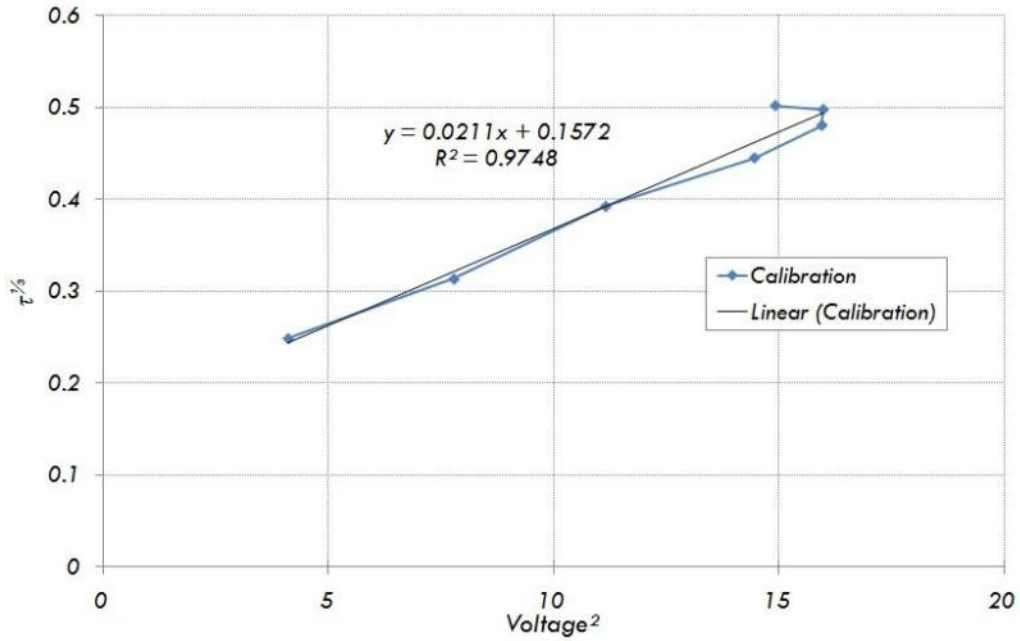

Fig. 2-27: Calibration of the 10.3 Ohm hot film from the smooth sphere.

2.4.3. Data Collection

The procedure for data collection had to be done with a large amount of caution. To limit hot films from breaking and losing data, the procedure was done, in order, of a single hot film plug on the landing strip of the baseball, then calibration for both hot films, and finally both hot film plugs inserted before and after a seam.

To record data with the hot film inserted into the landing strip of the baseball, the force balance with the modified sting and single slit chopper plate had to be installed into the wind tunnel. The decade controls in the mini CTA box had to be modified for the specific hot film to prevent the hot film from overheating. This was completed by using the Excel spreadsheet supplied by Dantec. The sensor resistance and desired wire temperature was inserted to give the necessary controls. A test was then done with the

Fig. 2-28: Photo of the setup for the hot film on the landing strip of the baseball.

specified hot film to make sure the hot film operated correctly. The BNC cable attaching the hot film to the CTA box was disconnected, while the power cord remained plugged in. The hot film plug was VERY CAREFULLY inserted into the baseball, copper wires first. Once the bottom of the plug was at the surface of the baseball, fingernails carefully pushed the plug into the baseball until the top surface of the plug was flush with the surface of the baseball. It was confirmed that the hot film was orthogonal to the direction of the wind. The continuity of the hot film was checked to verify that the hot film did not break. The baseball was then forced onto the shaft of the force balance. The wires from the BNC cable from the CTA box was led up through the force balance nacelle and wrapped around the shaft as many times as possible. Those wires were then twisted together with the copper wire leads from the hot film plug. Figure 2-28 is a photo of the setup. The wind tunnel was then set to 70 mph and the multiple data collection LabView program from appendix A-1.3 was compiled. The BNC cable from the hot film was then plugged into the CTA box. The electric motor was set to 50 rpm and data was collected for as many rotations possible or until the rotation rate of the baseball was noticeably slowed due to the tension of the wires. The BNC cable was then unplugged from the CTA box and the wind tunnel was turned off. The power cord was not unplugged from the CTA box because calibration would be lost. The leads from the hot film plug and from the BNC cable were untwisted.

The BNC cable wires were then spun around the shaft and data was collected until thirty valid rotations of hot wire data was collected while keeping the power cord plugged into the CTA box.

The force balance was then removed and the flat plate was installed into the wind tunnel. The hot film from the landing strip baseball was carefully removed and inserted into the flat plate. The wind tunnel was turned on to the desired velocity. The angle of the flat plate was found where there was no change in pressure. Calibration was then completed as discussed in section 2.4.2. Figure 2-29 is a photo of the calibration setup. The hot film plug was removed and the other hot film plug was inserted. Calibration was then completed for the other hot film, but with a different CTA box. Once done, the landing strip data and calibration was completed.

To finish the hot film data collection, the shear stress before and after a seam was

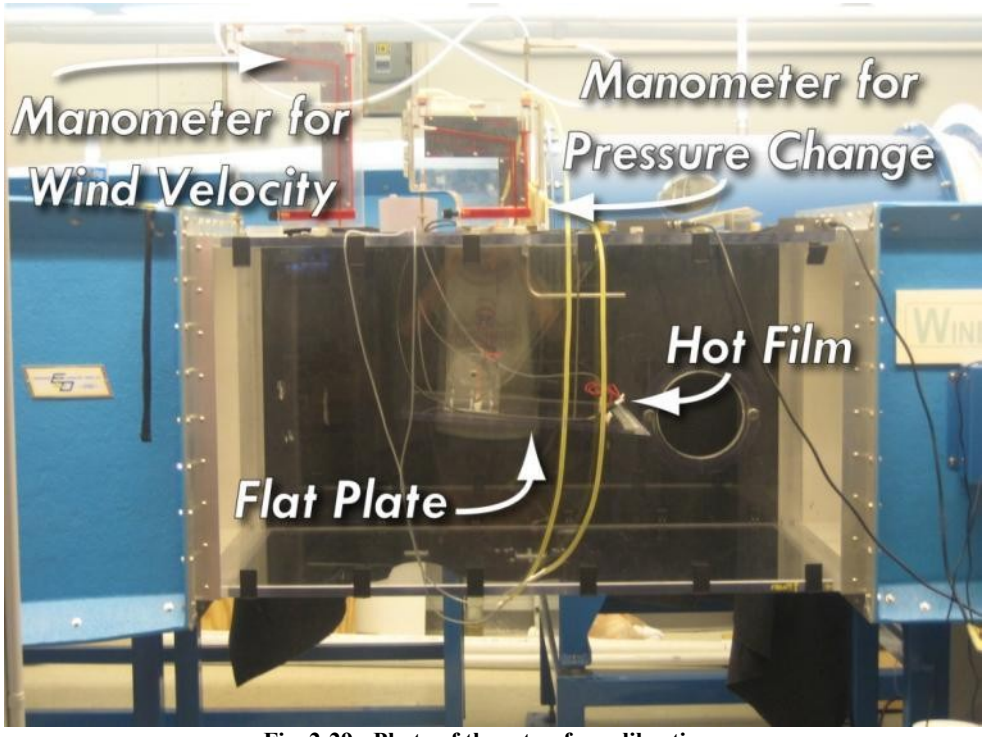

Fig. 2-29: Photo of the setup for calibration.

found. The flat plate had to be removed and the force balance was installed once again. The same process was completed as discussed for the landing strip baseball, except the hot film plugs were inserted before and after the seam. When installing these plugs, more caution was allowed because the copper wires from the hot film plugs crossed each other inside the baseball. Figure 2-30 is a photo of the hot films in the baseball.

Fig. 2-30: Photo of the hot films before and after a seam. Data was recorded for two different rotation directions to test if the second seam affected the shear stress at both locations.

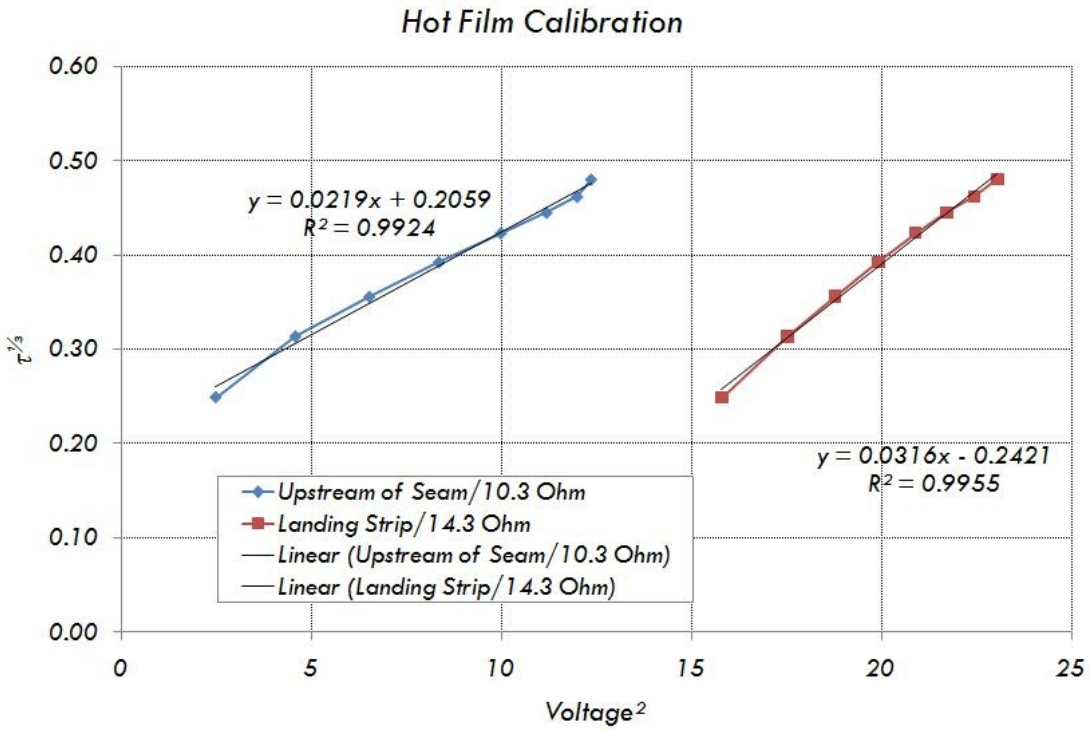

Fig. 2-31: Re-calibration curve of the shear stress on the baseball. The calibration done on the 14.3 Ohm hot film was done by using the data on the landing strip of the baseball. The 10.3 Ohm hot film was calibrated using the data from the hot film placed upstream of the seam.

Thirty rotations of data were collected in two directions, clockwise and counter-clockwise, for reasons discussed in section 3.3.3.

Once the shear stress on the baseball was recorded, there was a realization that the baseball should be calibrated on the smooth sphere and not the flat plate. Therefore, the shear stress on the smooth sphere was found, along with a series of tests with a trip wire on the smooth sphere. The calibration on the baseball was then retrofitted to fit the calibration on the smooth sphere. Figure 2-31 is the plot of the recalibration of the baseball. The data was then analyzed and discussed in section 3.3.

CHAPTER 3. DATA ANALYSIS

3.1. Force Balance

Once all the data from the force balance was collected, it was processed and analyzed. This was completed by a series of Matlab programs. However, to make certain that the apparatuses were functioning properly, the data first must be matched to previous published data. Once the apparatuses were deemed acceptable, the model was placed into knuckleball conditions, to find the lift and lateral forces acting on the baseball.

3.1.1. Comparison to Previously Published Data: Static Ball Position

With respect to the objectives of this thesis, the most interesting and important data from the literature review in section 1.3 was Watts and Sawyer's data in figure 1-13. In Watts and Sawyer's experiment, they rotated a baseball in the four-seam orientation on a force balance at 46 mph. They measured the lift of the baseball at known angles. The graph they compiled ended up looking like a sinusoidal curve. Watts and Sawyer also noted where large and small fluctuations of the data appeared at specific angles. Therefore, in order to determine if the current force balance was valid, the data from Watts and Sawyer's experiment was matched.

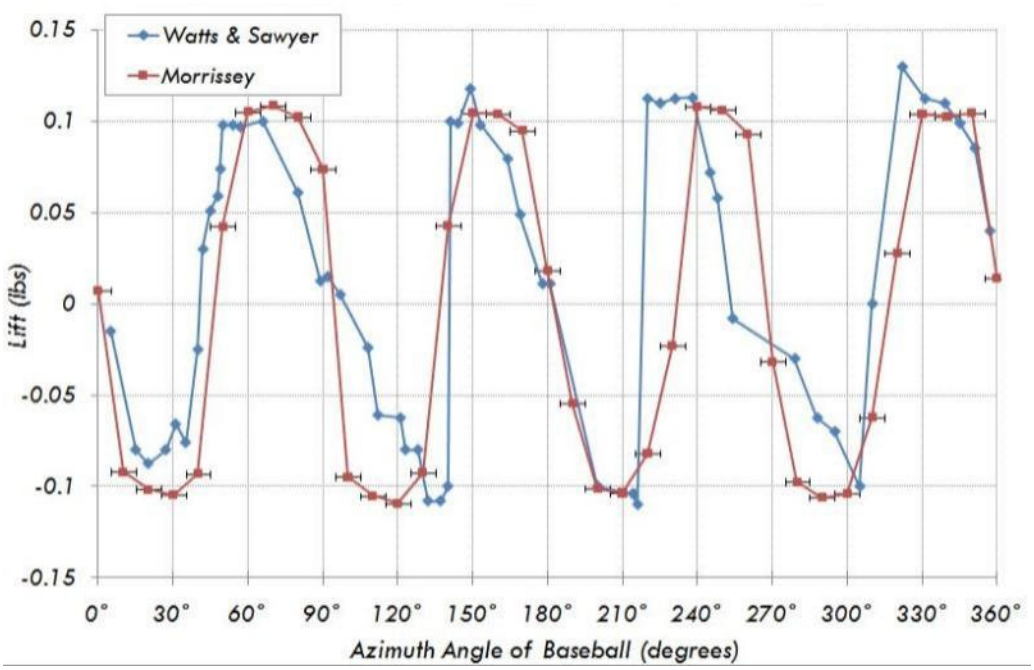

Fig. 3-1: Comparison of Watts and Sawyer data with Morrissey data. Conditions were a four-seam baseball at 46 mph and not spinning.

In order to match Watts and Sawyer's data, the modified, rigid strut was used, as discussed in section 2.2.1. A Major League Baseball was mounted onto the sting, and the lift was measured at every ten degrees, which was the same positioning Watts and Sawyer used as presented in figure 1-12. Nine trials were averaged. The comparison between Watts and Sawyer data to our data is shown in figure 3-1. Before any comparison was made, it was important to note that when Watts and Sawyer published their data in 1975, Major League Baseball changed the regulations on the official baseball so the surface can be made of cowhide instead of horse skin, due to the shortage of horses [2]. However, horsehide covered baseballs was not completely discontinued until 1995. This may leave some discrepancy within Watts and Sawyer's lift measurements. Regardless, the Morrissey data follows the same trend and ranges between -0.1 to 0.1 lbs. For the data presented here a positive force indicates lift (up) and a negative force

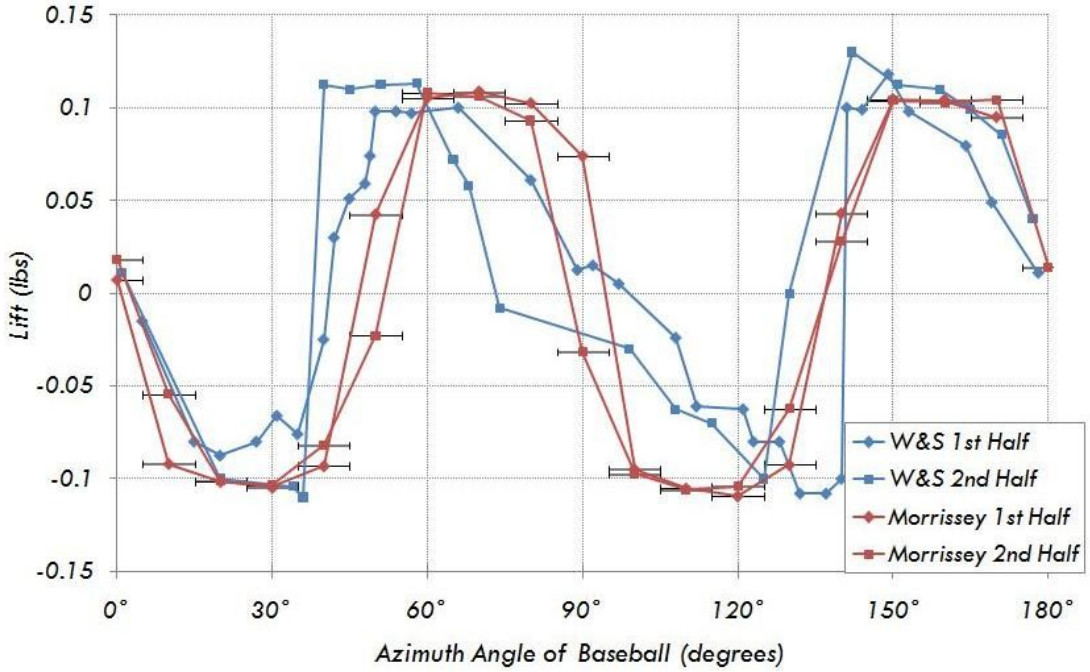

Fig. 3-2: Symmetry check comparison between Watts and Sawyer data with Morrissey data from figure 3-1. Morrissey's data is more consistent than Watts and Sawyer's data.

indicates down. In the four-seam orientation, a single 360 degree rotation shows that the seams on the ball are twice symmetric and twice asymmetric with respect to the stream-wise direction. Since the lift was measured along the plane of symmetry, one would expect that the lift data would repeat four times in one rotation. The Watts and Sawyer data demonstrate a larger variation in the lift force from each local minimum and maximum, as compared to the Morrissey data. The Morrissey data was more consistent from each local minimum and maximum than the Watts and Sawyer, meaning the data repeats itself. When the same data was compared and checked for symmetry, the Morrissey data lies upon itself more than Watts and Sawyer's data, as shown in figure 3-2.

One should bear in mind that the lift results from the presence of the seams; a smooth, non-rotating sphere would produce no lift. A Major League baseball can weigh

no more than 5 and ¼ ounces (0.32 lbs). Therefore, a lift of 0.1 lbs was a significant fraction of the total weight of the ball and can have a significant effect on the trajectory of the flight. Watts and Sawyer also mentioned how there seemed to be a large fluctuation and small fluctuation of forces at 52 and 310 degrees, respectively. A plot of the standard deviation collected in the experiments conducted here was constructed in respect to the position of the baseball, as shown in figure 3-3. There were fluctuations at 52 and 310 degrees, however, not as largely noted by Watts and Sawyer. To put the lift and standard deviation data into a more understandable plot, a polar graph was constructed. The polar graphs better illustrated how lift was affected by the seams of the baseball. Figures 3-4 and 3-5 are polar graphs of the lift and standard deviation, respectively. The polar graphs illustrate the data as if the ball was fixed, and the wind direction changed angular position, from a side view, thus the azimuth angle refers to the

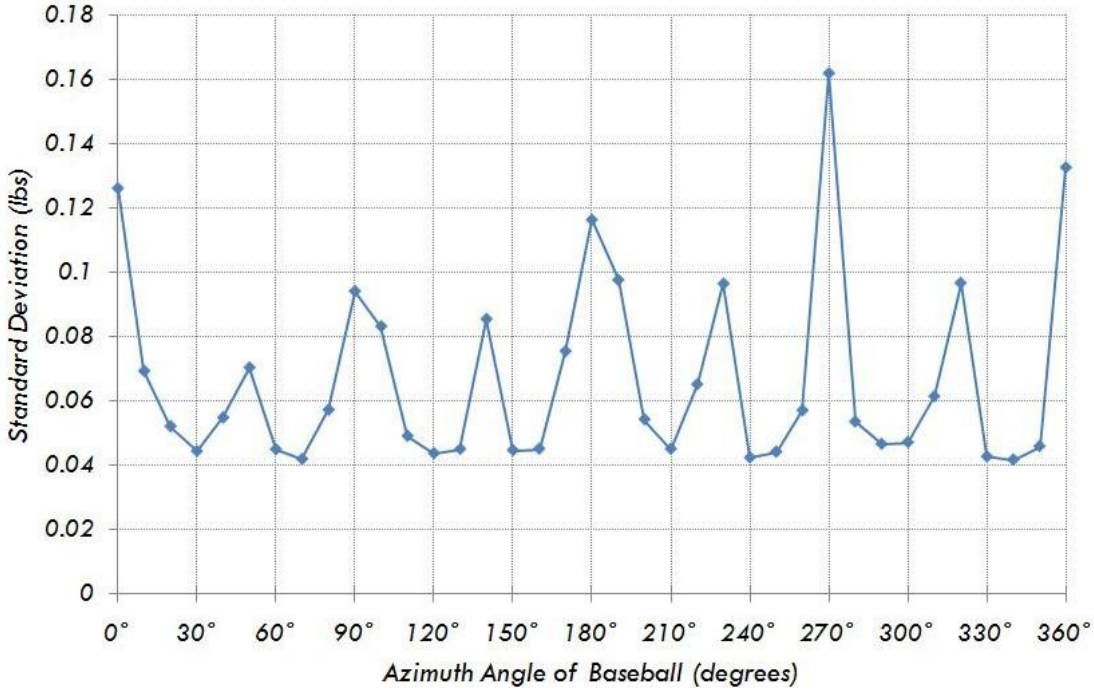

Fig. 3-3: Standard deviation of the lift on the baseball at ten degree intervals.

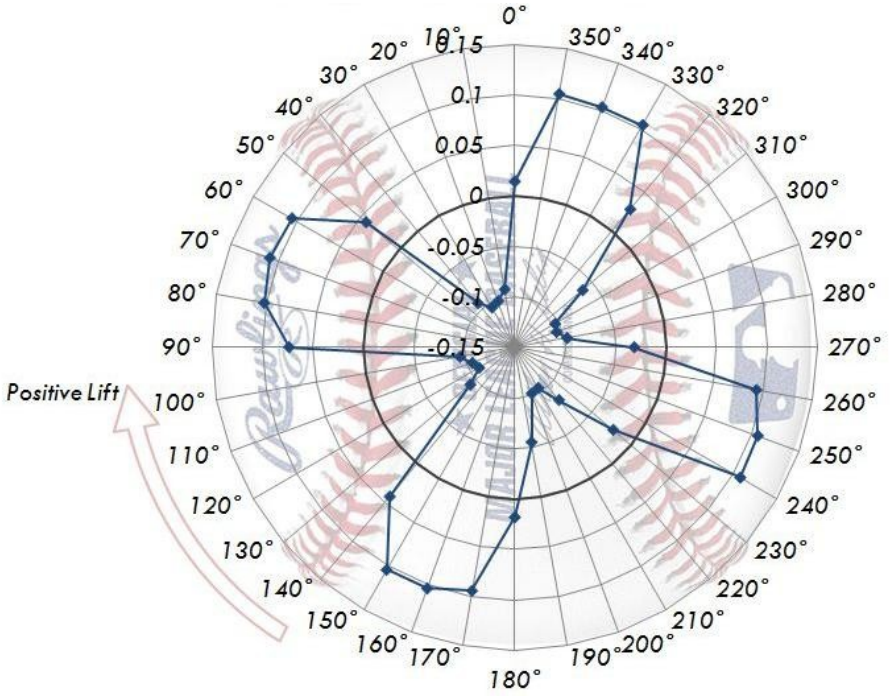

Fig. 3-4: Polar graph of average lift (lbs) at different positions of four-seam baseball at 46 mph. The axis of rotation goes perpendicular into the paper. This is a side view. Lift is tangent to stagnation.

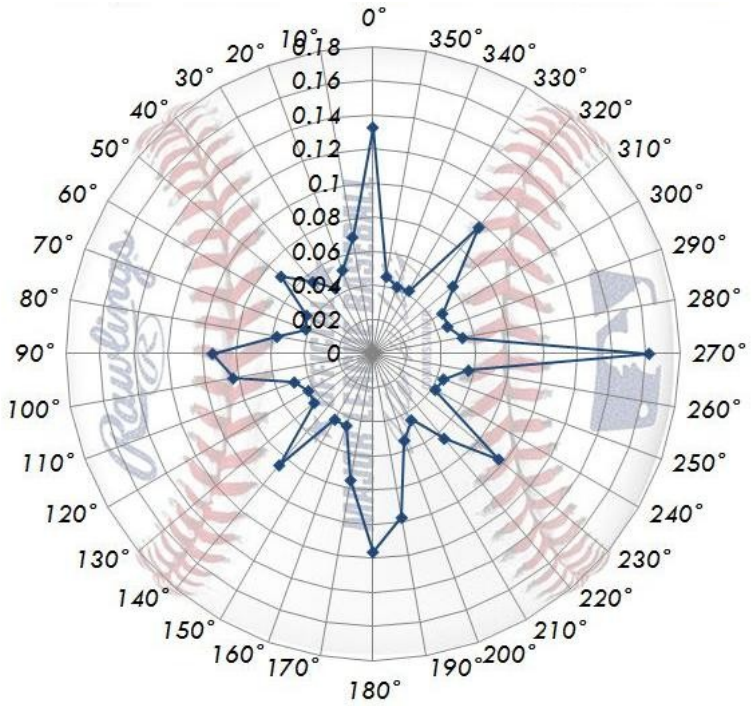

Fig. 3-5: Polar graph of standard deviation at different positions at 46 mph.

wind direction. The seams are positioned at 40°, 140°, 220°, and 320°. Figure 3-4 illustrates how the lift mirrors itself. The local minimums and maximums are the same amplitudes at 180 degrees from a given position. When the stagnation point was directly on a seam or at the midpoint between the two seams, lift was about zero and the sign of the lift changes.

Therefore, the seam disturbs the symmetry of the flow and induces lift in the direction of the seam. In other words, whichever side the nearest seam was to stagnation, lift will be the respective direction. For instance, when stagnation was at 70 degrees, the nearest seam was 30 degrees, clockwise, from stagnation; therefore, the lift of the baseball would follow tangent to stagnation in the clockwise direction. This process was repeated on each side of the seam. That was what makes the data periodic. The same can be said for figure 3-5. The plot itself appears to be like an eight pointed star. The local maximums were when the lift on the baseball was zero, or where a seam or the midpoint between the seams was at stagnation. The local minimums appear where the lift was at its absolute maximums. This means that when the position of the seams of a four-seam baseball was symmetrical (i.e., stagnation was at 0 or 40 degrees), lift was zero because each seam subtracts the lift from the opposite seam mirrored on the other side. Since Morrissey's data correlates with Watts and Sawyer's data, this confirmed that the force balance was acceptable to find the lift on a baseball.

3.1.2. Spinning Ball

The thrust of this thesis was to explore the aerodynamics associated with knuckleballs, i.e., slowly rotating pitches in a two-seam orientation. Therefore, most of

the data for the knuckleball was collected with the spinning strut that spun the baseball. The same procedure was done as discussed above, where lift was recorded every ten degrees. However, this was done with the spinning strut and laser diode system as discussed in section 2.2.3. In order to validate the spinning strut data, there was a comparison of the results to the non-spinning data presented in figure 3-1. Figure 3-6 is the comparison of all three data sets: Watts and Sawyer rigid strut, Morrissey rigid strut, and Morrissey spinning strut. The spinning strut data oscillates with the same trend and nearly meets the exact local minimums and maximums as the rigid strut data. Regardless, the spinning strut data collected here compares favorably to Watts and Sawyer's lift data. In nearly all instances it appears the lift for the spinning ball was less than that for the fixed ball. We must conclude that the aerodynamic maxima (established of delayed separation) was not achieved due to the motion of the ball.

In order to study the lift of a knuckleball, the baseball must be rotating while collecting data. To check if the spinning strut was acceptable to use, the lift data was collected while the baseball was spinning in a four-seam orientation using the procedure discussed in section 2.2.3. After collecting 300 rotations of lift data at 46 mph, the lift plot appeared as in figure 3-7. As shown, the data contains several hidden frequencies, some of which are attributed to the dynamics of the force balance coupled to the spinning ball apparatus. However, the plot seems to follow the same trend as figure 3-6. In order to isolate the lift signal, frequency filters were applied. This was completed through a series of Fourier transformations.

In order to isolate the model contribution of various components, three separate data sets were collected: rotating baseball with no wind (signal from the motor),

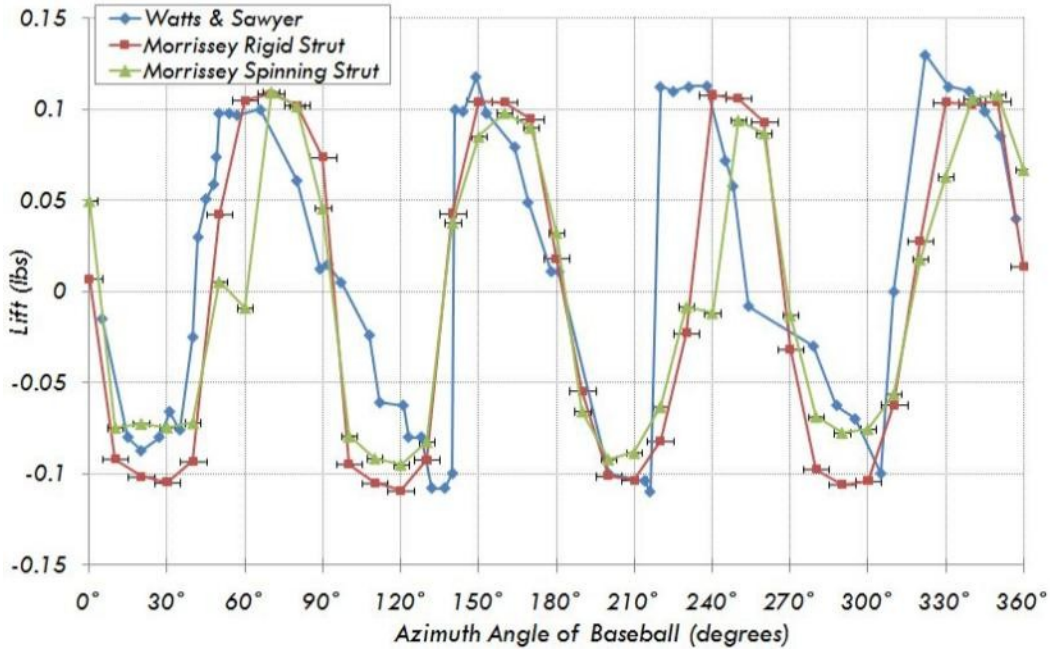

Fig. 3-6: Comparison of Watts and Sawyer, rigid strut, and still spinning strut.

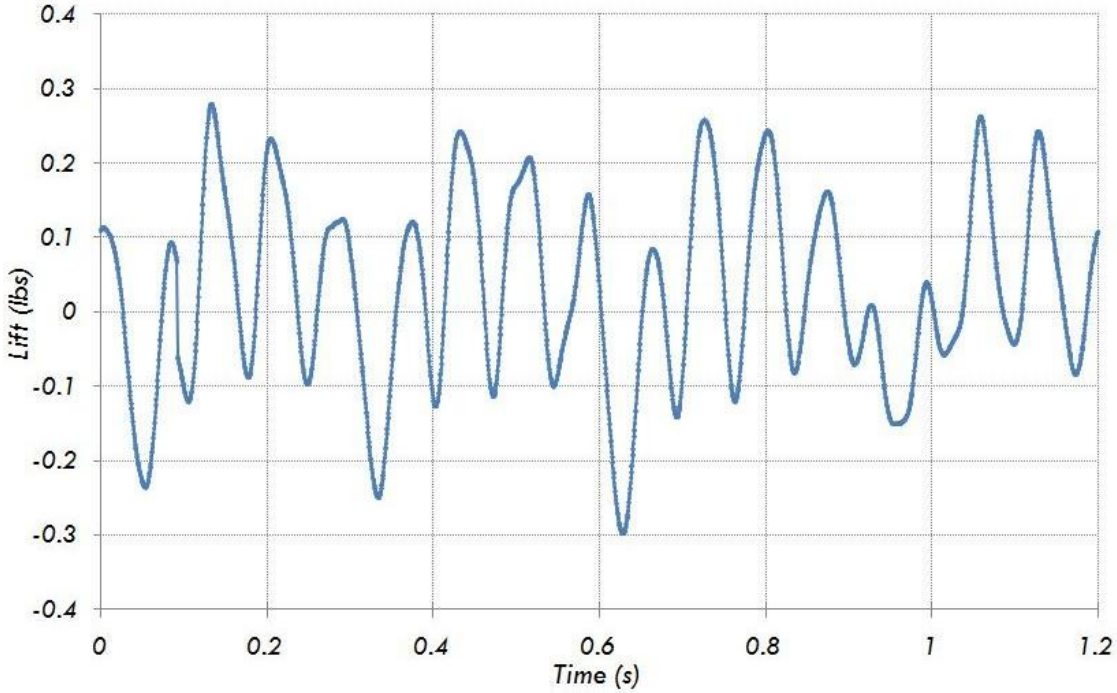

Fig. 3-7: Original lift data from spinning strut. There are frequencies that have to be filtered.

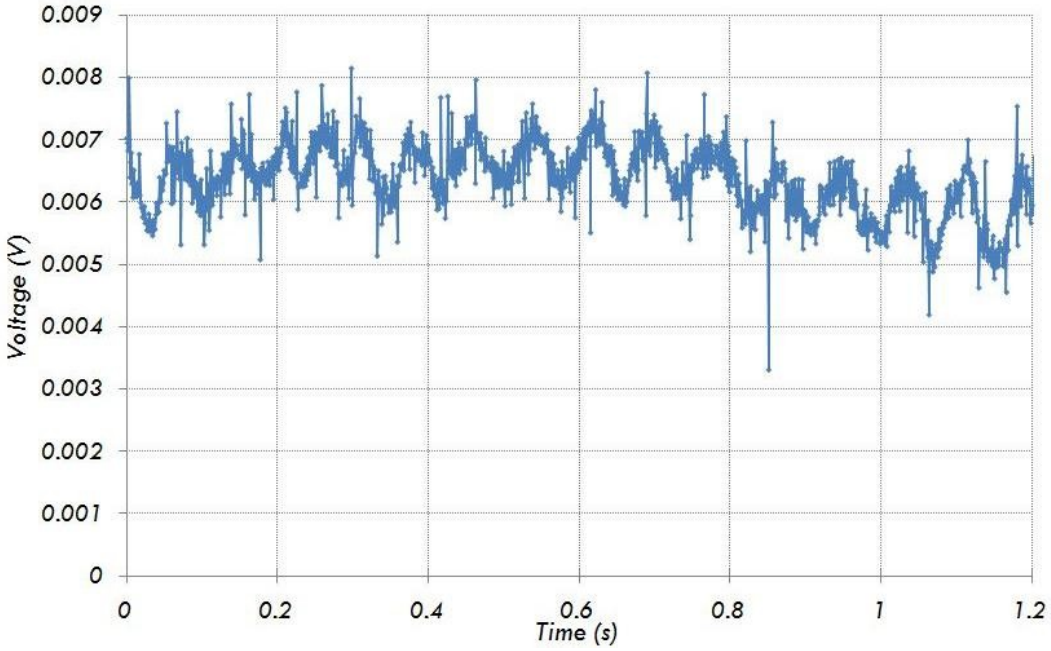

Fig. 3-8: Raw signal from motor rotating shaft and baseball. No wind velocity applied.

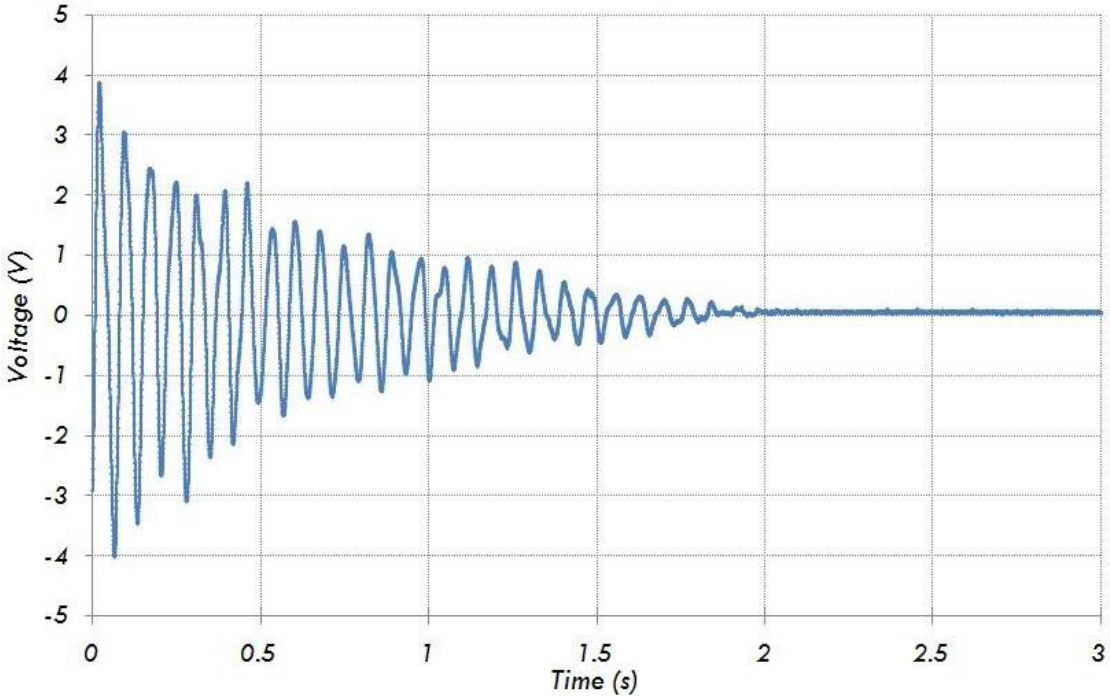

Fig. 3-9: Raw signal of spinning strut vibrating from finger flick.

vibration of spinning strut with ball attached with no wind, and rotating baseball with no wind. A procedure was then applied to filter out the unwanted frequencies from the rotating baseball data from figure 3-7 to extract the pure lift from the rotating baseball data.

Figures 3-8 and 3-9 are the signals from the motor rotating with the baseball on the shaft at 50 rpm and the vibration of the spinning strut when a step input was applied (flicked by a finger). The signal from the motor was consistent over the time duration data was collected. The vibrating strut plot illustrated a damped, natural frequency. The frequencies presented in figures 3-8 and 3-9 are superimposed within the spinning baseball data presented in figure 3-7. Both of these signals are contained within the data from figure 3-7. A Fourier transform was applied to the motor, vibrating strut, and rotating baseball data: figures 3-10 through 3-12 are their respected Fourier transformations. The amplitudes of the motor Fourier transform were much smaller than the amplitudes of the other transformations. Therefore, the motor contributes a very small amount towards any of the signal to the baseball data. However, the amplitudes of the vibrating strut were very strong relative to the signals collected for the rotating baseball. At about 13 Hz, the amplitude was about 0.45. The Fourier transform of the vibrating strut response was on the order of the baseball Fourier transformation. There was also a commonality of each graph at about 30 Hz. Therefore, the vibrating strut has a strong possibility of adding noise to the raw data of the rotating baseball.

The shedding frequency of the baseball measured in the wind tunnel operating at 70 mph was found by placing a hot wire in the near wake of the baseball. The frequency transform of this data is presented in figure 3-13. The maximum amplitude was centered

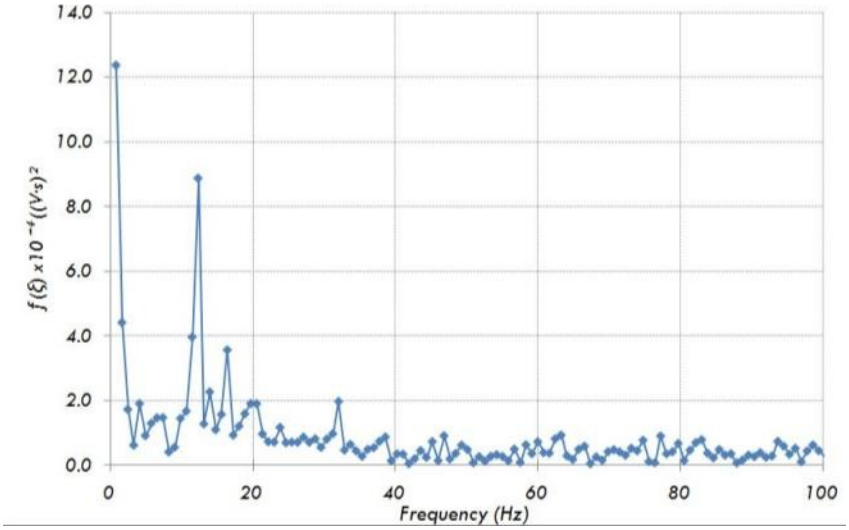

Fig. 3-10: Fourier transformation of the motor signal.

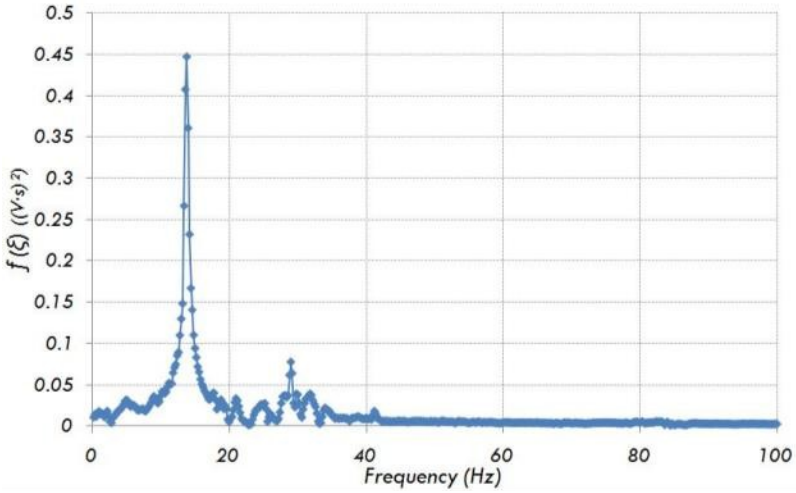

Fig. 3-11: Fourier transform of the vibrating strut. This Fourier transform has a greater amount of points because the data was collected for a large amount of time.

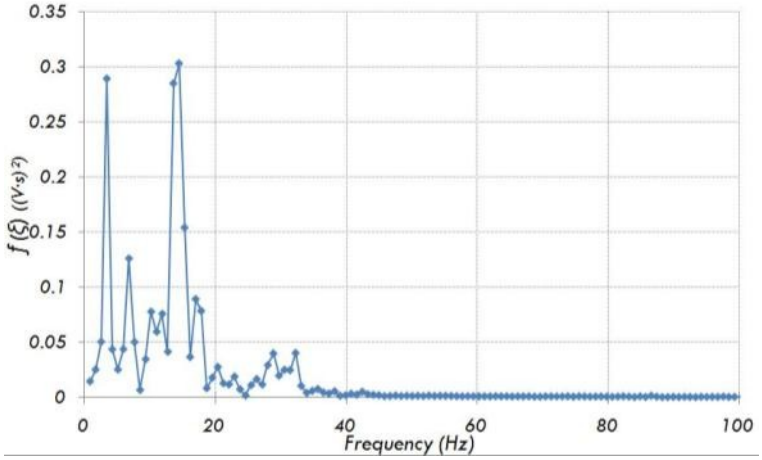

Fig. 3-12: Fourier transform of the spinning baseball at 50 rpm.

about a frequency of 96.8 Hz. In order to compare this frequency to published data, the Strouhal number, which is a dimensionless shedding frequency, was calculated using equation 3.1. The accepted Strouhal number for a circular cylinder is 0.2 [21], which is

$$St = \frac{fD}{U_o} \tag{3.1}$$

constant over a large range of Reynolds number, from 10^2 to 10^5. Table 3-1 presents all of the shedding frequencies and Strouhal numbers for a cylinder, sphere and baseball. Notice how the Strouhal number for the sphere was lower than both the cylinder and the baseball, whereas the baseball has the largest Strouhal number. The Strouhal number also increases when the baseball or sphere was spinning. Much like the lift, the shedding frequency from a sphere demonstrates a large dependence upon the presence of the seams and some dependence upon the presence of rotation, but to a lesser degree.

The shedding frequency of the spinning baseball was 98 Hz. Neither the shedding frequency nor the blade pass frequency of 280 Hz appears in the spectra of the lift data obtained.

Theoretically for a linear system, if the frequencies common to the vibrating strut are removed from the raw spinning baseball data, then the inverse Fourier transformation would be a time series indicative of the aerodynamic lift of the baseball. Figure 3-14 is a graph of all three Fourier transformations together. Notice between 13 to 29 Hz and 32 to 37 Hz, the strut

Table 3-1: Strouhal number for respective models at 70 mph. Spinning was at 50 rpm.

Model	f (Hz)	St
2" Cylinder	96.8	0.198
3" Sphere, still	63.4	0.154
3" Sphere, spinning	73.2	0.178
Baseball, still	96.4	0.236
Baseball, spinning	98.0	0.240

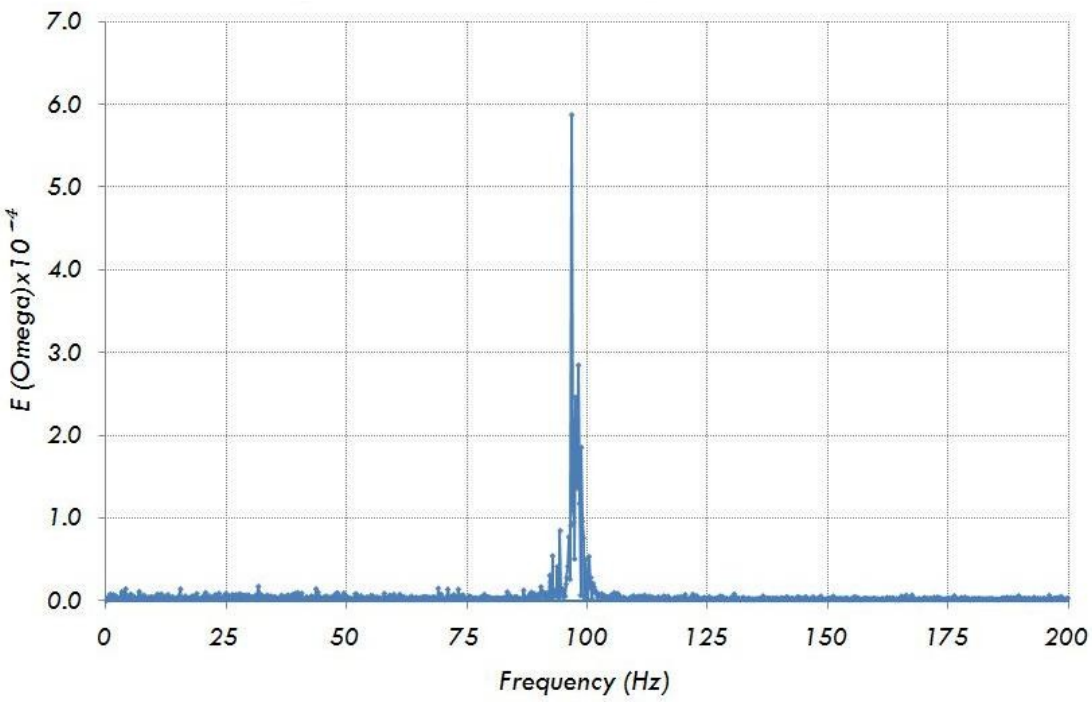

Fig. 3-13: Shedding frequency of a smooth cylinder at 70 mph; recorded by a hot wire. The peak is at 96.8 Hz.

amplitudes appear in the Fourier transform of the spinning baseball data. Therefore, as shown in figure 3-15, frequency content at 13 to 29 Hz and 32 to 37 Hz was filtered, as the purple line shows. The inverse Fourier transformation was applied to the filtered spinning baseball data and presented in figure 3-16. There was an obvious difference between the original, raw baseball lift data and the modified, frequency filtered baseball lift data. The filtered baseball data now appears more like figure 3-6. The spinning baseball data was ensemble averaged and presented in figure 3-17 along with the static data for comparison. The local minimums and maximums are about -0.1 to 0.1 lbs and the lift oscillates at the same period as the existing data. However, the spinning data appears to contain higher frequency information than the static ball data; to preserve as much of the raw lift data, these frequencies were not filtered.

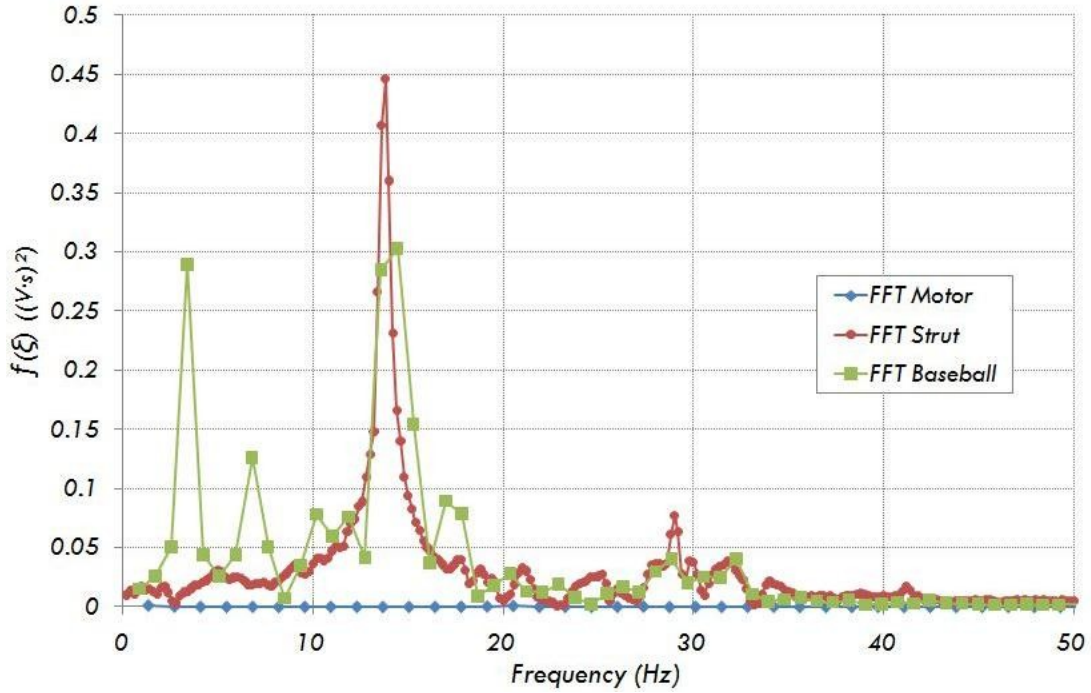

Fig. 3-14: Comparison of all three Fourier transformation data sets. Notice how the baseball amplitudes are in common at the same frequencies as the strut. The amplitudes of the motor is negligible.

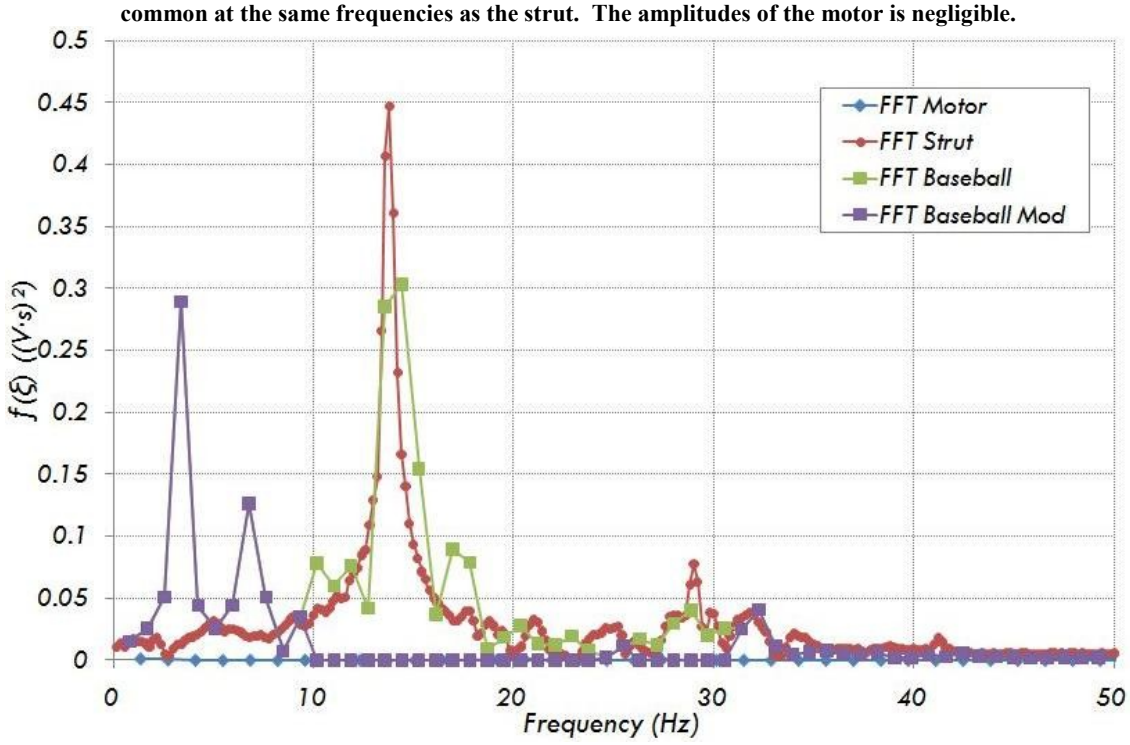

Fig. 3-15: The same plot as in figure 3-14, except the modified baseball amplitudes are included. All amplitudes in common with the strut amplitudes are set to zero. Those frequencies include from 13 to 29 Hz and 32 to 37 Hz.

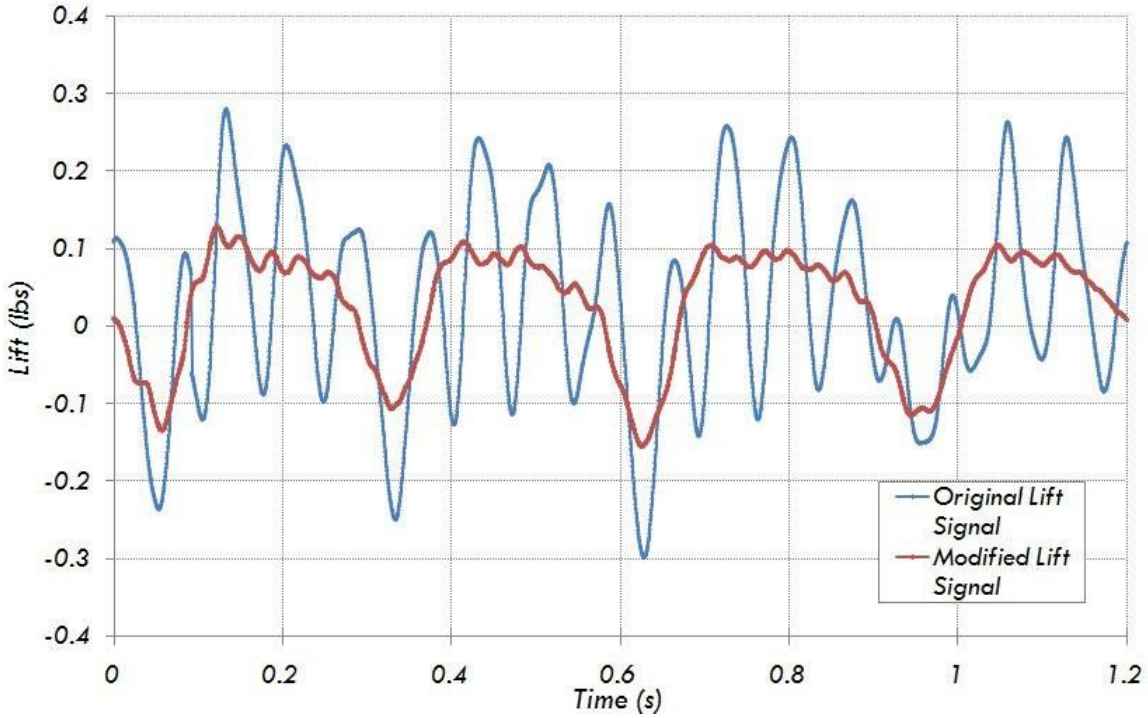

Fig. 3-16: Comparison from the raw baseball data to the modified baseball data.

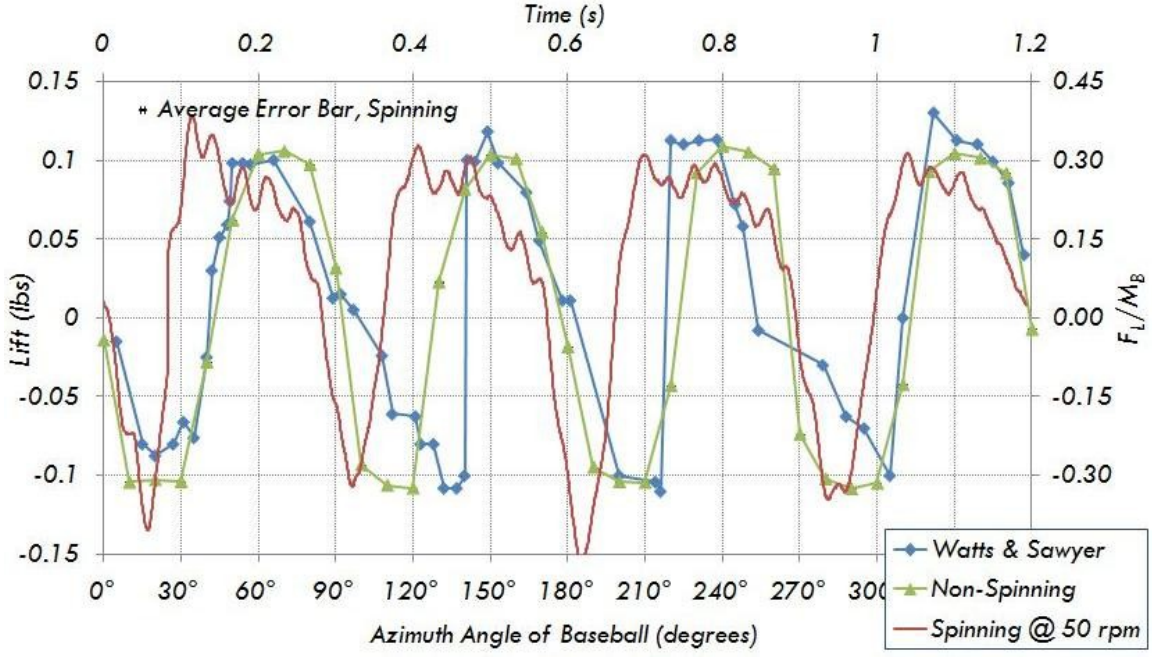

Fig. 3-1: Lift comparison of Watts and Sawyer, non-spinning, and spinning data with their respective error bars. Data was collected at 46 mph and in the four-seam orientation.

An interesting feature of this data was that there appears to be a bias toward positive lift. One may think that it may be because of the Magnus force [22]. To find the lift on a smooth spinning sphere, equation 3.2 was applied, where C_L is the coefficient of

$$L = \frac{1}{2}\rho {U_o}^2 A C_L \tag{3.2}$$

lift due to the Magnus force only. The lift coefficient can be computed through equation 3.3, which also equals the spin parameter in equation 1.3. It was found that the coefficient of lift for a smooth sphere under the conditions given was only 0.001014. This made the Magnus force to only be 6.579×10^{-7} lbs, via equation 3.2. Thus, the

$$C_L = \frac{\omega r}{U_o} \tag{3.3}$$

Magnus force was not sufficient enough to affect the overall lift of the baseball or cause the bias in the data that we observed.

The standard deviation of each data point was calculated by taking the standard deviation at each angle, as shown in appendix A-2.4. The standard deviations for the spinning data were also larger than for the non-spinning data. This can be a mix between the frequency filter and the actual fluctuation the baseball experiences while rotating. The comparisons between the still and spinning baseball standard deviations are in figure 3-18. Overall, the spinning baseball has a greater standard deviation than the still.

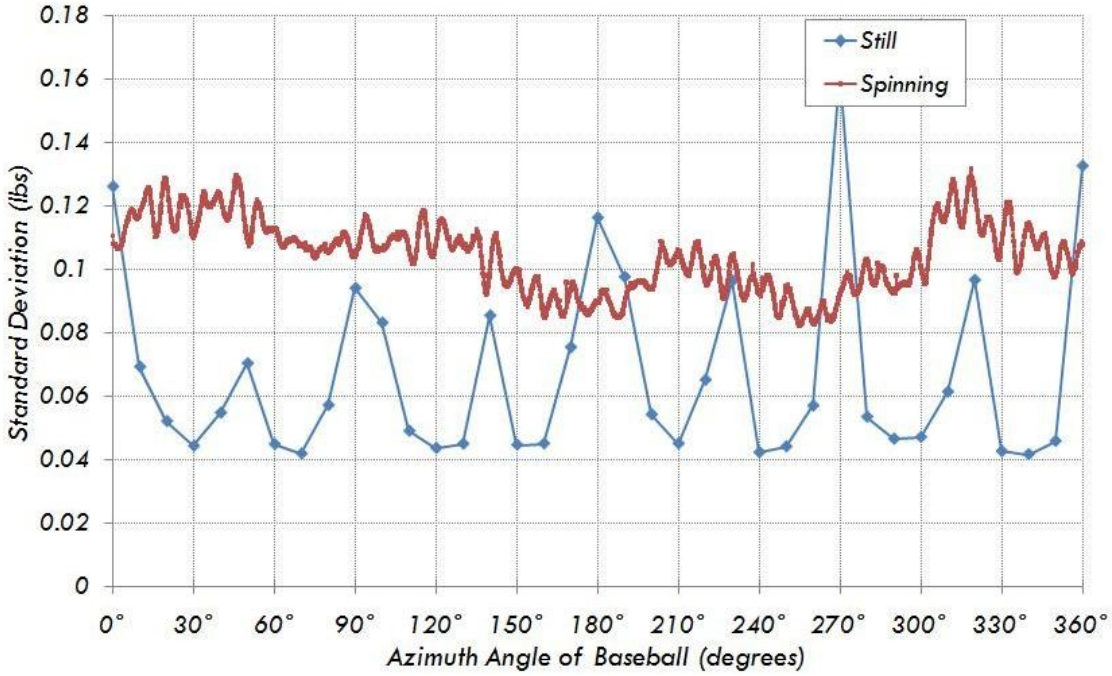

Fig. 3-18: Comparison of standard deviations between four-seam spinning and still lift data.

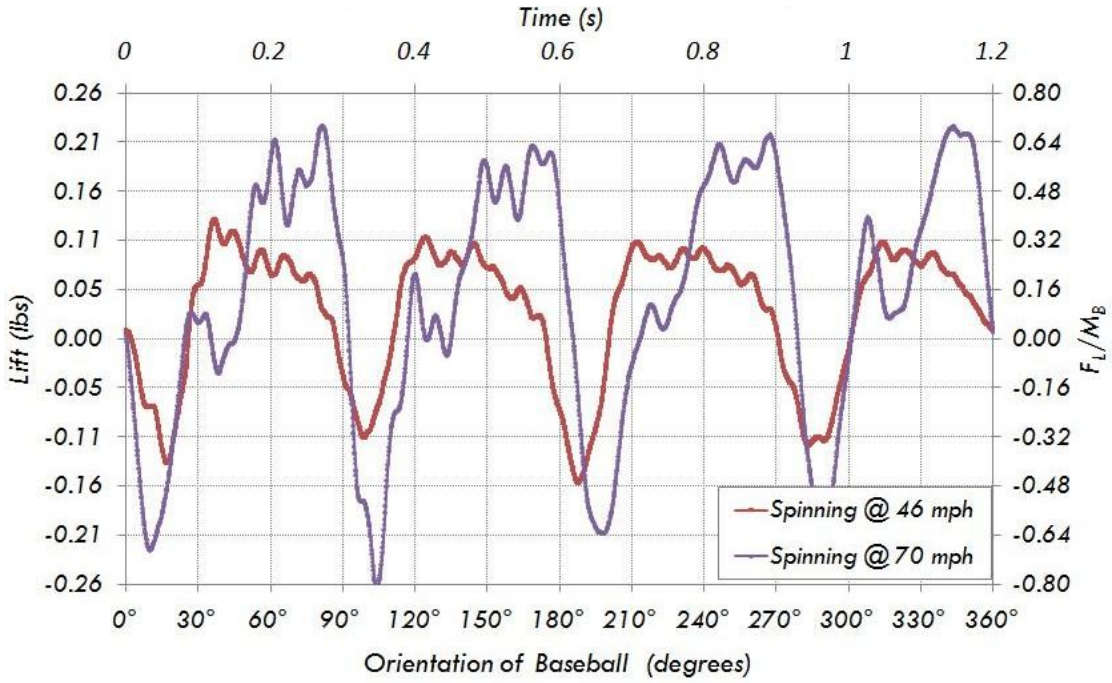

Fig. 3-19: Comparison of lift at 46 and 70 mph of a four-seam baseball rotating at 50 rpm.

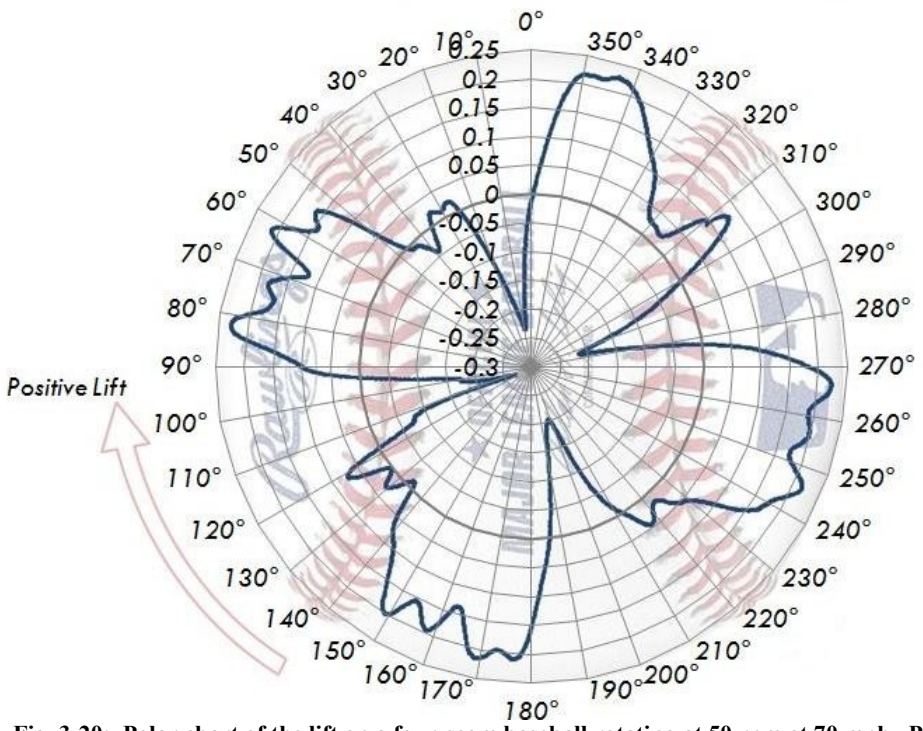

Fig. 3-20: Polar chart of the lift on a four-seam baseball rotating at 50 rpm at 70 mph. Positive lift is clockwise and tangent from the surface of the baseball.

However, the still baseball has more of a fluctuation.

One part of interest with the forces on a baseball was when the velocity was increased. Figure 3-19 is a direct comparison of the lift of a four-seam baseball at 46 and 70 mph. When the baseball was traveling at 70 mph, the lift forces were almost double that of the 46 mph baseball. Keeping in mind that the baseball weighs just over 0.3 lbs, a 70 mph knuckleball nearly produced enough lift to overcome the weight of the baseball. The Reynolds numbers for a baseball at 46 and 70 mph is 1.045×10^5 and 1.62×10^5, respectively. This results in nearly no change in lift if the baseball was a smooth sphere. Therefore, this large difference in lift was due to the presence of the seams. The 70 mph baseball also seems to experience a sudden decrease of lift at about 40, 140, 220, and 320 degrees. When the lift was plotted in a polar graph, as in figure 3-20, it was evident that the sudden decrease was a result of the stagnation point on the seams of the baseball.

This occurrence does not happen at the midpoint between the seams. Conclusively, as the velocity increased, the magnitude of the lift increased and the seams affect the lift when there was a stitch at stagnation.

3.1.3. Two-Seam Knuckleball Conditions

Since the force balance data was consistent with the accepted data from literature, it was with some confidence that the focus shifted towards more realistic knuckleball conditions. All of the experiments performed previously were in a four-seam orientation. This was done to compare our data with published data. However, most modern knuckleball pitchers utilize a two-seam orientation, thus it was desired to conduct experiments in this orientation. In addition, much of the data in the literature was obtained at a lower velocity (46 mph), whereas practical knuckleball pitches are in the range of 65 to 75 mph. We suspect this was due to the limitations of the wind tunnel available at the time. Irrespective, this section focused on obtaining data from the ball while at 70 mph in a two-seam orientation. The baseball was still rotating at 50 rpm.

Figure 3-21 is a plot of the lift data between a baseball rotating continuously and a baseball collecting data at every ten degrees. Once again the trend was about the same and the local minimum and maximums are about the same. The standard deviation was greater for the spinning baseball as compared to the still baseball, which was consistent with data discussed before. The standard deviation of the still and spinning baseball data appears in figure 3-22.

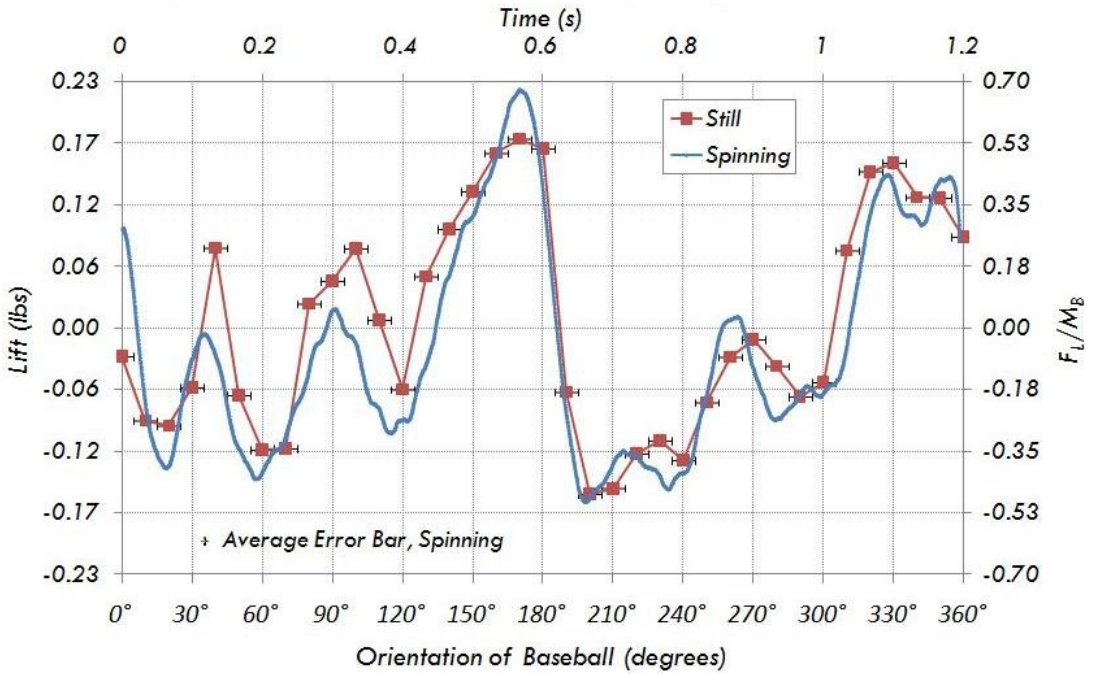

Fig. 3-21: Comparison of lift between a rotating and still two-seam baseball in 70 mph wind.

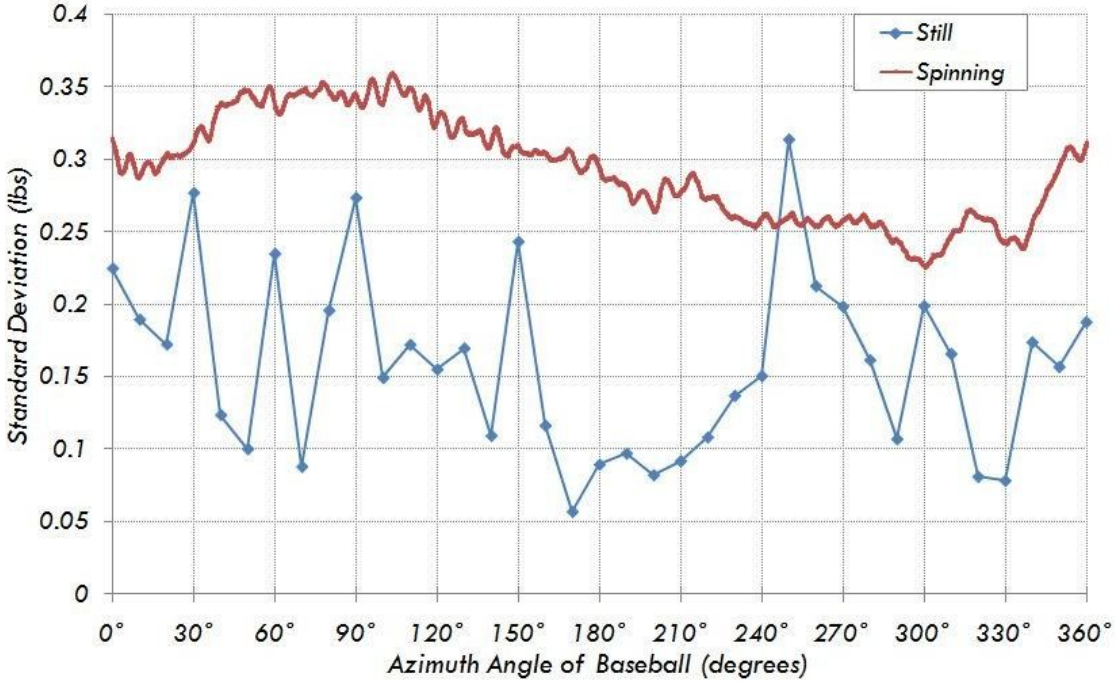

Fig. 3-22: Comparison of standard deviations between a still and spinning two-seam baseball at 70 mph.

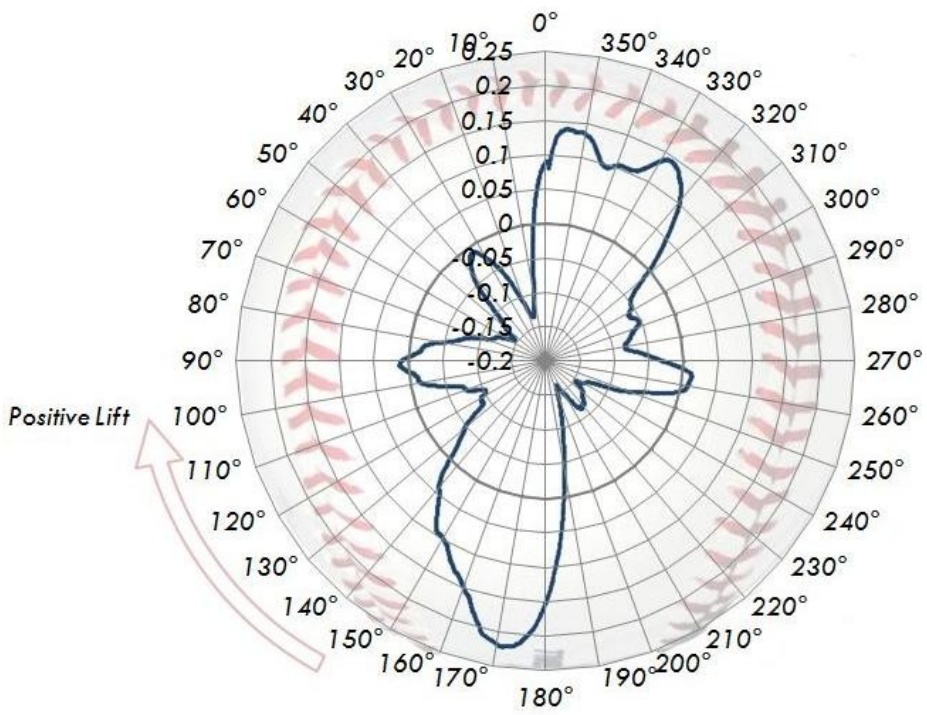

Fig. 3-23: Polar graph of the lift forces on a two-seam baseball rotating at 50 rpm at 70 mph.

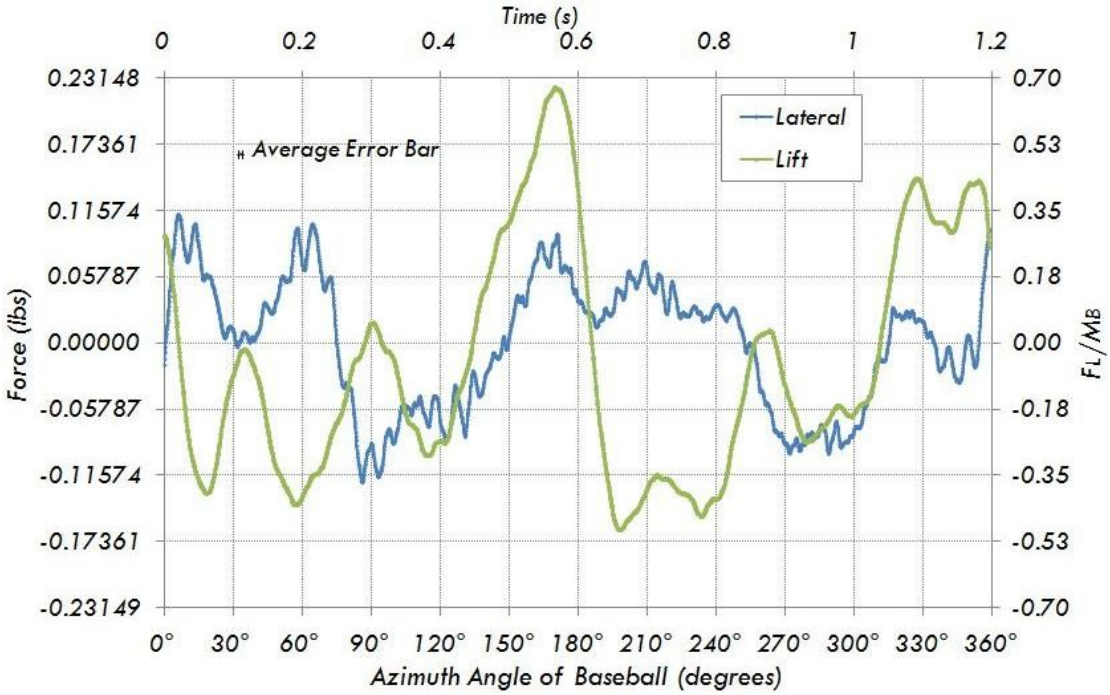

Fig. 3-24: Lift and lateral force data for a two-seam baseball, rotating at 50 rpm at 70 mph.

The spinning baseball lift data was plotted in a polar graph, as shown in figure 3-23. This graph varies greatly from figure 3-20, for when a seam was near stagnation, lift will increase tangent in the direction of the nearest seam. However, in the two-seam orientation, this did not occur. The lift on the two-seam orientation nearly repeated itself at every 180 degrees with very minor discrepancies. The lift was positive for a greater time duration than negative. However, there was a large and sudden drop in lift when stagnation passes the first seam. Before the second seam passes through stagnation, there was even a greater positive change in lift. There was also a decrease and strong increase in lift at 350 degrees, but not as great at 170 degrees. This was interesting because of how the knuckleball dips up and down during flight.

The lift force data was also plotted with the lateral force data. Figure 3-24 is the graph of the filtered, Fourier transformed lateral and lift forces of a two-seam, spinning baseball at 70 mph. There were no found publications of lateral force on a rotating baseball, so the lateral force may not be correct. However, considering that the apparatus was sufficient to record the lift force, the lateral force may be satisfactory. The negative lateral force points to the right side from the view of the catcher. The greatest change in the lateral force begins approximately at 90 degrees where the first seam was 60 degrees away from stagnation. Both lift and lateral forces seem to be correlated between 0 to 120 and 200 to 360 degrees, which nearly covers the whole surface of the ball, except the smaller area between the seams.

In figure 3-25, both forces are somewhat mirrored. The graph had to be mirrored instead because the first half of the azimuth angles would not be the same as the second half. All of the lift data was not correlated until about 90 degrees. At that point, stagnation was 90 degrees away from the midpoint between the seams. From 120 degrees, the lift on the first half decreases much more quickly than the second half. This could be from the ball rotating away from stagnation during the second half. Therefore, the seams did not have to go against the wind, as they did while rotating towards stagnation. The lateral force should be the same at 90 degrees. That was because the view from stagnation was the same, with an exception of a seam crossing the top or bottom part of the baseball. Also, the magnitude of lift at 0 degrees should be equal to the lateral force magnitude at 180 degrees and vice versa. These are illustrated in table 3-2.

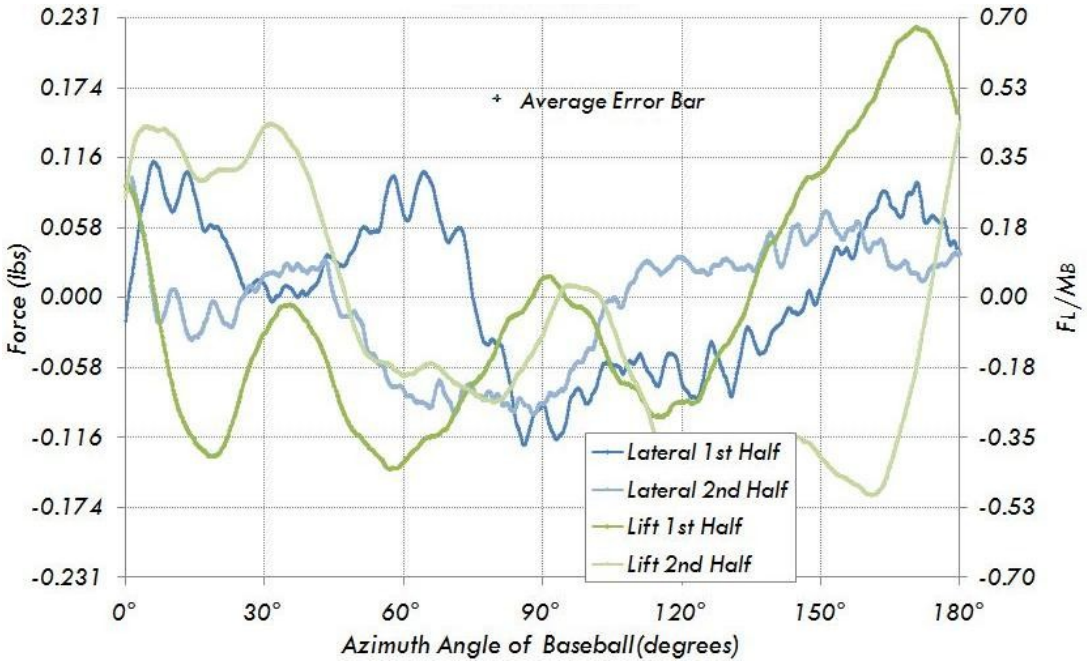

Fig. 3-25: Mirror check of the lift and lateral forces on a two-seam, spinning baseball at 70 mph. Note that the second half is when the baseball was rotating away from stagnation.

Table 3-2: Forces that theoretically equal to each other due to geometry similarities.

Theoretical Correlated Forces		
|Lift| 0°	=	|Lateral| 180°
|Lift| 180°	=	|Lateral| 0°
|Lift| 90°	=	-|Lift| 270°

Unfortunately, that did not happen. This could attribute to the complex three-dimensional flow. Considering that the forces also have such a high variance, the forces can be stronger or weaker than shown. This non-correlation and fluctuation of forces is what causes a knuckleball to move erratically.

3.2. Flow Visualization

There were a few ways to analyze the flow visualization around the baseball. Two techniques were applied: one that superimposed all of the images collected at one azimuthal location (ball rotational position) onto one image to create a still image, and a second technique that strung these images together in order to create a movie. Once again, this process was completed with a series of Matlab programs. Each of these methods was used to find separation. The angle of separation was then compared to our lift data in order to develop an overall understanding of the aerodynamics involved in knuckleball pitches.

3.2.1. Match Pre-Existing Data

Several researchers, using a number of different techniques, have investigated the separation angle on a smooth sphere. Thus, these results were used in order to verify the flow visualization method and the data collected here as applied to a baseball. According to Paul Chang's book, *Separation of Flow*, separation on a smooth sphere should be at

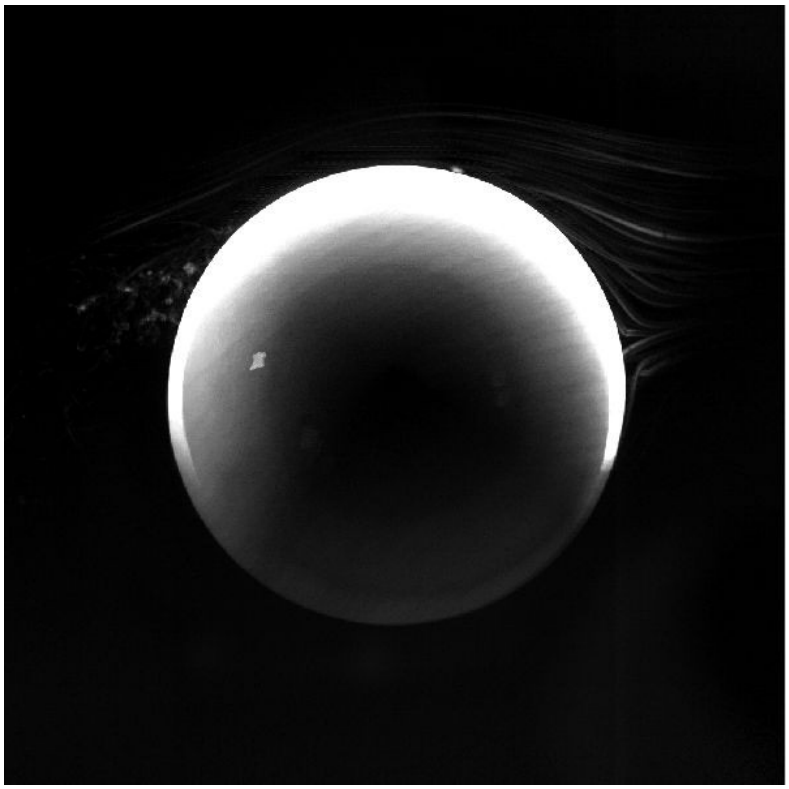

Fig. 3-26: Superimposed photo of a smooth sphere.

Fig. 3-27: Image of the angle of rotation conformation. The difference in angles was 9.89°.

about 110 degrees when the Reynolds number is greater than 10^5 [23]. To confirm that the helium bubble flow visualization system measured the same results; a smooth, three inch wooden sphere was placed on the force balance with the static sting (no rotation). The wind velocity was set at 70 mph which corresponds to a Reynolds number of $1.6x10^5$. 1024 images were collected at 500 frames per second, which roughly corresponds to 117 shedding cycles (that will be explained in section 3.2.2), while injecting neutrally buoyant helium bubbles into the flow. The Matlab program Multiple Exposure Photo in appendix A-2.1 was used to superimpose all of these images in order to produce one ensemble image. Figure 3-26 is an example of an ensemble image for the smooth sphere. To help calculate where separation occurs, a protractor was laid over the sphere. Once completed, it was noticed that stagnation was not at zero degrees due to a bias in the orientation of the camera. The camera was not aligned to the free stream. Therefore, the image had to be rotated 12 degrees, clockwise, in order to align the image to the free stream. The rotation was confirmed by finding the difference of the angle of the force balance to the axis of the camera. A photo of the force balance was taken with the high speed camera without the sphere. The photo was then opened in Gimp, and the measure tool was used to find the angle of the force balance in respect to the axis of the photo. The resultant difference in the angle was about 10 degrees, clockwise, as presented in figure 3-27. Therefore, the angle has an error of 2 degrees, which was only 0.0523" on the surface of the baseball, which was much smaller than the diameter of the helium bubbles. A fiduciary marker was placed by hand by the user for each ensemble image where separation occurs. Figure 3-28 is the post-processed ensemble image, incorporating the 12 degree rotation and illustrating the protractor and fiduciary marker.

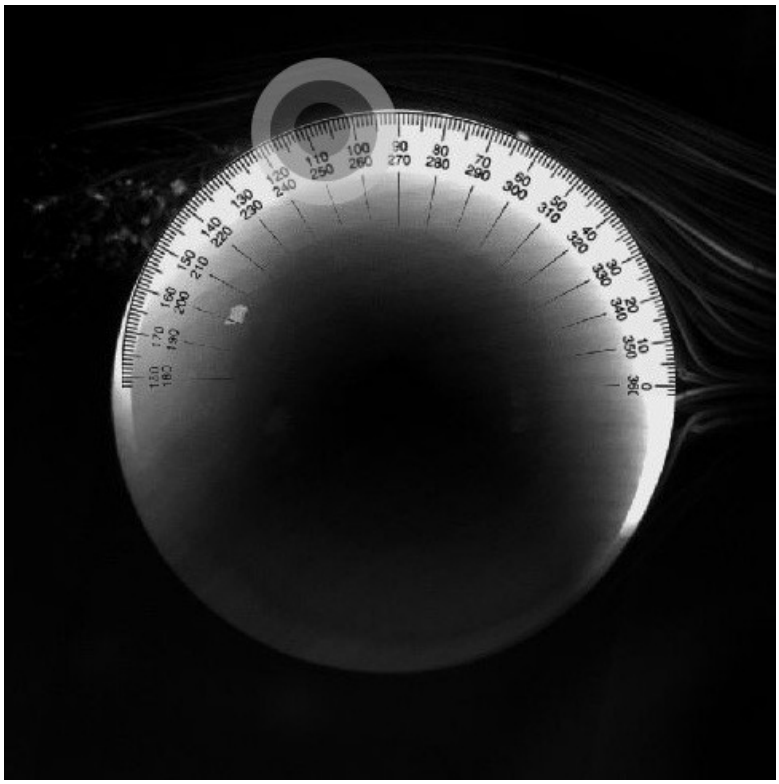

Fig. 3-28: Modified superimposed photo of a smooth sphere. Separation was at 107°.

As shown, separation on the smooth sphere occurs at an angle of about 107 degrees with respect to the free stream, which was very near the 110 separation angle measured by others.

3.2.2. Knuckleball Conditions

For the knuckleball measurements, the sphere was replaced with the baseball in the two-seam orientation. The same process described above for the sphere was repeated for the baseball to find separation on the landing strip and across the seams as the baseball was stationary. A video was then compiled to observe how separation changes as the baseball rotates at 50 rpm.

Initially, the location of separation was found on the landing strip to compare it to the location of separation on the smooth sphere. Figure 3-30 is the photo of the superimposed image of separation on the landing strip of a two-seam baseball. Separation was located at about 104 degrees. Since separation on the smooth sphere was at 107 degrees, an argument can be made that the landing strip of a baseball acts as a smooth sphere.

To study how a seam affects the location of separation, the baseball was oriented to have the seam where the landing strip was located. Figure 3-29 is the superimposed image of separation across the seams. Separation begins at the second seam. Separation has slightly moved upstream than the landing strip image in figure 3-30. The seam also creates a larger wake than the landing strip. Both of these observations are evidence that the seam was sufficiently raised from the surface of the baseball, that it begins separation, rather than a tripping wire that delays separation. The seam has an average height of 0.04933 inches, or 1.252 mm. When the height of the seam was applied to the equation 3.4 at 70 mph and a kinematic viscosity at 20° Celsius, Re_k becomes 2613.95.

$$\frac{U_o k}{\nu} \approx Re_k \tag{3.4}$$

In Frank White's book, *Viscous Fluid Flow* [21], and Hermann Schlichting's book, *Boundary- Layer Theory* [24], it was expected for a wire to "trip" flow when Re_k was about 850 for a flat wall or 120 for distributed roughness. As Re_k increases, separation creeps closer to the location of the roughness. Since Re_k was so large at the seams, separation occurs at the location of roughness, or the seam.

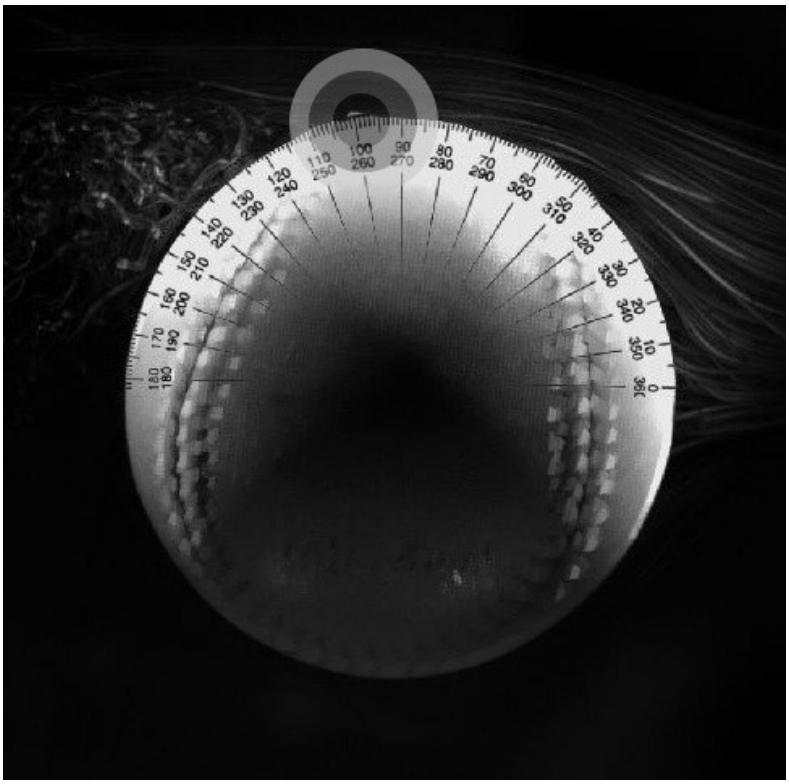

Fig. 3-29: Separation across a seam.

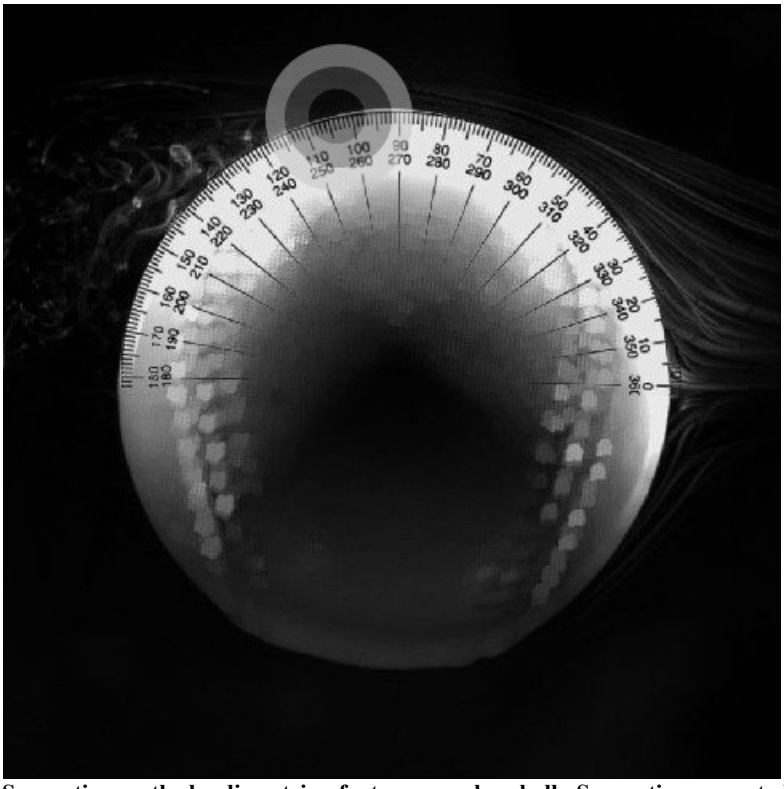

Fig. 3-30: Separation on the landing strip of a two-seam baseball. Separation was at about 104°.

Now that conclusions have been built upon how the landing strip acts as a smooth sphere, and the seam initiates separation, it's time to observe how the location of separation changes as the two-seam baseball rotates. Each photo was superimposed upon each other at every 0.6 degree. This calculates to 600 ensemble images per rotation. A video was compiled using the Tracer Movie Compiler (as shown in appendix A-2.6). Figure 3-31 is snapshots from the video at a baseball azimuth angle at every 60 degrees. When viewing and discussing these images it was important to note that there were two angles of interest. The first was the angle the baseball makes with the wind, which was defined as the center of the landing strip pointing directly upstream, or azimuthal angle. The second angle of interest was the angle at which the flow separates from the baseball, or separation angle. As shown, the tracer moves up and down the surface of the baseball. One should bear in mind that the fiducial marker was placed onto each image by hand.

When viewing the video, one observes that the separation angle for the two seam knuckleball pitch varied from 88 to 122 degrees when the ball rotated at 50 rpm. This was rather a large variation when one considers the fixed smooth sphere separation angle was at 110 degrees. At an azimuthal angle of about 44 degrees, separation moved upstream and began to cling to the first seam. Separation remained fixed to the seam as the seam rotated downstream until the baseball rotated to about 73 degrees, at which point separation released itself from the first seam and moved to a separation angle of about 90 degrees. Separation then danced between the two seams until the ball was at 90 degrees. Separation then clung to the second seam until the baseball rotated to 134 degrees. At this location, separation was the furthest upstream than at any other time

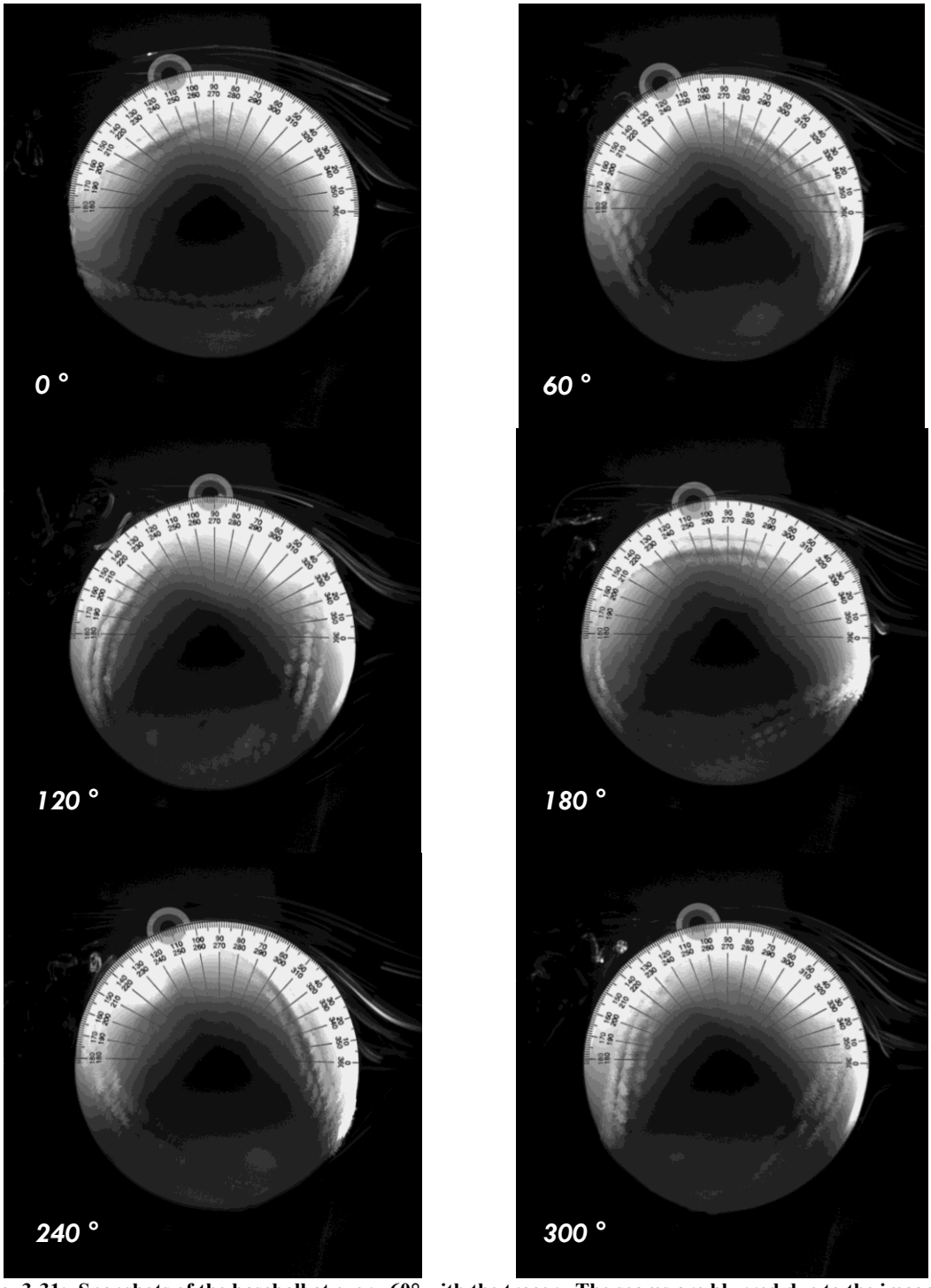

Fig. 3-31: Snapshots of the baseball at every 60° with the tracer. The seams are blurred due to the images overlaying each other.

during the baseball's rotation. At an azimuthal angle of about 141 degrees, separation was located at 104 degrees, where the separation angle for the landing strip was applied. Separation remained to be at that position for most of the remaining rotation. This change in separation was different than what a curveball pitch experiences. This asymmetry was ultimately responsible for the lateral forces generated on the curveball and result in the "curve" of the pitch. The effect, for the most part, was deterministic on the rotation rate of the baseball. The greater the rotation rate, the more lift, or curve, and vice versa. The curveball was spinning too fast for the flow to respond to the variations in the orientation of the seams. The knuckleball pitch has such a low rotation rate that the seams dominate the effects of separation. The end effect was an averaged shift in the angle of separation due to the seams. The position of the seams on the surface of the baseball has a direct effect on how separation changes.

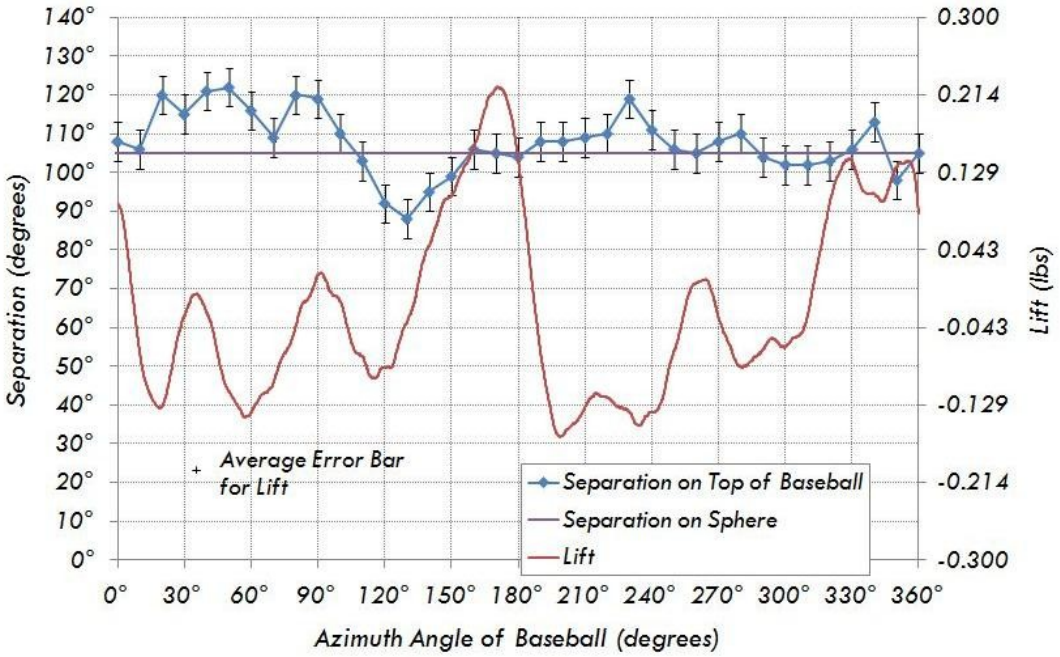

Fig. 3-32: A plot of separation on the top of the baseball, separation on a smooth sphere, and lift of a two-seam baseball rotating at 50 rpm in 70 mph free stream velocity.

A graph of the lift and lateral forces were plotted along with the location of separation in figure 3-32. The location of separation was slightly correlated to the lift forces. However, there was a slight lag. For instance, the largest decrease in the location of separation was between 90 and 130 degrees. The largest decrease in lift was between 120 and 170 degrees. This occurs during the whole rotation. However, when the change in separation was not great, there was not as much of a lag in lift. Table 3-3 summarizes all of the notes from above. As the separation caught onto each seam, separation moved upstream. Once separation let go, separation moved downstream. These episodes, in effect, change lift. This observation has to be taken lightly though, considering that the measurement of separation was on the top half of the baseball.

Table 3-3: Important locations of separation on baseball.

Orientation of Baseball	Notable Description
44° - 73°	Separation is on first seam
90° - 134°	Separation is on second seam
160° - 360°	Separation stays mostly about 104°

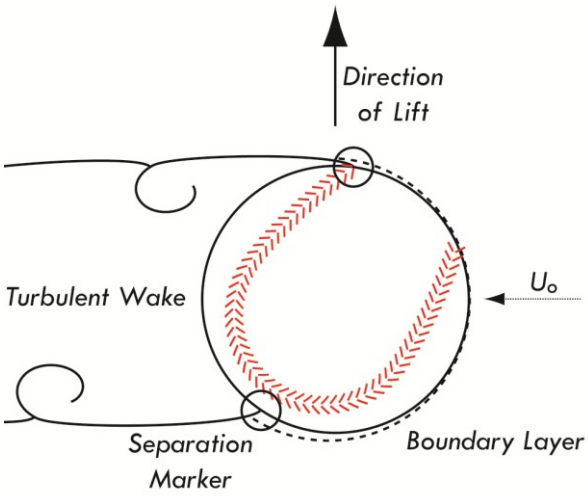

Fig. 3-33: A drawing of how a difference in separation can cause lift. The effects caused by the seam near stagnation are ignored.

This correlation between the separation and lift is explained in figure 3-33. As illustrated, separation on the top of the baseball was caused by the seam; therefore, its position was more upstream than the separation on the bottom of the ball. That difference in the angle of separation causes asymmetrical

pressure on the ball. The pressure difference lies in the turbulent wake. The turbulent wake creates less pressure on the baseball than the boundary layer. Since the turbulent wake begins earlier on the top half than the bottom half, the baseball wants to go in the direction of lower pressure, so there was a upward lift on the baseball.

Of course, the angle of separation was only found on the top half of the baseball. A baseball is a complex model because of the design of the seams on the surface, whereas a smooth sphere does not have any design of roughness on the surface. Thus, unlike the smooth sphere, separation on a baseball was not toroidal. At a given angle of baseball, separation at all points do not lie on a plane. Because of the scattering of separation, separation on the landing strip was not at 107 degrees because the seams on the opposite side of the baseball were ducking up separation.

3.3. Hot Film Anemometry

Hot film anemometry was used to measure the viscous shear stress on baseball as it rotated 360 degrees. There were two locations on the ball which were of interest: the landing strip and the seams. By comparing the shear stress in these areas, it was determined what relative effect the seams have on the aerodynamics of the knuckleball pitch. However, first the shear stress profile must be compared to published data to know if the hot film technique was sufficient. The hot films were then applied to a smooth sphere with a trip wire for comparison.

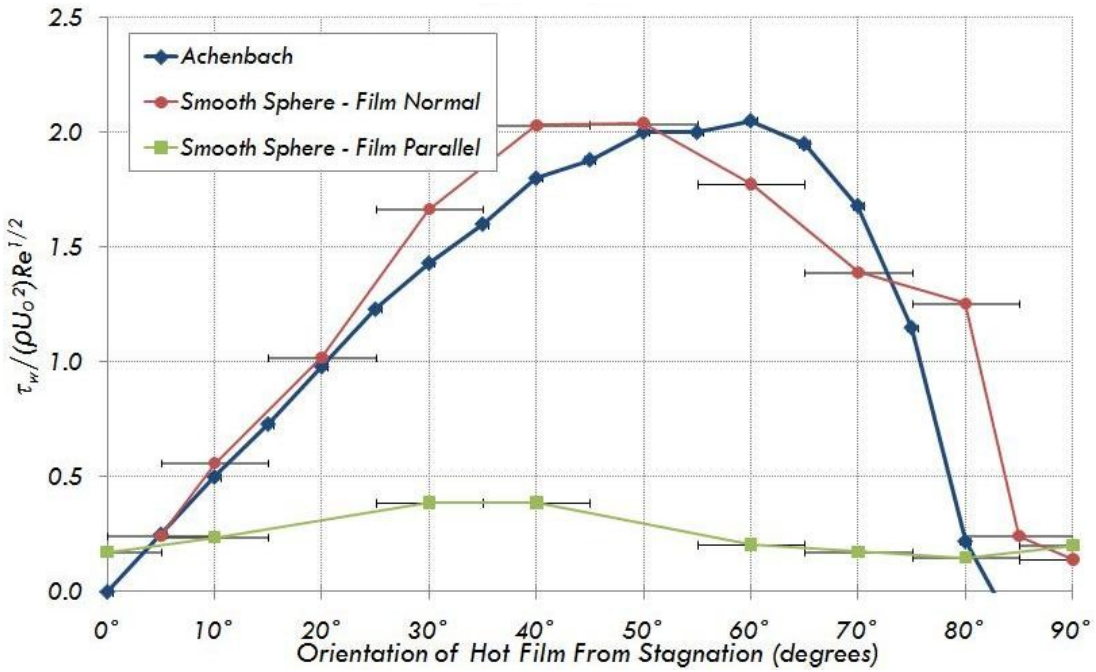

Fig. 3-34: Comparison of Achenbach's and Morrissey's smooth sphere shear stress data at a Reynolds number of $1.62x10^5$. Morrissey's data matches when the hot film was placed orthogonal to the direction of the free stream. Morrissey's data did not match when the hot film was place parallel to the direction of the free stream. The shear stress profile was much too low.

3.3.1. Shear Stress on a Smooth Sphere with a Trip Wire

Once a realization became a fact that the flat plate was not sufficient enough to calibrate the hot films for use on a baseball, the hot films were calibrated on a smooth sphere. This was completed by placing a hot film on a smooth sphere and rotating the sphere a known azimuthal angle. Those voltages recorded were calibrated with Achenbach's data shown in figure 2-17 at a Reynolds number of $1.62x10^5$. As a result, the shear stress on a smooth sphere was plotted in figure 3-34. Data was recorded when the hot film was placed perpendicular and parallel to the direction of the free stream. The shear stress for the hot film placed parallel to the free stream was very low as opposed to the hot film placed orthogonal to the free stream, which matches Achenbach's data. This

was significant for two reasons: the hot films are satisfactory to use for recording shear stress on a sphere model and that a hot film placed parallel to the free stream will record a very low shear stress. In other words, when a hot film records shear stress, it means that either there was a low amount of shear normal to the direction of the hot film and that maybe the greater shear was parallel to the hot film.

Now that Morrissey's data matches previously published data, a tangent can be drawn to new investigations. An experiment was built where a trip wire on the same scale as the seam was placed 20 degrees upstream and downstream of a hot film on a smooth sphere. The shear stress was recorded at different angles of the sphere. The shear stress profiles are plotted in figure 3-35. Once again, the hot films placed parallel to the free stream direction recorded very low shear stresses. Except for the hot film

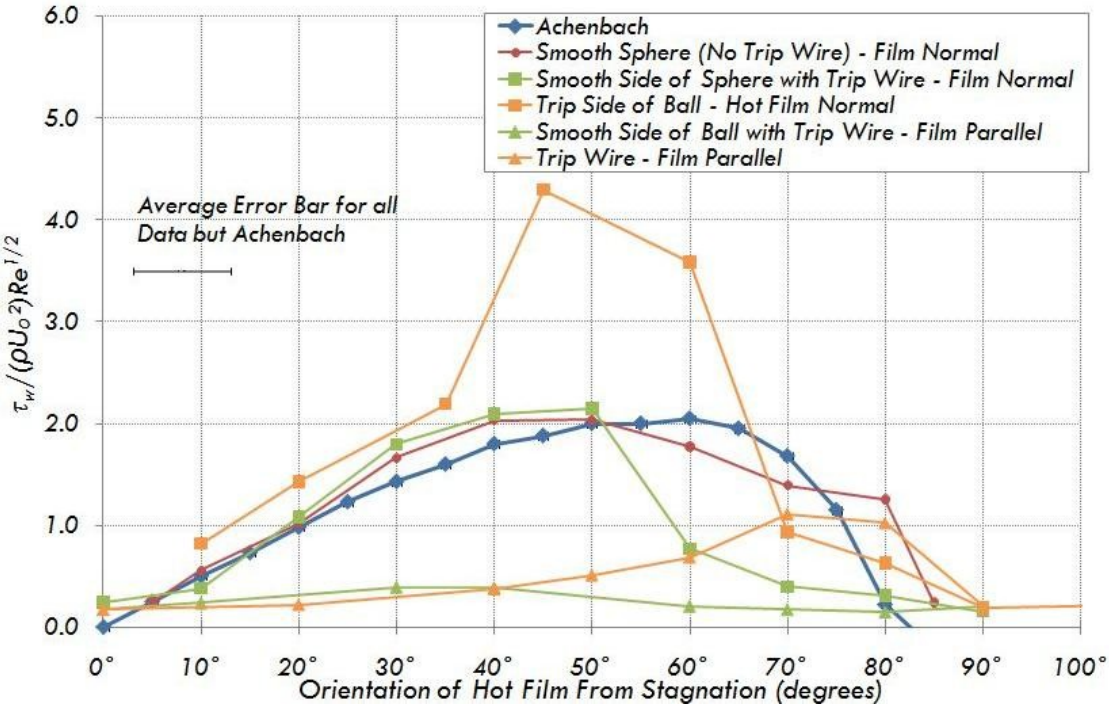

Fig. 3-35: Comparison of Achenbach's smooth sphere with Morrissey's with a trip wire 20° upstream and downstream of the hot film. The hot film was placed parallel and perpendicular to the free stream direction.

placed downstream of the trip wire. Between 60 and 70 degrees the shear stress grows. That was due to the turbulent wake. In a turbulent wake, pressure decreases while the shear stress increases. It was also noteworthy that the hot film placed upstream of the trip wire decreases in shear from 50 to 60 degrees as the hot film placed downstream of the trip wire increases when compared to Achenbach's and Morrissey's smooth sphere shear stresses. Regardless, for all hot films placed perpendicular to the free stream direction, the shear stress profiles are the same from 0 to 40 degrees. Since that was true, those azimuthal angles were used to re-calibrate the hot films on the baseball.

An attempt was made to study the effect of a trip wire on a smooth sphere. It was well known that a trip wire on a flat plate delays flow, but it was of interest to observe the effects of a trip wire on a smooth sphere. Therefore, a trip wire was placed 60 degrees

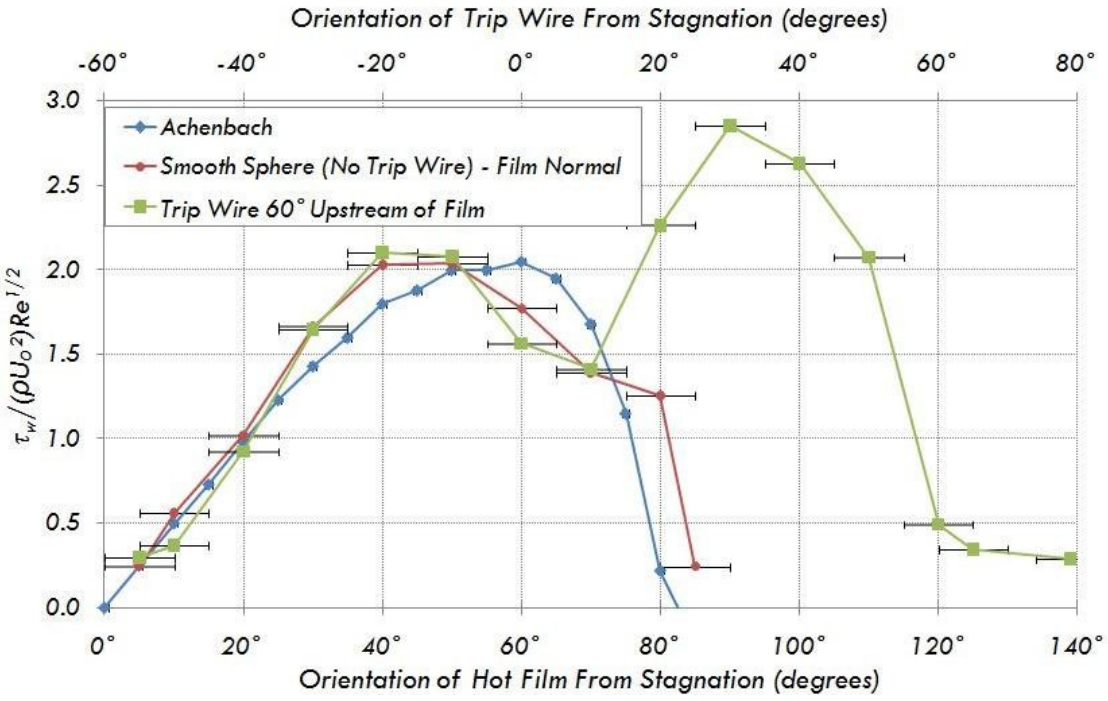

Fig. 3-36: The delayed separation on a smooth sphere due to a trip wire.

upstream of a hot film on a smooth sphere. The shear stress was recorded at different angles and the results were plotted in figure 3-36. As presented, from 0 to 70 degrees, the shear stress profiles of the smooth sphere and the smooth sphere with the trip wire are the same. However, at 70 degrees, the shear stress from the hot film 60 degrees downstream of the trip wire dramatically increases and finally lowers at about 120 degrees. This was a strong sign that the trip wire has an effect on delaying separation. Therefore, when the trip wire was 10 to 60 degrees from stagnation, there was a delay of separation on the smooth sphere. This basis will be an argument later in this paper.

3.3.2. Matlab Analysis

There were three different sets of data recorded on the baseball: a hot film placed on the landing strip of the baseball, a hot film placed before and after a seam on the baseball while rotating clockwise, and a hot film placed before and after a seam on the baseball while rotating counter-clockwise. Data was collected for thirty rotations for each hot film configuration. A Matlab program was used to ensemble average each trial for analysis, the Matlab program was included in appendix A-2.7.

Figure 3-37 presents the hot film data collected from the landing strip for a single rotation of the baseball spinning at 50 rpm while the wind speed was 70 mph. It was important to note that the data was shifted in figure 3-37 such that stagnation was at 180 degrees. Applying the orientation used throughout this paper, the hot film would begin at stagnation and rotate 360 degrees around until it meets stagnation again. This creates a discontinuity between each hump. Therefore, the hot film on the landing strip was set at

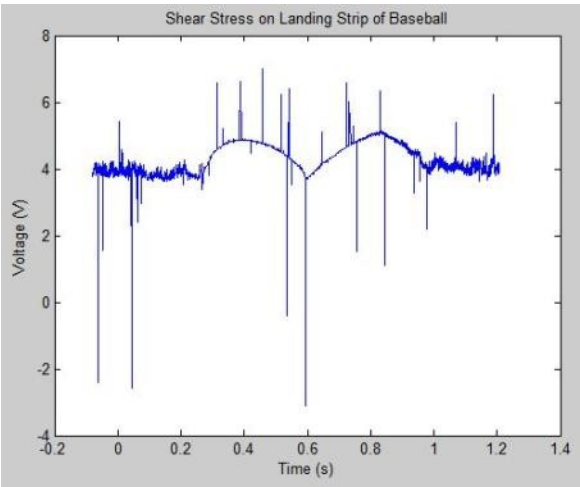

Fig. 3-37: A sample of hot film data from a single rotation on the landing strip of the baseball.

180 degrees and rotated through stagnation so there was no discontinuity between the humps at stagnation on the hot film data.

Figure 3-38 presents the time series of shear stress measured on the ball for 30 rotations. In figure 3-38, it was evident that from zero to 0.26 seconds and from 0.98 to 1.2 seconds the hot film was in the turbulent wake. All other durations were when the hot film was in the attached boundary layer, before separation. The two humps were when the hot film experienced the most shear stress and where the hot film was not in the turbulent wake. Halfway through the second hump seems to have a bit more variation than the first hump. This could occur because that was when the hot film was rotating in the direction of the free stream velocity. However, it was not certain on why there were some random points that reach as far as -3 volts and as high as 7 volts. Regardless, this was only observed randomly and was insignificant.

When all thirty rotations were shifted such that stagnation was centered at 180 degrees, the results are

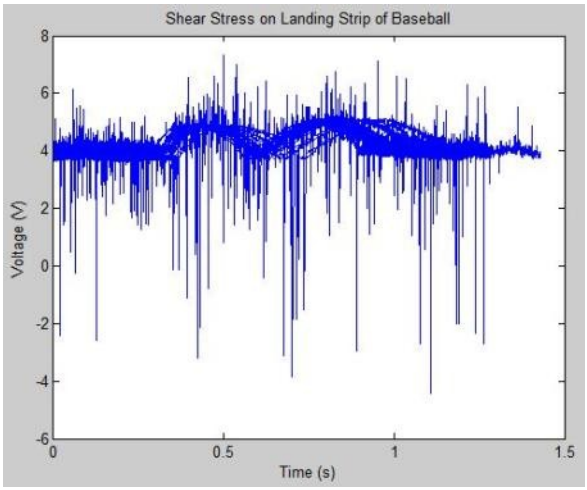

Fig. 3-38: All 30 trials of the hot film data lay upon each other.

presented in figure 3-39. It was obvious that the positioning of the baseball and the rotation rate was not perfectly lined up during each rotation because stagnation was not at the same position for each rotation. This occurred because the wires from the hot film were allowed to wrap around the sting supporting the baseball. The tension in the wires from the CTA box affected the rotation of the baseball. Therefore, the data from each rotation was shifted so that the local minimum was centered at 0.6 seconds, where stagnation should appear.

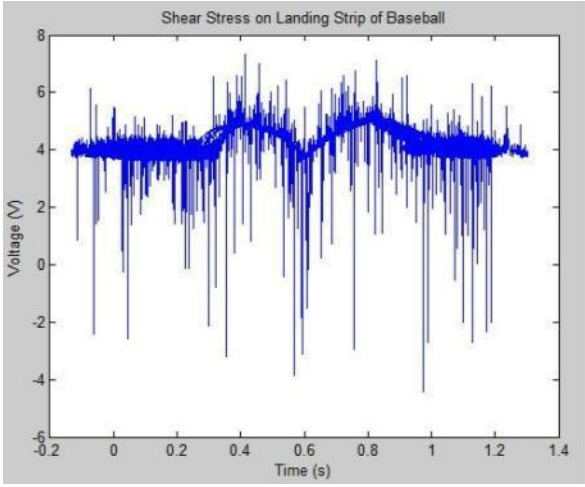

Fig. 3-39: All thirty trials centered at 0.6 seconds.

Once the data was centered, all thirty trials appeared as it does in figure 3-39. Unfortunately, this shift of each trial left some of the hot film data to be plotted before zero and after 1.2 seconds. That did not matter because that data was when the hot film was in the turbulent wake. Any signal received in the turbulent wake would be consistent with any other data that represented the hot film in the turbulent wake. Regardless, the point of interest was what the shear stress was when the hot film was in the boundary layer. Now that all thirty rotations were centered, an ensemble average of the voltages was converted to shear stress using the calibration obtained from the flat plate.

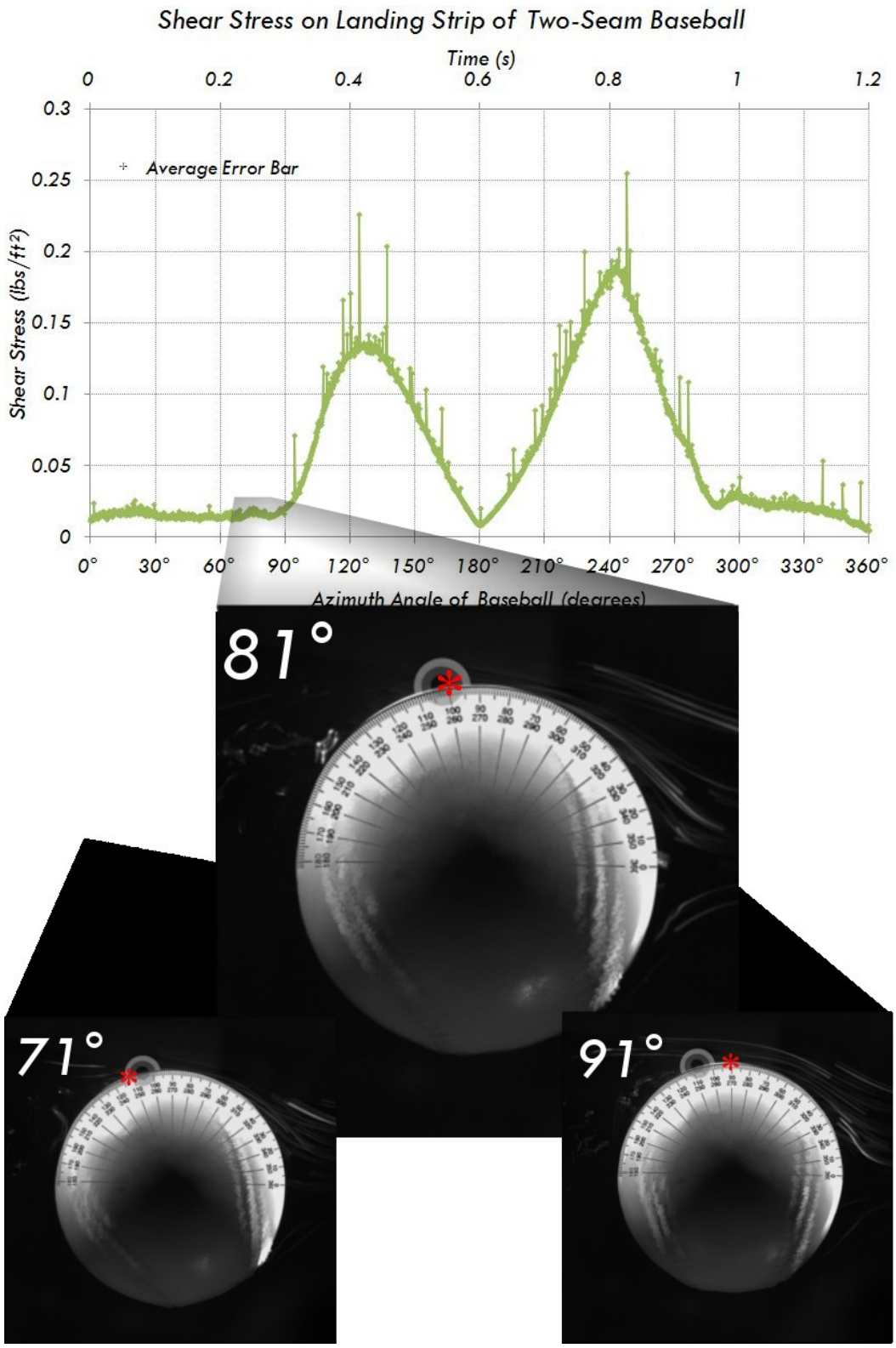

Fig. 3-40: Ensemble average of the shear stress of thirty rotations on the landing strip of a two-seam baseball. Separation occurs at 81°, as supported by the flow visualization photo at the same position. The two surrounding photos are the images when the ball is at 71° and 91° respectively. The red asterisk represents the approximate location of the hot film on the landing strip.

3.3.3. Shear Stress on the Knuckleball

Figure 3-40 presents the shear stress acquired from the landing strip of the rotating baseball while in a two-seam configuration. The rotation angle has been adjusted such that stagnation (the upstream location on the ball) was at 180 degrees. The shear stress should be zero at stagnation and increase as the flow negotiates the curvature of the ball. The boundary layer continues to grow along the surface of the ball and shear stress reaches a maximum near 60 degrees from stagnation. At this point, the boundary layer begins to experience a negative pressure gradient and the flow nearest to the ball begins to slow down. At some short time after, the flow cannot continue to slow and separates from the ball. At this point, the shear stress measure was in the wake and relatively small. It was evident from the variation in the shear stress signal that separation occurs at approximately 81 and 288 degrees. This assertion was cooperated by comparing the flow visualization to the hot wire data. Thus, figure 3-40 includes three images from the flow visualization where the baseball was at different flow angles around 81 degrees with the red asterisk representing the approximate location of the hot film. The figures illustrate that the separation tracer was first upstream of the hot film, then located at the hot film, and then downstream where the hot film would be. The images before and after 81 degrees illustrates how the hot film moved past separation. The shear stress was quite symmetrical at 180 degrees, which was where the hot film passes through stagnation. This was predicted by the assumption that the landing strip acts as a smooth sphere from the flow visualization data. Other the variances at the turbulent wakes were decreased due to the ensemble average. However, as shown in figure 3-37, it was evident that the hot film was in the turbulent wake in those respected positions. Lastly, there was slightly

greater shear stress as the hot film rotated away from stagnation. This does not agree well because there was a greater local Reynolds number as the hot film rotates towards stagnation. Therefore, there should be a greater shear stress.

However, when the shear stress of the landing strip was plotted from stagnation, as presented in figure 3-41, another argument was built. As shown, the shear stress on the landing strip rotating towards stagnation was greater up to 40 degrees. However, the shear stress decreases due to separation. The shear stress on the landing strip rotating away from stagnation was greater due to delayed separation. Therefore, the shear stress was allowed to increase over 60 degrees. As a result, the landing strip delays separation on the bottom half of the baseball due to rotation.

When the shear stress profiled was compared to Achenbach's shear stress profile

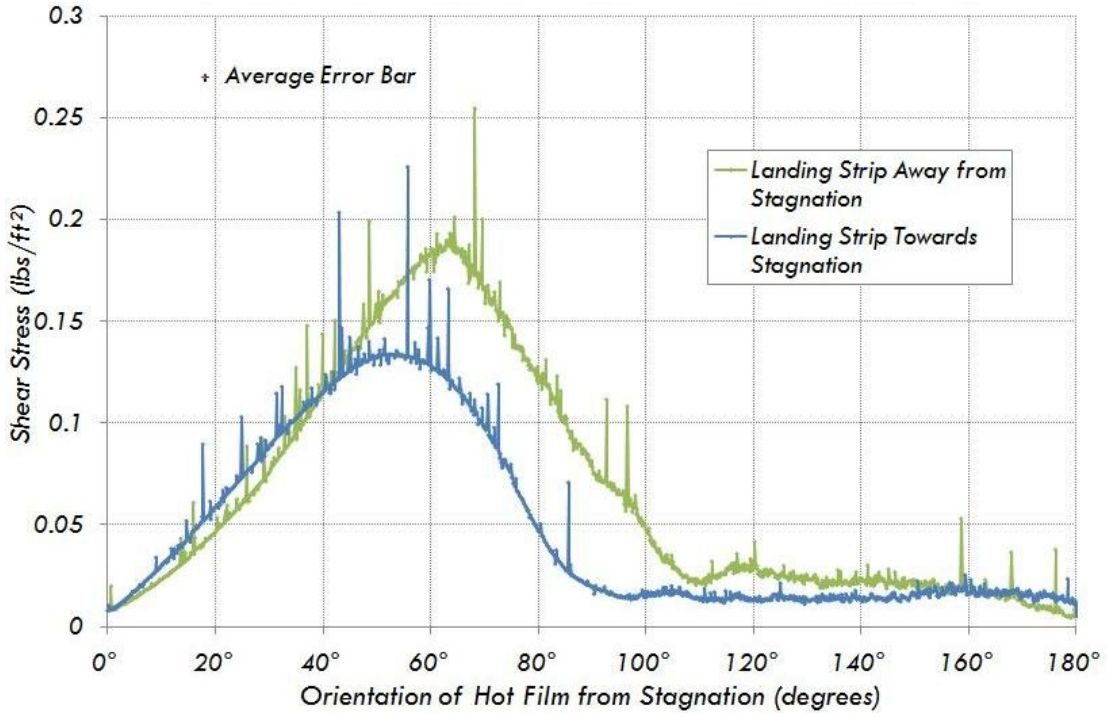

Fig. 3-41: Comparison between the shear stresses on the landing strip.

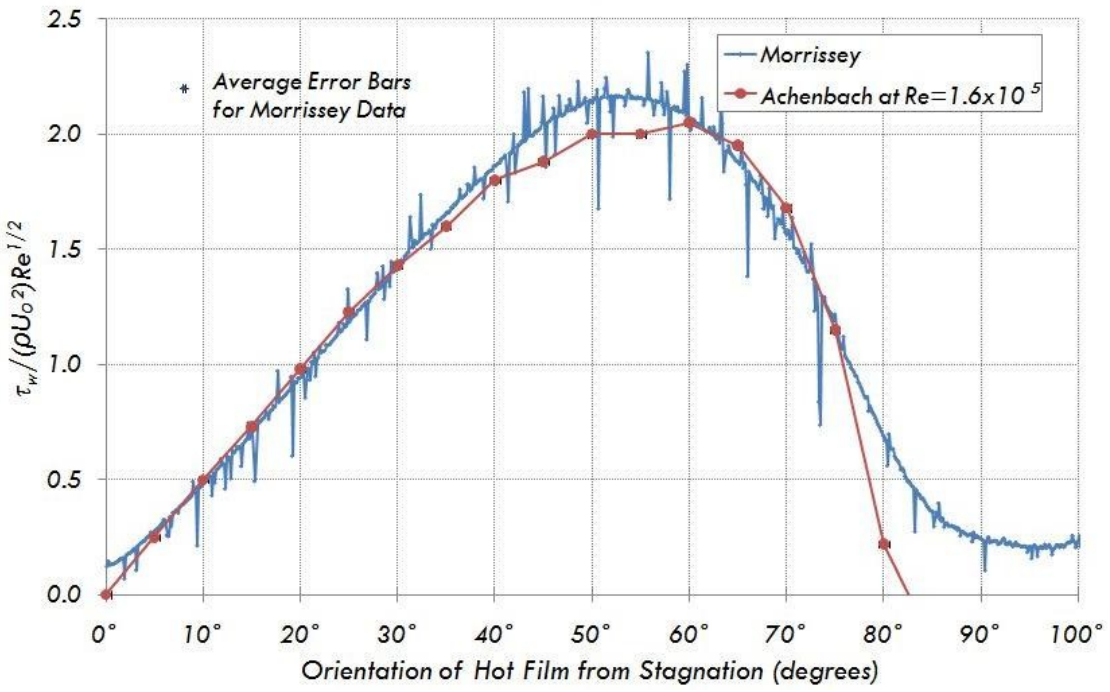

Fig. 3-42: Comparison of Achenbach and Morrissey's landing strip shear stress. The profiles match each other except after 75°. Achenbach used pressure taps; therefore, was able to measure direction, unlike hot films.

at the same Reynolds number, a strong conclusion was built. As presented in figure 3-42, Achenbach's data matches to the landing strip data when the hot film was rotating towards stagnation. This concludes that the landing strip acts as a smooth sphere when considering shear stress.

Now since the flow visualization agreed with the hot film data, it was fair to find the separation at each point on the baseball where a hot film was placed. As discussed in section 2.4.3, a hot film was placed on the landing strip of one baseball and before and after a seam on another baseball. Figure 3-43 presents two schematic drawings of the hot films placed before and after a seam, as well as on the landing strip of the baseball. The hot films on each side of the seam surround one seam. To find the shear stress on the other seam, the baseball was rotated counter-clockwise. If all of the hot films were

placed on a single baseball, this would essentially create a total of five hot films on the baseball, as presented in figure 3-44. Each seam was named to not create any confusion. To clarify, "seam A" would cross stagnation first when rotating clockwise, with "seam B" following. The benefit of this procedure was that the distance of each hot film from the seam was equal on "seam A" and "seam B." The hot films placed before and after the seam in figure 3-43 was surrounding "seam A."

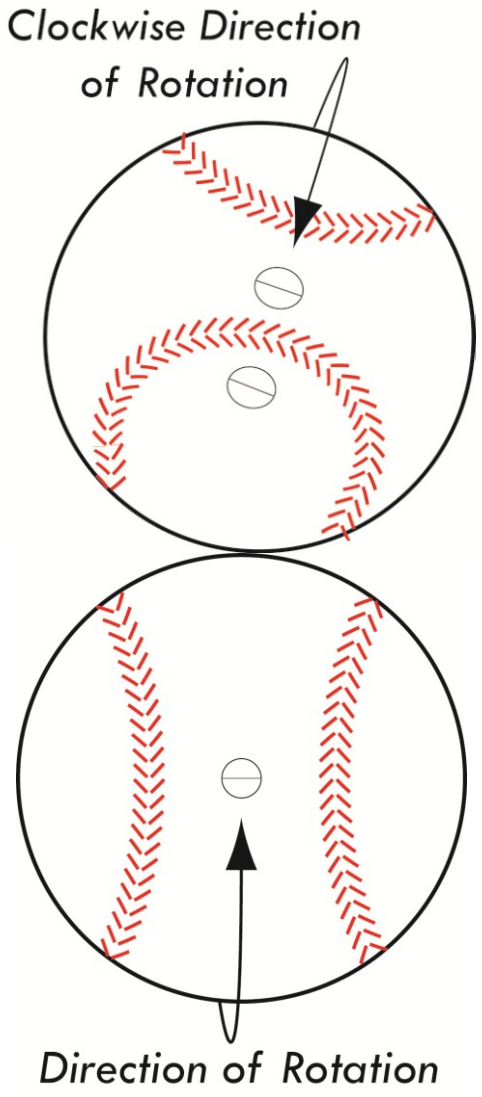

Fig. 3-43: Schematic drawings of a rotating baseball with the hot films before and after the seam (top image) as well as a hot film placed on the landing strip (bottom image).

Interestingly enough, a plot of each hot film surrounding "seam A" in each rotation direction is presented in figure 3-45. For this plot, stagnation has been shifted to an azimuth angle of zero degrees. As shown, the data for each rotation was shifted when compared to its respected data set. For instance, all of the shear stresses recorded clockwise were shifted to the right of the data recorded counter-clockwise. However, the maxima, minima, and trend are the same. The only difference was where separation starts and ends at a small difference at time.

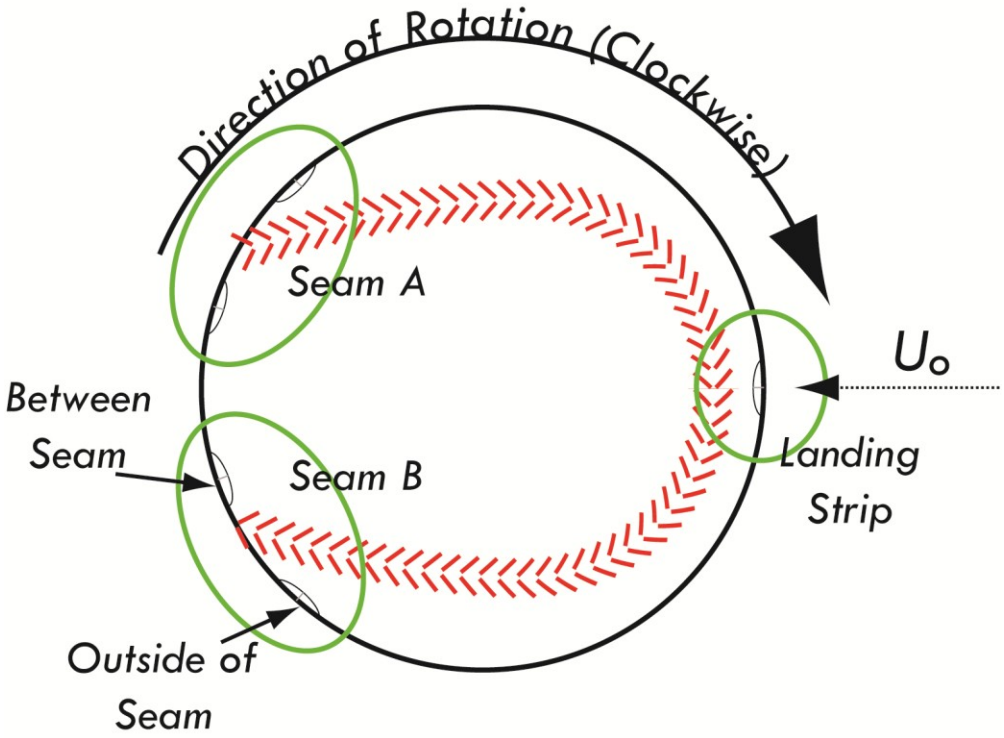

Fig. 3-44: Schematic drawing of all five hot films placed on the baseball as well as the terms. This orientation of the baseball would be at 0°. Free stream velocity is right to left.

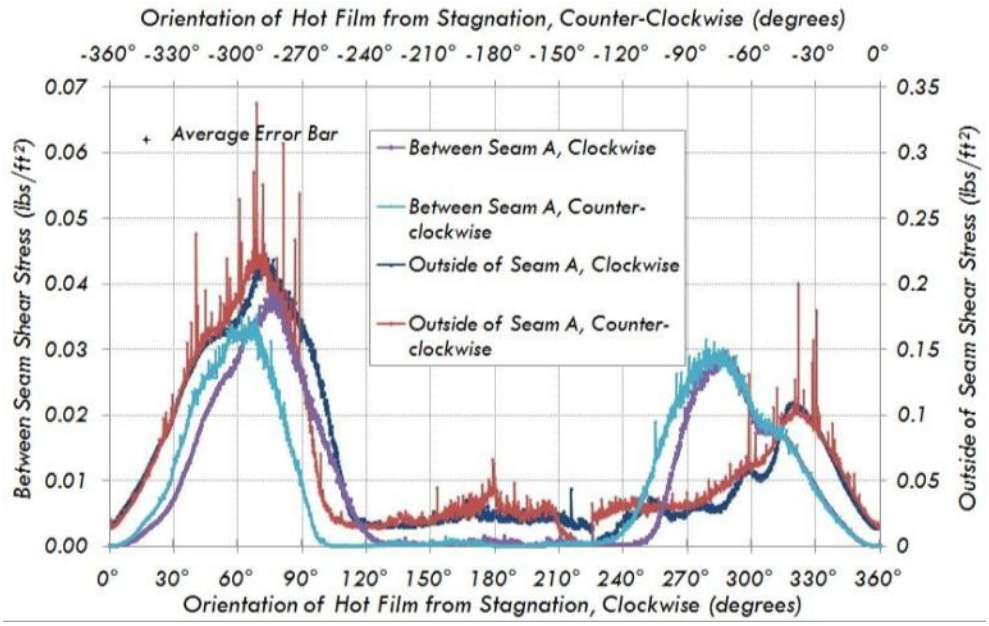

Fig. 3-45: Comparison of the hot films surrounding "seam A" with the baseball rotating each direction. Stagnation is at 0°.

The positioning for the hot film data had to be confirmed. As shown in figure 3-23, the seams are approximately at 150 and 210 degrees. The hot films were placed one half width of a seam from the end of each seam. The simple arc length formula was used to find the distance from the center of the seam on the surface of the baseball, as shown in equation 3.5. The width of a seam was about 7/16th of an inch, which is s.

$$s = r\theta \tag{3.5}$$

The radius, r, of a baseball is 1.5", which makes theta 16 degrees. Table 3-4 presents the following positions of each hot film on the baseball. The stagnation points from the "landing strip," "outside seam A," and "between seams, B" hot films were centered at their respective position on the baseball. The "between seams, A" and "outside seam B" hot film stagnation points were automatically shifted due to the centering of the previous mention hot films. Table 3-4 was confirmed when the shear stress from each hot film was plotted together.

Figure 3-46 presents the shear stresses from all five hot films as a function of the azimuth angle of the baseball. Each stagnation point represents where the hot film was placed, for example, the landing strip stagnation was at zero degrees. A key observation of this graph was how the data mirrors itself at 180 degrees, irrespective of which hot film. This was expected due to the symmetry of the baseball. The oddest observation in this graph was the hot film "outside seam A." There was no seam in

Table 3-4: The hot film locations on the surface of the baseball.

Hot Film	*Position on Baseball*
Landing Strip	*0°*
Outside Seam A	*134°*
Between Seams, A	*166°*
Between Seams, B	*194°*
Outside Seam B	*226°*

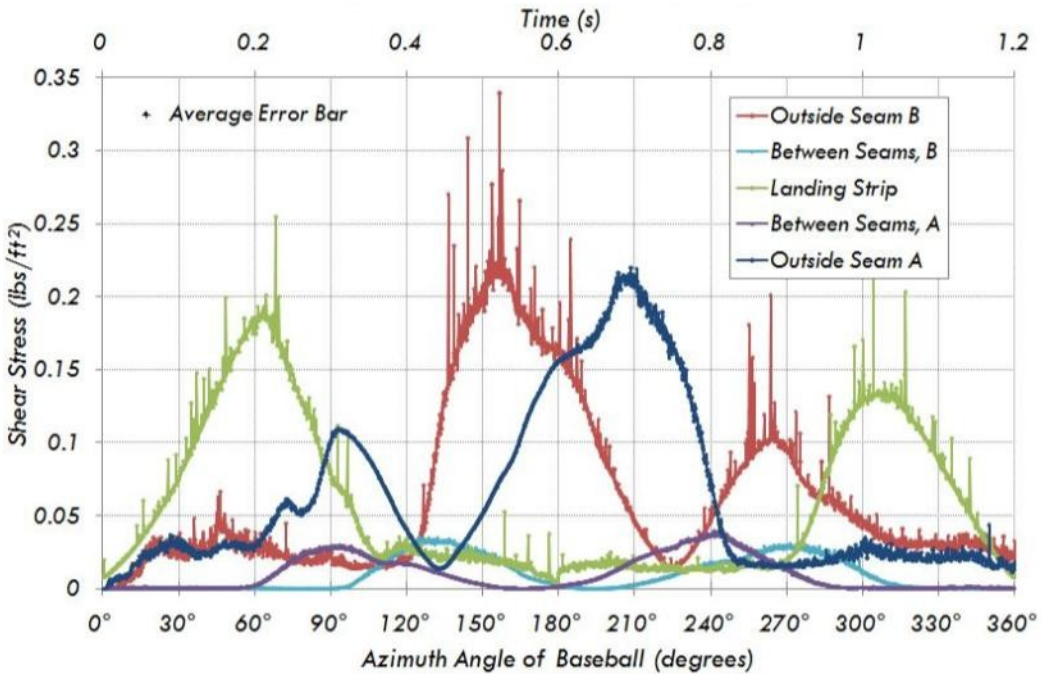

Fig. 3-46: Shear stress data from all five hot films.

front of the direction of rotation on that particular hot film; however, it experiences the greatest amount of shear as the ball rotates away from stagnation, when the seam was between the hot film and stagnation. There was an explanation though, as the hot film "outside seam B" illustrates, the greatest shear was when the hot film was rotating towards stagnation. During that time, there was a seam between the hot film and stagnation. The magnitude of shear and placement of the hot film would conclude that the seam creates a turbulent wake, while the area before the seam and towards stagnation there was a laminar boundary layer. The laminar boundary layer was proven by the lack of the variance of stress on the first maxima of "outside seam A" while there was a larger amount of variance of stress on the second maxima of "outside seam A." That argument was also supported by the large amount of shear stress while the hot wire was behind the seam from stagnation. There was a greater amount of shear in turbulent than laminar flow. An odd observation was how there was very little shear between the seams as

opposed to the landing strip. This could be because of the orientation of the hot films on the baseball. Figure 3-47 illustrates how the seams can direct the flow of the fluid because of their height. Due to this interaction, the shear stress at that specific location was greatly influenced from the possible flow direction. Since the hot films used only measures the shear stress in one direction, any flow parallel to the hot film would record no shear. Thus, applying this hypothesis, the hot films between the seams would record a very minimal shear stress.

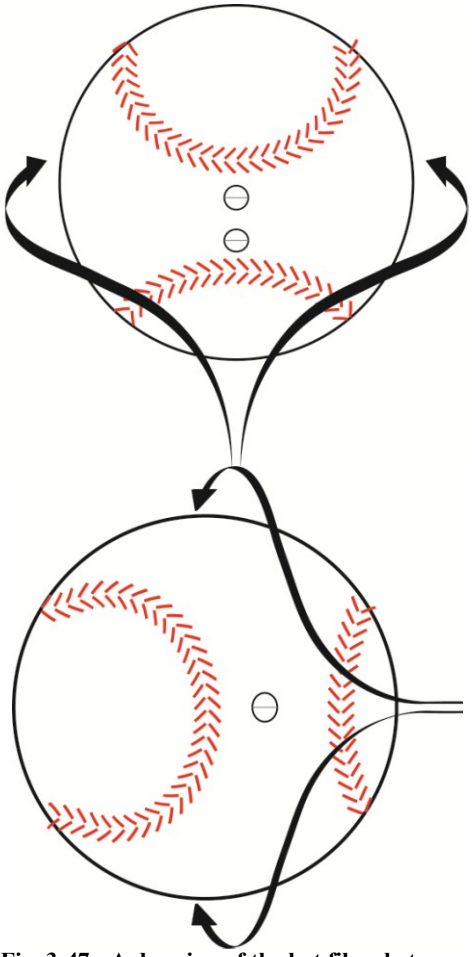

Fig. 3-47: A drawing of the hot films between the seams (top) and the hot film on the landing strip (bottom). The arrows represent the pathlines of the fluid. The seams interact with the pathlines to direct where the fluid travels. In the top image, the hot films are parallel to the pathlines. In the bottom image, the hot film is perpendicular to the pathlines. Thus, the hot film in the landing strip will record more shear stress than the hot films between the seams because of the direction of the flow.

Another way to view the data presented in figure 3-46 is a polar graph, shown in figure 3-48. The color of the hot film location marker corresponds to the color of the respective hot film data. At zero degrees, all of the hot films experience nearly no shear stress. At 210 degrees, where "seam B" was at stagnation, the hot film at "outside seam A" was experiencing the greatest shear. This graph is only useful to observe what the shear stress at any given location on the baseball for each hot film and tells nothing about separation.

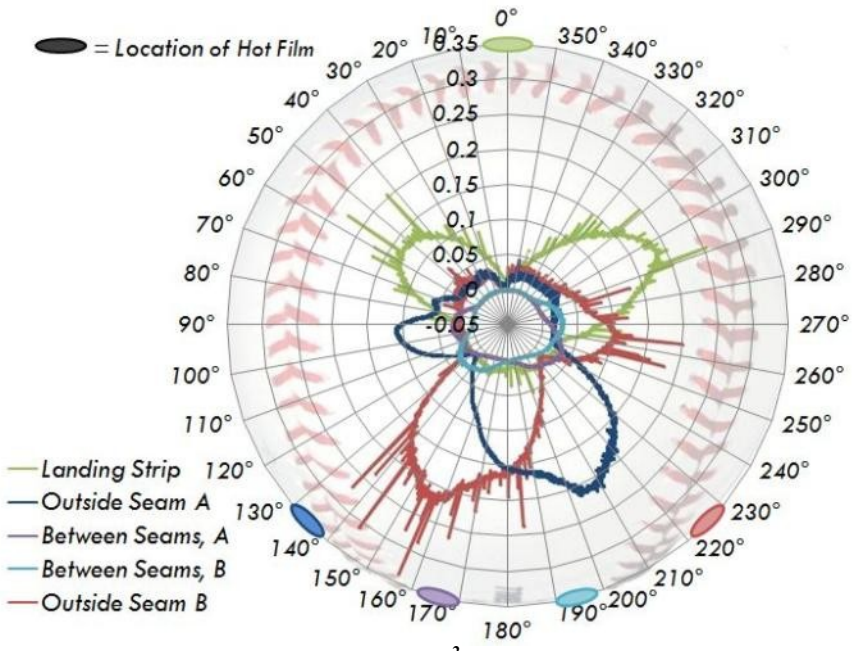

Fig. 3-48: A polar plot of the shear stress (lbs/ft^2) the hot films experienced at orientations of the baseball. The color of the hot films corresponds to the color of the shear stress data.

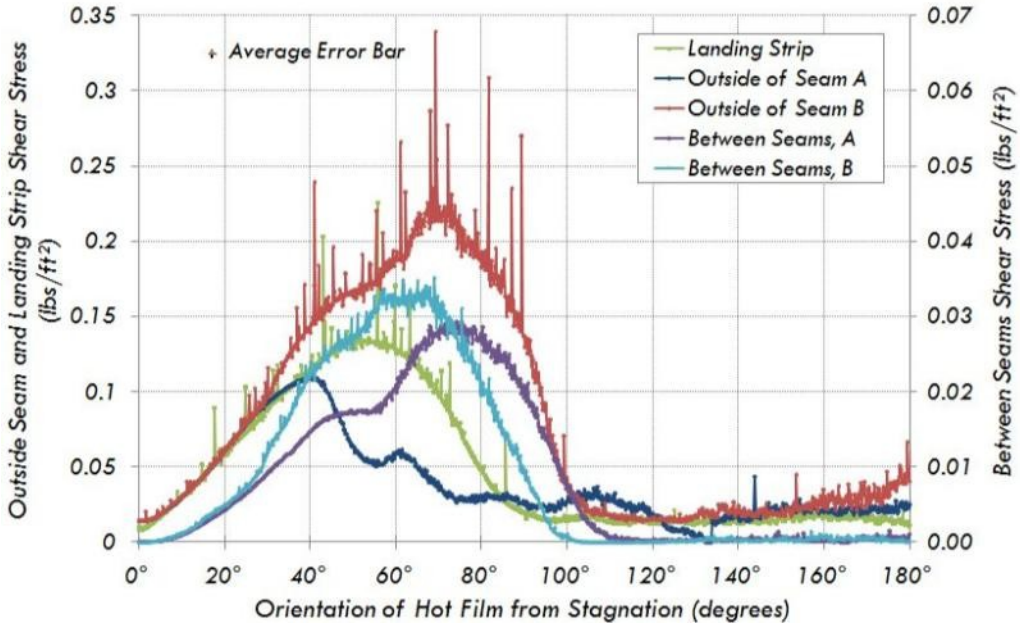

Fig. 3-49: A plot of the shear stress for each hot film as a function of degrees from stagnation. The shear stress experienced here was while the hot films were rotating towards stagnation.

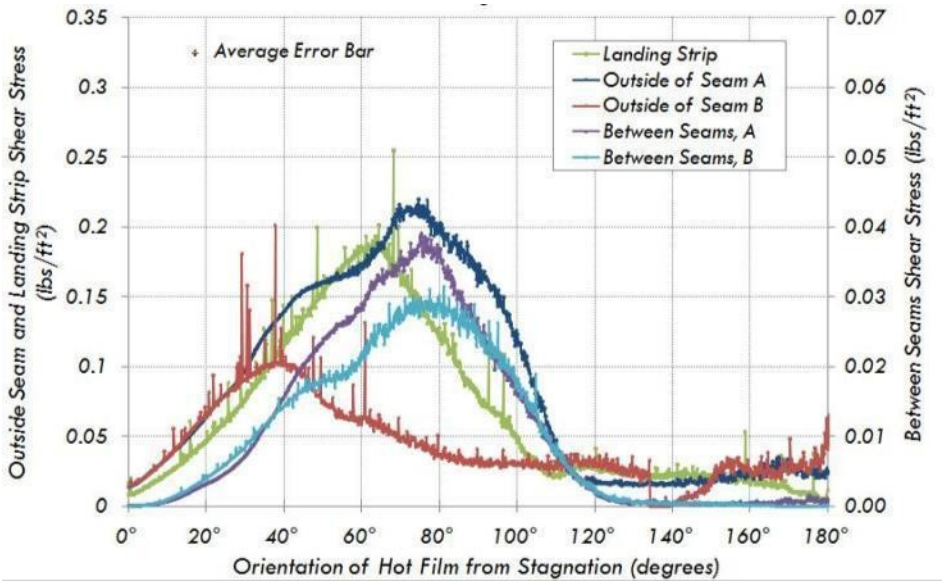

Fig. 3-50: A plot of the shear stress for each hot film as a function of degrees from stagnation. The shear stress experienced here was while the hot films were rotating away from stagnation.

To better illustrate the effect of separation on shear stress for each hot film, figures 3-49 and 3-50 are presented. Separation occurs when there was a rapid decrease in shear stress. Figure 3-49 presents shear stress data that was collected when the hot films were rotating toward stagnation, while figure 3-50 presents shear stress data that was collected when the hot films were rotating away from stagnation. When the hot films were rotating away from stagnation, separation was delayed more than when the hot films are rotating towards stagnation by about ten degrees. In both graphs, at about 40 degrees, there was a change in the slope of shear stress for all hot films except the landing strip. Coincidently, the landing strip's hot film experiences the greatest amount shear stress at that that same point. It was also noticeable that the three largest maximums are nearly at the same angle. Most importantly, there was a greater shear stress when the hot film was downstream of the seam and a lesser amount of shear stress when the hot film was upstream of the seam.

Those observations were also made in figure 3-36 when the trip wire was placed 60 degrees upstream of the hot film on the smooth sphere. Figure 3-51 compares the shear stress of the hot film when placed upstream and downstream of a trip wire or baseball seam. The comparison of these two data sets was not completely fair, due to the smooth sphere recording data statically and the baseball was rotating. Regardless, the same trend appeared when the hot film was placed upstream of the trip wire and seam. The same can be said to an extent when the hot film was placed downstream of the trip wire and seam. The hot film experiences a greater amount of shear than the other hot films. The only difference was that separation was more downstream for the hot film on the baseball. Therefore, one can say that the seam acts like a seam.

Overall, the seams has a significant effect on the baseball. The landing strip

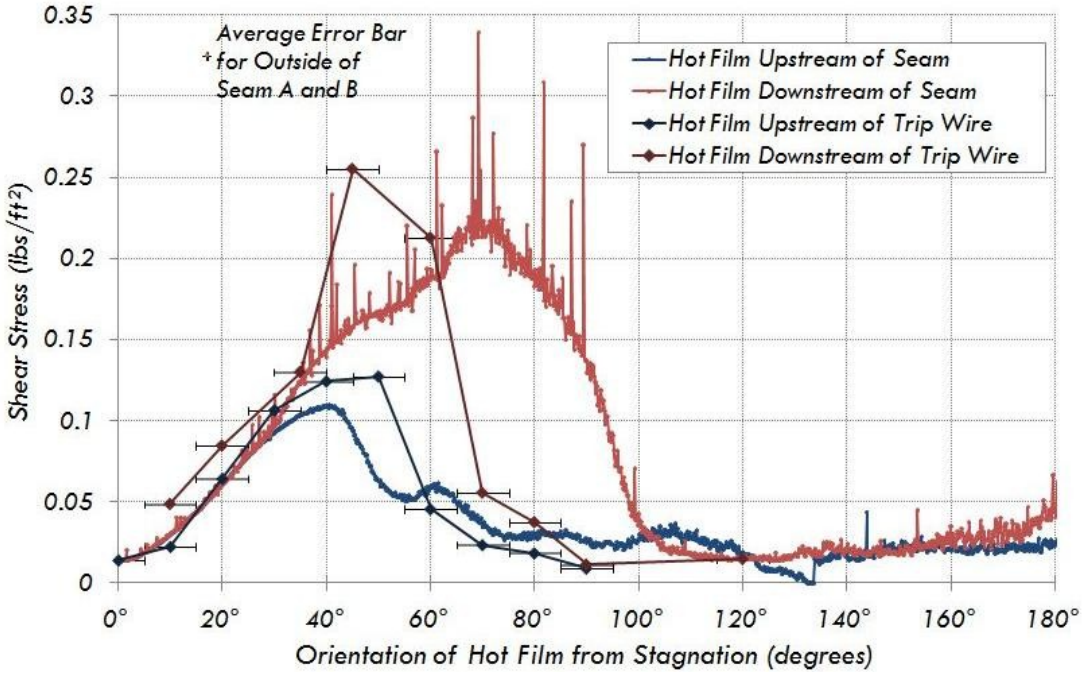

Fig. 3-51: Comparison of shear stress when a hot film was placed upstream and downstream of a trip wire or baseball seam.

replicates the same shear stress profile as a smooth sphere with the same Reynolds number. It was also noticed that when the hot film on the landing strip was rotating towards stagnation, shear stress was greater than when rotating away. However, it was only momentarily, this was due to the bottom half of the baseball delaying separation. This was also noticed for the hot films around the seams. Lastly, a strong argument can be built that the seam delays separation. This was supported by figure 3-51. Since the seams create the same shear profiles as the trip wire, the seams can be modeled by the trip wire. It was proven that the trip wire delays separation in figure 3-36. Therefore, the seams delay separation.

CHAPTER 4. CONCLUSION

4.1. Final Conclusions

With each technique and data collection analyzed, a quick summary will be done for each method and how it pertains to the movement of the knuckleball.

4.1.1. Force Balance Conclusions

The conclusions for the force balance came from the four-seam and two-seam orientations. It was first noticed when comparing the four-seam, static Morrissey data to Watts and Sawyer's data was that the seam has a dramatic effect on the lift of the baseball. The seam disturbs the symmetry of the flow. That asymmetry of the flow around the baseball leads to lift. It was found that the lift goes in the direction to the seam nearest stagnation for both the four-seam and two-seam orientation. When the free stream velocity was increased from 46 mph to 70 mph, the lift nearly doubled. It was calculated that there was nearly no Magnus effect acting on a baseball rotating at 50 rpm.

When the baseball was in the two-seam orientation at a free stream velocity of 70 mph, the lift was not as great as a four-seam baseball. The two-seam orientation did not have a periodic effect as the four-seam. The greatest change in lift in the two-seam baseball occurred between 120 and 200 degrees. Between 120 and 170 degrees, the maximum of lift was 0.22 lbs, or two-thirds of the weight of the baseball, and the minimum was -0.16 lbs, or nearly one-half of the weight of the baseball. The largest magnitude in slope was from 170 to 200 degrees. The two-seam spinning baseball also had a large standard deviation in lift compared to the four-seam spinning baseball. This could be accounted to the complex three-dimensional flow as well as the unpredictability

of the path of the pitch. The four-seam baseball was much more symmetric than the two-seam baseball, both in geometry and lift plots. The geometry of the four-seam baseball repeats itself four times in one rotation; the two-seam baseball repeats its geometry only once. The only occurrence that the geometry was relevant was when the baseball was at 0 and 180 degrees, when stagnation was directly on the landing strip and between the seams. The lateral forces of the two-seam baseball, rotating at 50 rpm in a 70 mph wind were measured as well. There was not nearly as much fluctuation as the lift data. However, no published data was found for the lateral force on a baseball. Therefore, any conclusions made upon the lateral force may not be satisfactory.

4.1.2. Flow Visualization Conclusions

Some key observations of the flow visualization were how the landing strip and seams of the baseball affect the boundary layer separation. The landing strip of the baseball has nearly the same separation of a smooth sphere at the same Reynolds number. Therefore, one could point that the landing strip acts as a smooth sphere when pertaining to separation. The seams were found to be an initiator of separation. This was found by the turbulent wake observed whenever the seams were placed upstream of the landing strip separation. The seams did not show any evidence of delaying separation. This could be at fault of the user finding separation on the surface. It was found that due to their height and the Reynolds number, the seams are significantly too high to trip the flow. Separation, on top of the baseball, changed positions many time from 0 to 160 degrees. After 160 degrees, separation nearly stayed constant with minor discrepancies. It was also found, as expected, that separation had a strong hold on lift.

4.1.3. Hot Film Anemometry Conclusions

The hot film data presented some interesting observations. The hot film data was supported by the separation of the flow visualization on the landing strip at an azimuth angle of 81 degrees of the baseball. The shear stress nearly mirrored itself at an azimuth angle of 180 degrees of the baseball. This was expected considering the geometry of the baseball. However, going against earlier thought, rotation direction did make a small difference in separation. Separation was more upstream when the hot films where rotating towards stagnation than when the hot films were rotating away from stagnation. The reasoning behind this was not due to the rotating rate of the baseball, but rather the seams "carrying" separation. As the seams were rotating towards stagnation, separation was carried upstream. When the seams were rotating away from stagnation, the seams carry separation downstream. Therefore, separation was delayed on the bottom half and induced on the top half when the seams were present. The landing strip also carried separation upstream when rotating towards stagnation and downstream when rotating away from separation. The shear stress on the landing strip was greater when rotating towards up to 40 degrees from stagnation. However, since the landing strip delays separation on the bottom half of the baseball when the landing strip was rotating away from stagnation, the shear stress on the landing strip rotating away from stagnation continued to increase. It was also found that the landing strip has the exact same shear stress profile when compared to Achenbach's published data. That was significant because, once again, the landing strip acts like a smooth sphere.

Some key observations were also made on the smooth sphere when a trip wire was present. It was shown that when a trip wire was 10 to 60 degrees from stagnation,

separation was delayed. Also, the trip wire created its own turbulent wake, just like a seam. It also decreased shear stress just upstream of the trip wire. That observation was found with a seam as well. Therefore, the seam acts like a trip wire.

4.1.4. Summary of Complete Work and How it Relates to Baseball Conditions

When these observations were gathered, many conclusions can be built upon how and what makes the knuckleball move. As stated before, the most common knuckleball was thrown at 70 mph in a two-seam orientation with a half rotation from the pitcher's hand to home plate. An assumption was made from the interview from R.A. Dickey that the baseball was held at a 120 degree azimuthal angle upon release. That would mean that the knuckleball would rotate from 120 to 300 degrees. Reviewing some of the

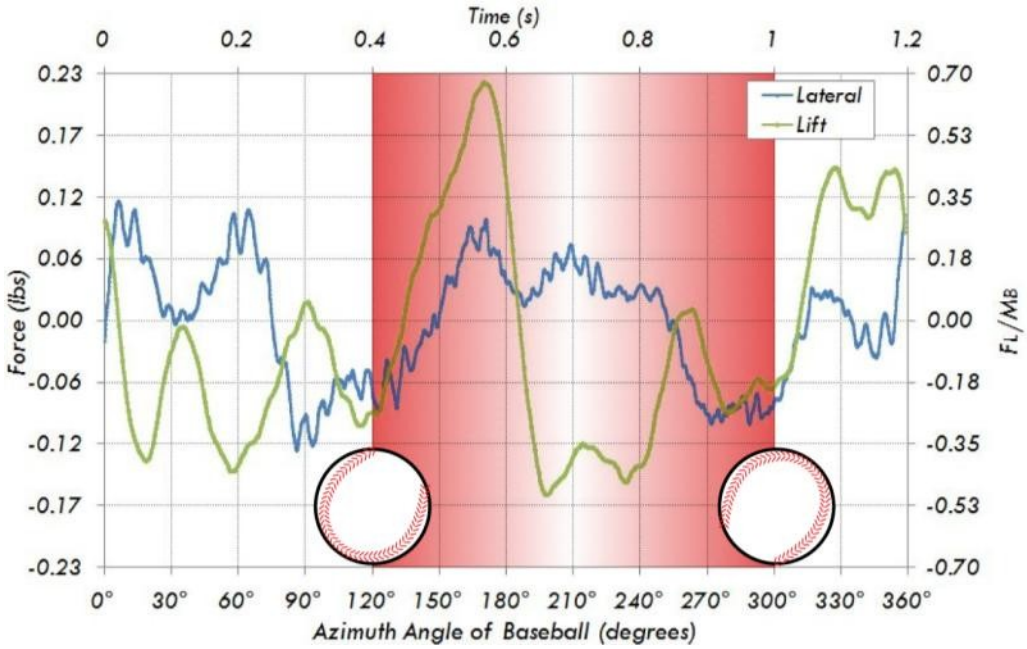

Fig. 4-1: The lift and lateral forces a two-seam baseball experiences at 70 mph while rotating at 50 rpm. The red area represents the area a common knuckleball is thrown today. Positive lift is up, negative is down. Positive lateral force is right field, negative is left field. Baseballs shown are the orientations of the baseball at the beginning and end of the knuckleball with the wind direction flowing right to left.

graphs above and focusing on those angles will help understand the knuckleball.

Figure 4-1 presents the lift and lateral force data from section 3.1.3, but with a highlight of the positions the knuckleball experiences. R.A. Dickey said that you want to rotate the baseball so the seams cross the front of the ball, otherwise the landing strip was exposed and the baseball moves like a batting practice pitch with very limited movement. As shown, the greatest difference in lift was in this area the knuckleball was thrown. The lateral force does not fluctuate as much as the lift. Regardless, there was a small amount of forces pushing the ball side to side. When considering the lift force during the flight of the pitch, the hitter would find that the baseball does not drop as much initially, but then half way to home plate, the ball will dramatically drop. As the baseball crosses home plate, the drop was no longer as severe, but the ball still moves downward. This dramatic drop and change in the slope of lift would fool the hitter to swing in the wrong place. However, the highest standard deviation in the lift forces of the baseball was at 120 degrees, as presented in figure 3-22. This would mean that the initial lift the baseball experiences each time may be different. So it would be rare for a hitter to see the exact same path of the pitch again. This was unfortunate for the pitcher as well, because that means it was difficult to control the pitch each time.

In figure 4-2, one can observe how the seams affect the lift. As stated before, lift goes in the direction of the nearest seam. As a pitcher, this is very beneficial. The pitcher's goal is to create as much movement on the pitch as possible. Therefore, the two-seam knuckleball would be applicable. Since the two-seams are so close to each other as opposed to the four-seam, lift changes in a shorter amount of time than the four-

seam. However, there would be no great change in lift in such a short time period if the knuckleball was thrown with backspin and stagnation went through the landing strip.

The flow visualization confirms that the seams control separation on the top half of the baseball. From the video, it was shown that the seams carry separation until the pressure recovers over the seam. Figure 4-3 shows that separation controls lift. As separation was pushed forward, lift increases. This was due to the Bernoulli principle. Unfortunately, the flow visualization only shows separation on the top half of the baseball. Therefore, any effect the seams have rotating away from stagnation was not recorded.

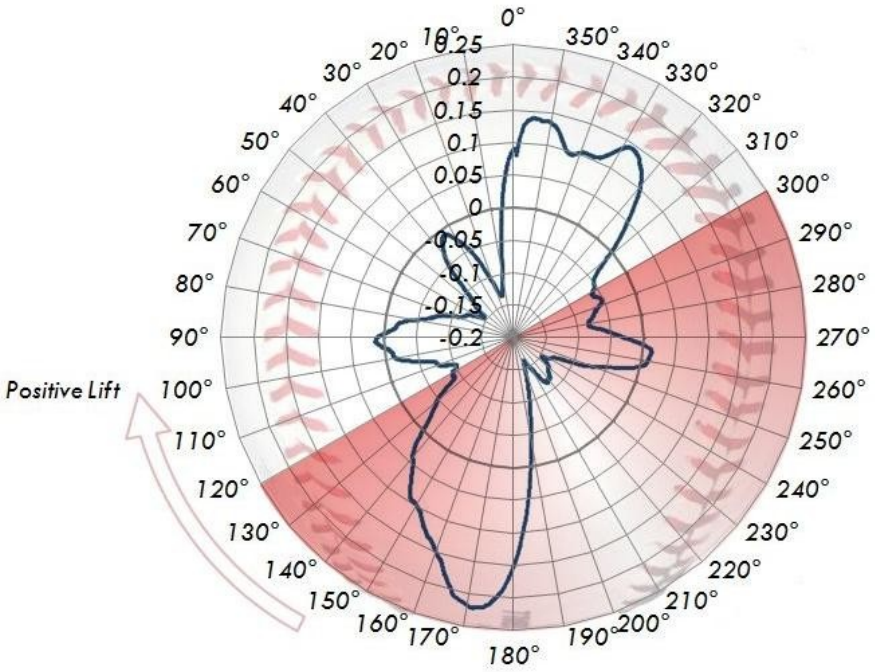

Fig. 4-2: The lift (lbs) a two-seam baseball, rotating at 50 rpm, in a 70 mph wind. The red area represents the area the knuckleball experiences.

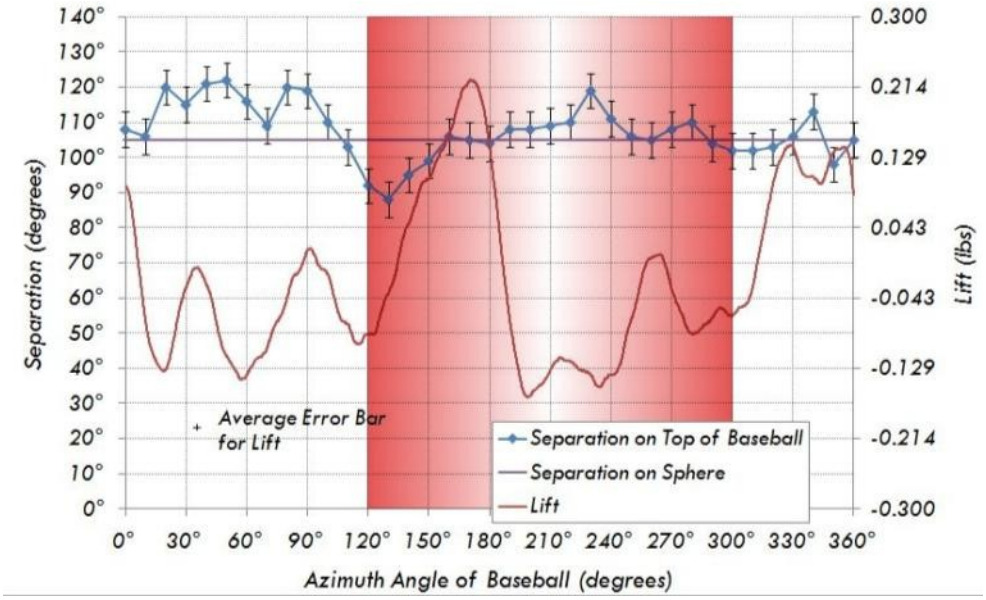

Fig. 4-3: A plot of separation on the top half of the baseball along with lift. The red area represents the area a common knuckleball is thrown today.

The hot film anemometry illustrates the importance of shear stress and separation on the baseball. As stated above, separation on the bottom part of the baseball was not recorded. However, separation was found through the hot films. Therefore, separation can be found on the bottom half of the baseball. It was shown through figures 3-49 and 3-50 that separation was more upstream as the hot films were rotating towards stagnation than when the hot films were rotating away from separation. This was a illogical arguments because the Magnus effect was so low. However, it was shown through Brown's photos from University of Notre Dame that a baseball can have lift when there was no rotation.

When the knuckleball was initially thrown, the azimuth angle of the baseball was at 120 degrees. As presented in figure 4-4, the shear stresses are initially low at 120 degrees; however, when stagnation hits the first seam at 150 degrees, the ball wants to rotate in the opposite direction due to the turbulent wake downstream of the second seam.

This was the critical motion that can make the knuckleball to be effective or not. If the shear stress downstream of the second seam was too strong, then the baseball will not rotate correctly, stagnation will go through the landing strip and the pitch be slow and flat. However, that same seam that creates the shear stress was also what changes separation, which makes the baseball move erratically. This was the toughest skill to master for knuckleballers. The pitcher must add just enough torque on the baseball so the ball does not rotate backwards, exposing the landing strip.

Lastly, because the seams act like a tripping wire, and the tripping wire delays separation, an argument can be built that the seam delays separation. Unfortunately, this was not seen in the flow visualization data. However, when referring to figure 4-2, lift has the greatest maximum between the seams, at 170 and 190 degrees. At 170 degrees,

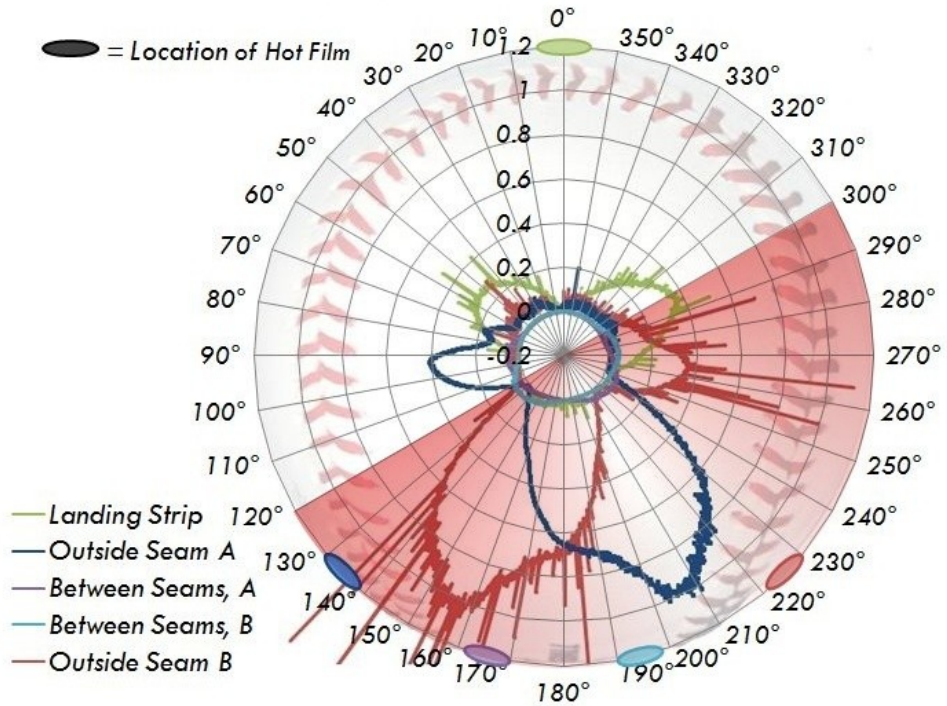

Fig. 4-4: Polar plots of the shear stress each hot film experiences. The red area represents the area a common knuckleball is thrown today.

the two nearest seams are 20 and 40 degrees away. Since a trip wire can delay separation when placed 10 to 60 degrees from stagnation, both of these seams should delay separation. However, 10 to 60 degrees is a large part of the surface of the baseball. So if this area was narrowed down, then the seam 40 degrees away from separation should delay separation. If this was true, then the lift of the baseball should be in the direction opposite of the side of the delayed separation. This was true for both maximum magnitudes of lift at 170 and 190 degrees. Although not fully proven, there was evidence that the seam does delay separation.

To organize these points better, a list was made below along with the supporting technique:

- Landing Strip acts as a smooth sphere
    - Separation from flow visualization
    - Shear stress profile from hot film
- Seams carry separation toward and away from stagnation
    - Separation from flow visualization
    - Indication of separation from shear stress profile from hot film
- Seams initiate and delay separation
    - Initiate at when seam is 90° to 120° from stagnation
        - Separation from flow visualization
        - Indication of separation from shear stress profile from hot film
    - Evidence that separation is delayed when seam is 10° to 60° from stagnation
        - Indication of separation from shear stress profile from hot film

- Evidence that rotation of baseball delays separation (not confirmed)
    - Indication of separation from shear stress profile from hot film rotating towards and away from stagnation

4.2. Future Work

While writing this thesis, many ideas were thought of to expand the research of the knuckleball, as well as some possible faults.

It would be very interesting to study how a knuckleball's lift and lateral forces as a function of humidity and ambient pressure. This would apply to a more relevant study of a knuckleball in different stadiums. For instance, the lowest humidity in any city that has a Major League ballpark is in Chase Field in Phoenix, Arizona. Chase Stadium is an indoor facility; however, spring training still exists outdoors. The stadium with the greatest humidity is Minute Maid Park in Houston, Texas. The stadium closest to sea level, thus highest pressure, is Fenway Park in Boston, Massachusetts. The stadium with the highest altitude, thus lowest pressure, is Coors Field in Denver, Colorado. It has been said that a ball will travel faster and farther but experience less aerodynamic forces in Coors Field due to the low pressure.

As stated before, there would be a better understanding if there was flow visualization data on the bottom half of the baseball. Then it could be proven if the seams carry separation away from stagnation. It would be equally as impressive if there was flow visualization data on the side of the baseball. The seams do not travel through the sides, but rather around. It would be very interesting to see how separation reacts with the seams.

Other tests that include recording the shear stress on a baseball, statically. This could help support the evidence that the seam acts like a trip wire and delays separation.

Lastly, there is interest of the shear stress between the seams. As stated in section 3.3.3, the reason there is no large amount of shear between the seams is because of the direction of the hot films. Thus, using the flow visualization technique with ink dots and solvent on the surface of the baseball between the seams can solidify this hypothesis. If the streaks of the ink dots perpendicular to the seams are not as long as parallel to seams, then this hypothesis would be correct.

This list of future work and others can help solidify on why a knuckleball "knuckles."

REFERENCES

1. Clark, D., *The Knucklebook*. 2006, Chicago: Ivan R. Dee.

2. Dickson, P., *The New Dickson Baseball Dictionary*. 2009, New York: W. W. Norton and Co.

3. Newton, I., *New Theory of Light and Colours.* Philos. Trans. R. Soc., 1672: p. 678-688.

4. Magnus, G., *On the Deviation of Projectiles; and on a Remarkable Phenomenon of Rotating Bodies.* Memoirs of the Royal Academy, 1852: p. 210-231.

5. Prandtl, L., *Essentials of Fluid Dynamics*. 1952, New York: Hafner Publishing Company, Inc.

6. Briggs, L.J., *Effect of Spin and Speed on the Lateral Deflection (Curve) of a Baseball; and the Magnus Effect for Smooth Spheres.* American Journal of Physics, 1959. **27**: p. 589-596.

7. Brown, F.N.M., *See the Wind Blow*. 1971, Department of Aerospace and Mechanical Engineering, University of Notre Dame.

8. Watts, R.G. and E. Sawyer, *Aerodynamics of a Knuckleball.* American Journal of Physics, 1975. **43**: p. 960-963.

9. Weaver, R., *Comment on 'Aerodynamics of a Knuckleball'.* American Journal of Physics, 1976. **44**: p. 1215.

10. Drury, J., *The Hell It Don't Curve*, in *The Fireside Book of Baseball*, C.E. Einstein, Editor. 1956, Simon and Shuster: New York.

11. Watts, R.G. and R. Ferrer, *The Lateral Force on a Spinning Sphere; Aerodynamics of a Curveball.* American Journal of Physics, 1987. **55**: p. 40-44.

12. Granger, R., *Fluid Mechanics*. 1985, New York: Holt, Rinehart and Winston.

13. Mizota, T., *Baseball and Golfball Aerodynamics.* The Japan Society of Mechanical Engineers, 2001. **15**: p. 2-3.

14. Alaways, L.W. and M. Hubbard, *Experimental Determination of Baseball Spin and Lift.* Journal of Sports Sciences, 2001. **19**: p. 349-358.

15. Aoki, K., et al., *Dependence of Aerodynamic Characteristics and Flow Pattern on Surface Structure of a Baseball.* Journal of Visualization, 2003. **6**: p. 185-193.

16. Nathan, A.M., *The Effect of Spin on the Flight of a Baseball.* American Journal of Physics, 2008. **76**: p. 119-124.

17. *GIMP - The GNU Image Manipulation Program*, in *Gimp 2.6*. 2009. Photoediting Software.

18. Achenbach, E., *Experiments on the Flow Past Spheres at Very High Reynolds Numbers.* Journal of Fluid Mechanics, 1972. **54**: p. 565-575.

19. Foss, J.F., *Hot Wire Anemometry Probe Fabrication Manual*, in *Hot Wire Anemometry Probe Fabrication Manua*, Turbulent Shear Flow Laboratory, Michigan State University.

20. Jorgensen, F., *How to Measure Turbulence With Hot-Wire Anamometers-A Practical Guide*. 2002, Skovlunde, Denmark: Dantec Dyamics, Publication no.: 9040U6151.

21. White, F.M., *Viscous Fluid Flows*. 1991, New York: McGraw Hill, Inc.

22. White, F.M., *Fluid Mechanics*. 2008, New York: McGraw Hill, Inc.

23. Chang, P.K., *Separation of Flow*. 1970, Oxford, New York: Pergamon Press.

24. Schlichting, H., *Boundary-Layer Theory*. 1979, New York: McGraw Hill, Inc.

25. Achenback, E., *Experiments on the Flow Past Spheres at Very High Reynolds Numbers.* Journal of Fluid Mechanics, 1972. **54**: p. 565-575.

26. Watts, R.G. and J. Walton, *The Kinematics of Baseball Pitches.* 1984: p. 3.

27. Mehta, R.D., *Aerodynamics of Sports Balls.* Annual Review of Fluid Dynamics, 1985. **17**: p. 151-189.

28. Adair, R.K., *The Physics of Baseball*. 1994, New York: HarperCollins.

29. Mehta, R.D. and J.M. Pallis, *Sports Ball Aerodynamics: Effects of Velocity, Spin, and Surface Roughness.* Materials and Science in Sports, 2001: p. 185-197.

30. Allman, W.F., *Pitching Rainbows: The Untold Physics of the Curveball.* Science, 1982. **82**: p. 32-39.

31. Allman, W.F., *Flight of the Knuckler.* Science, 1983. **83**: p. 92-93.

APPENDIX

A-1. LABVIEW PROGRAMS

A-1.1. Real Time

Front Panel

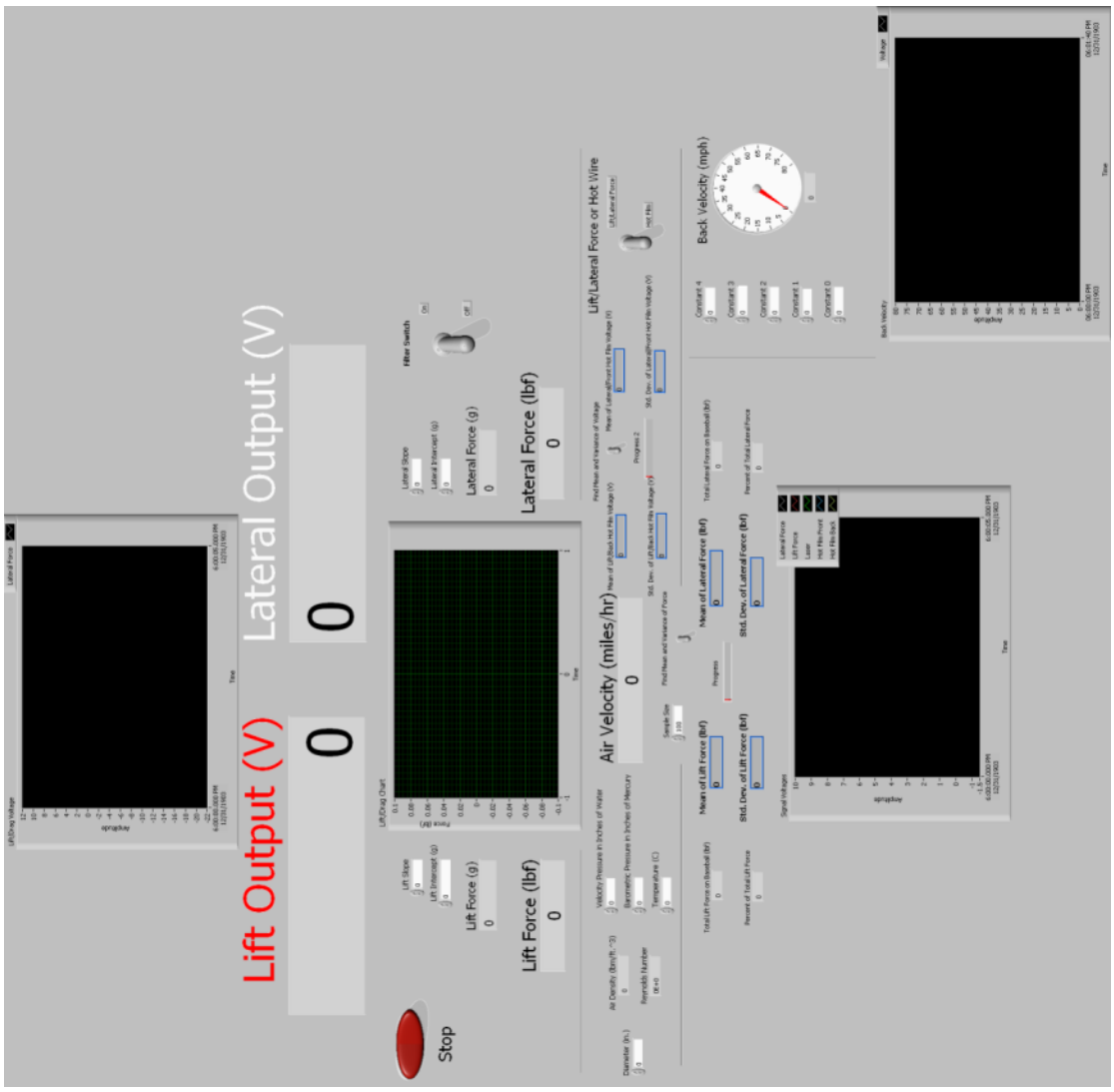

Block Diagram

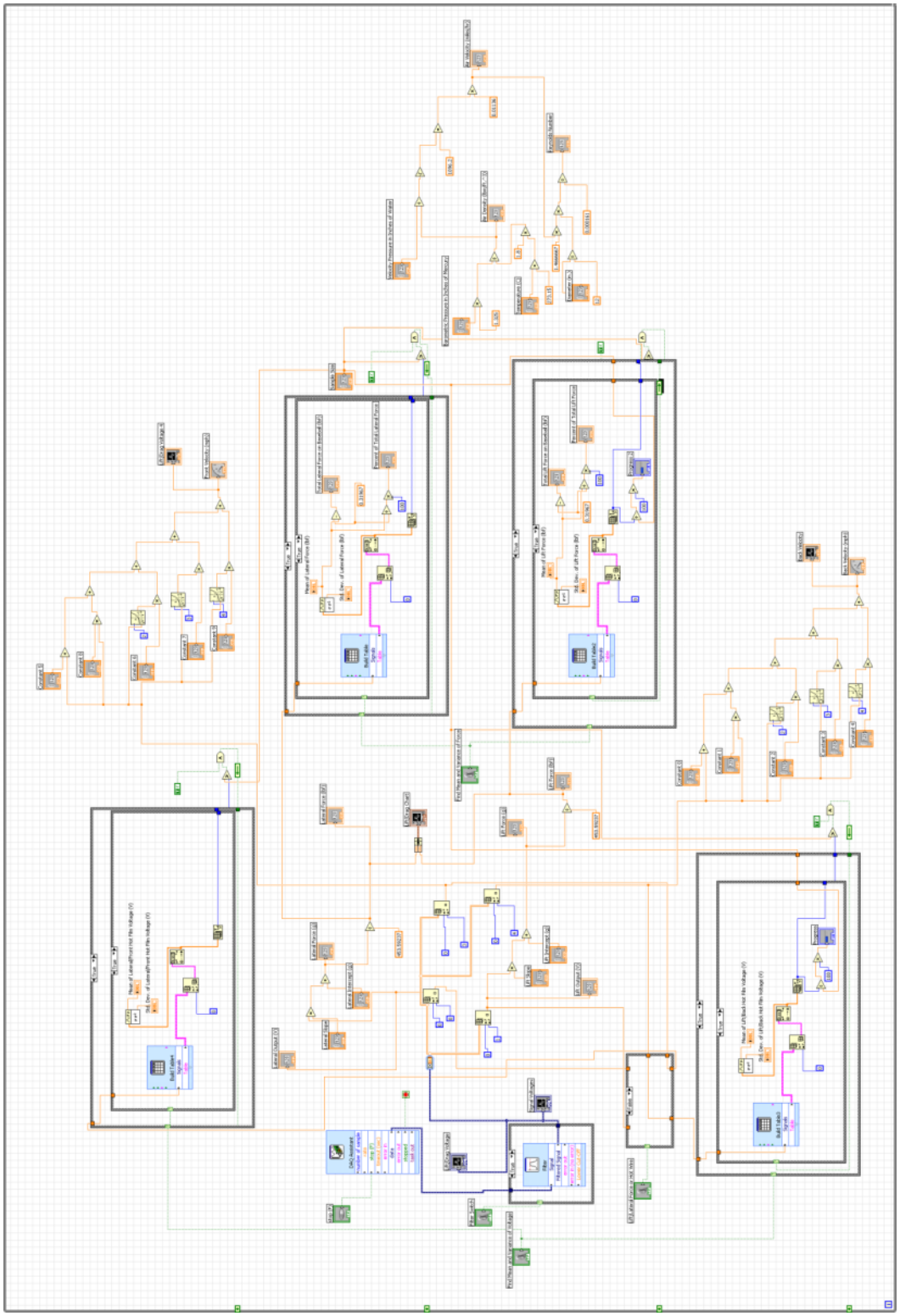

A-1.2. Single Data Collection

Front Panel

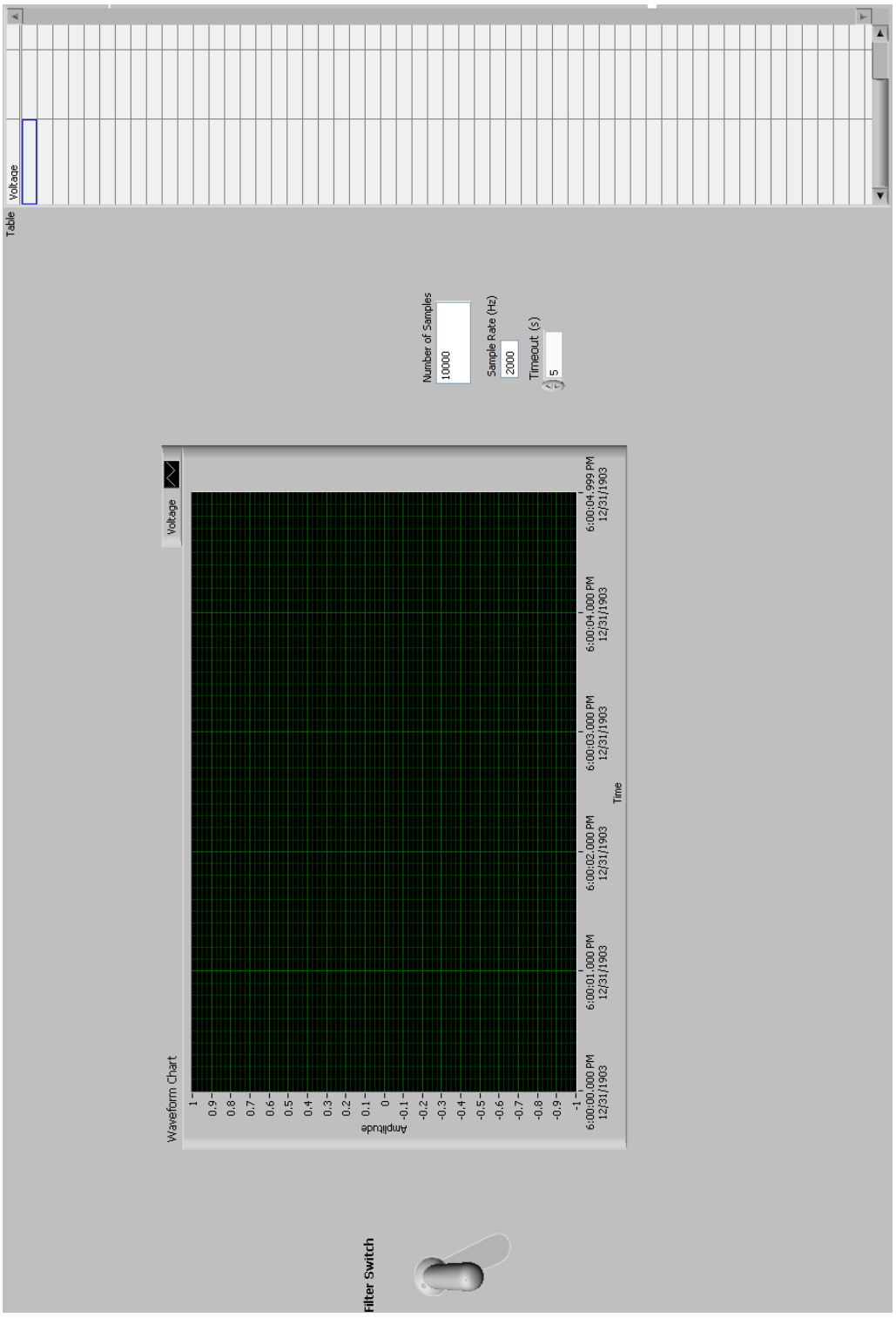

Block Diagram

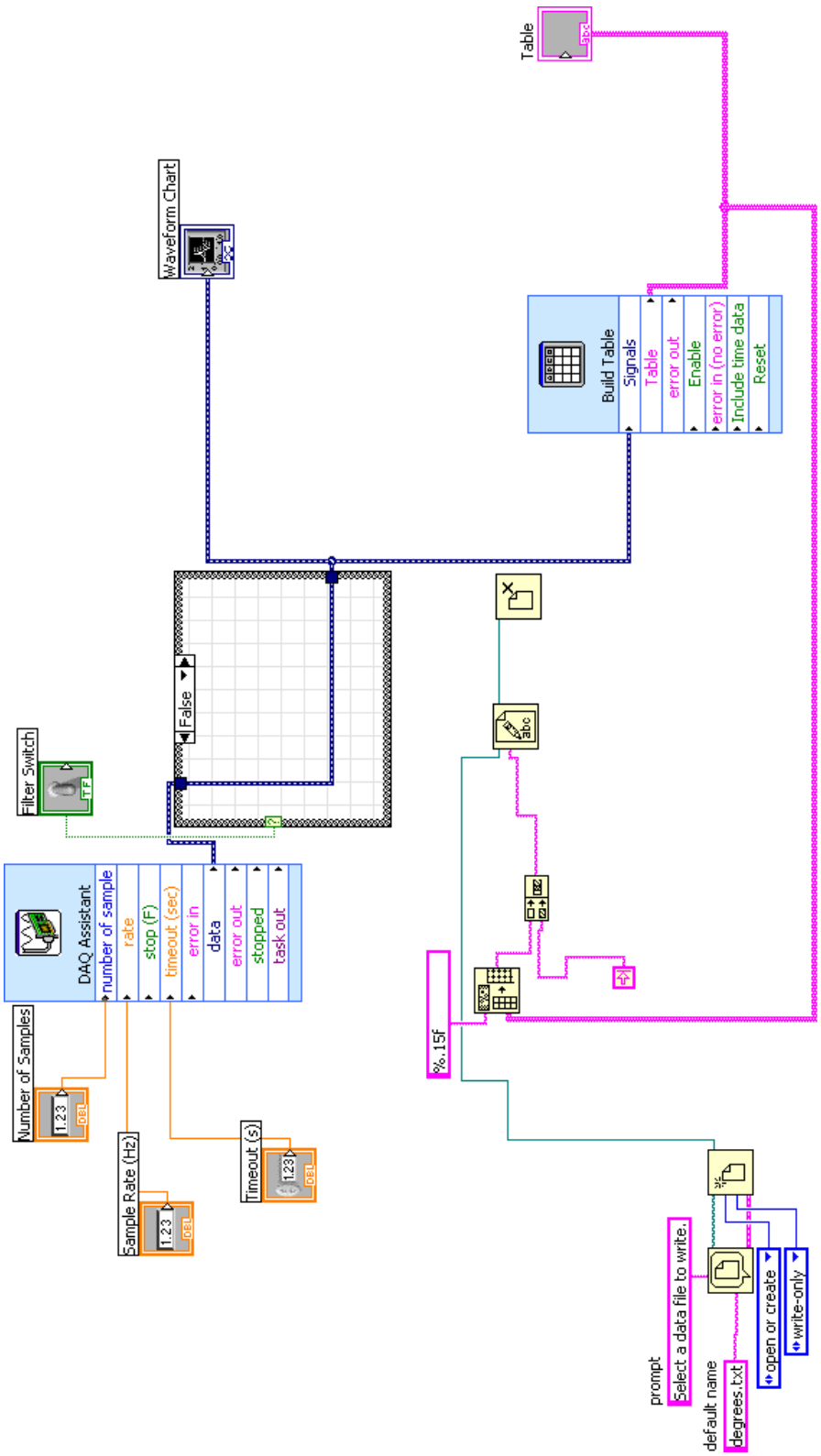

A-1.3. Multiple Data Collection

Front Panel

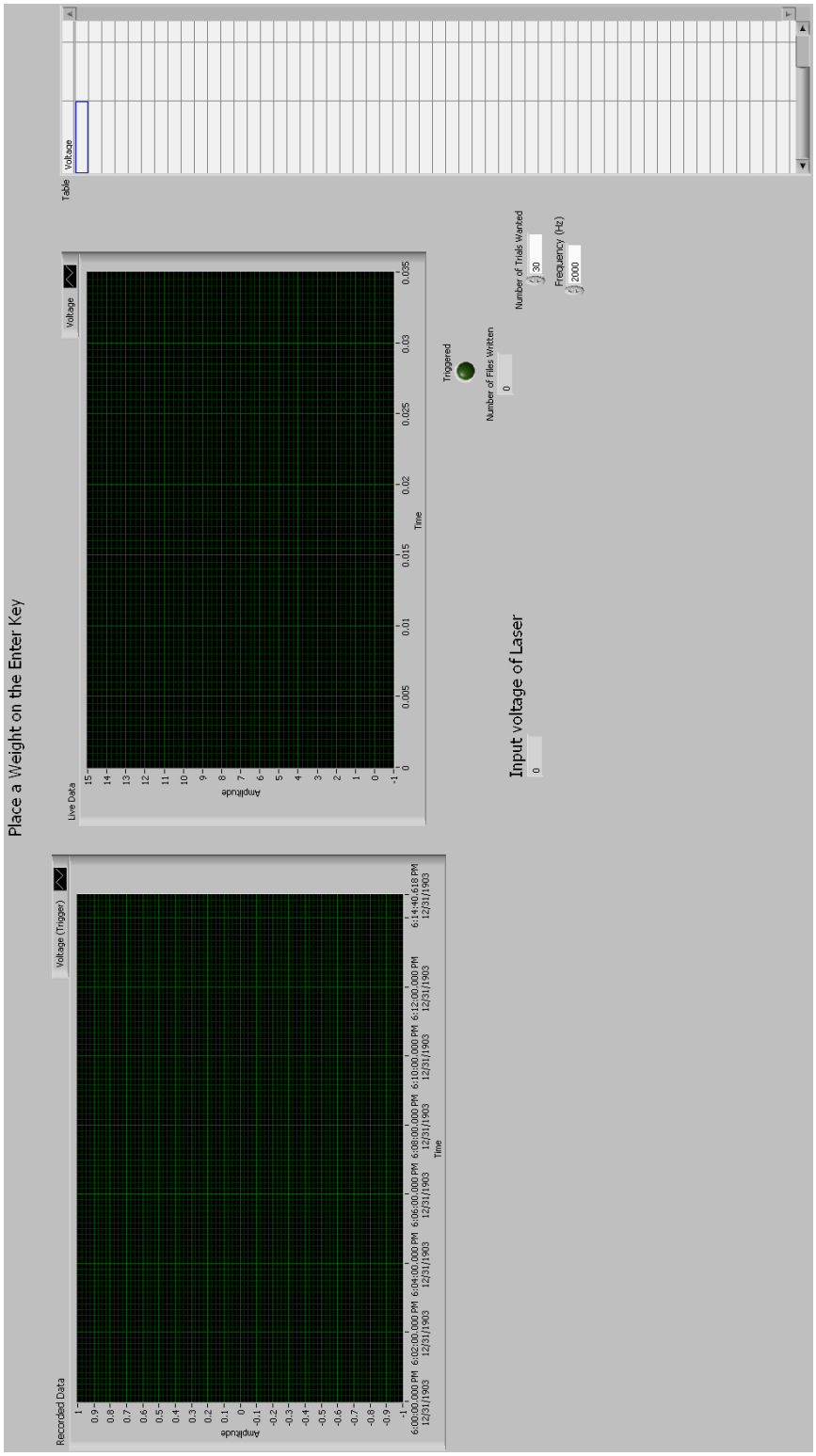

Block Diagram

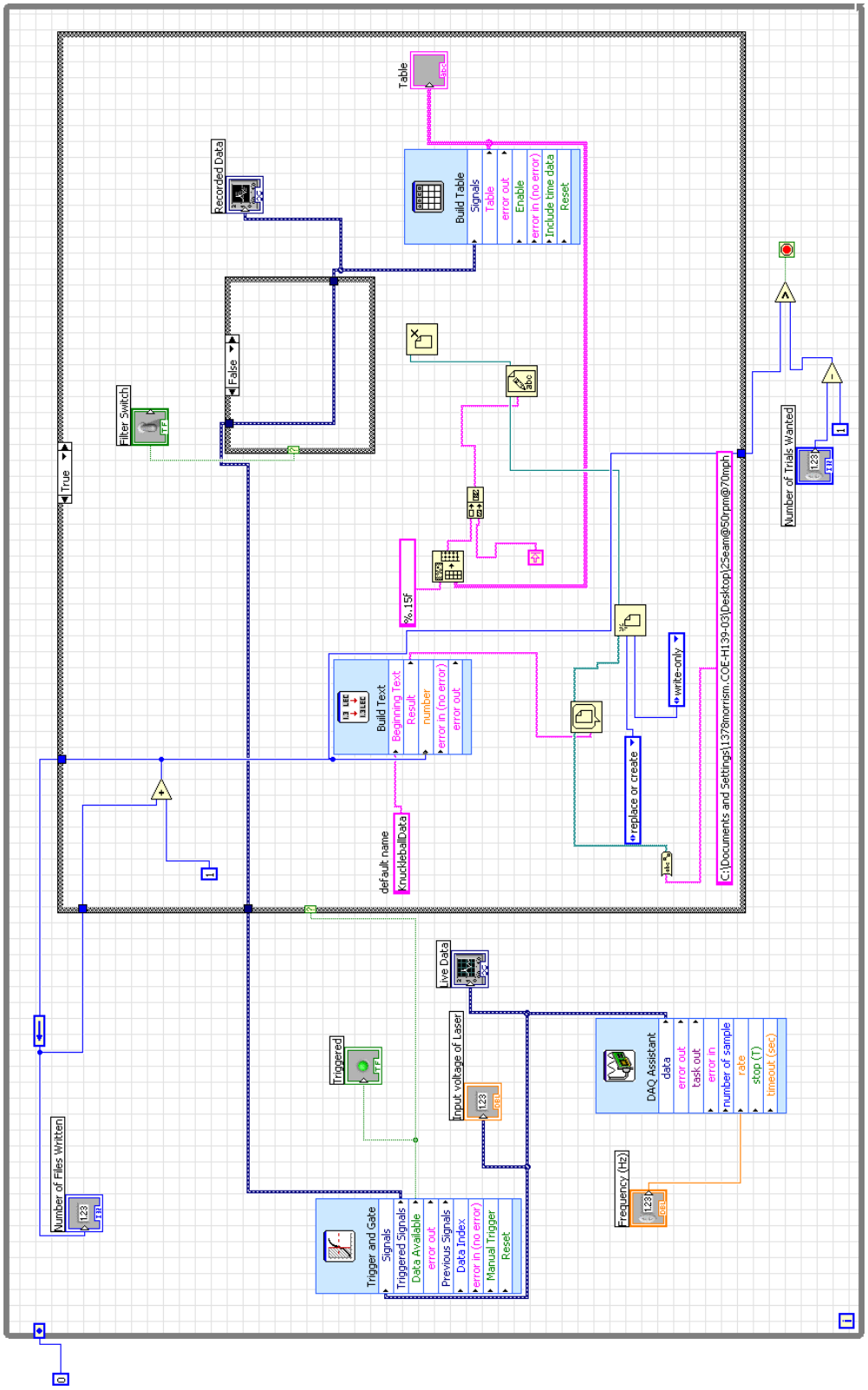

A-2. MATLAB PROGRAMS

A-2.1. Multiple Exposure Photo

```
clc; clear all;

%************************************************************
%This program superimposes images into a single image by taking the higher pixel
%************************************************************

%Number of images wanted to superimpose
image_num = 500;  %500 for still images, 600 for target images
trials = 1024;

root = input('Are you collecting Baseball(bb) or Smooth Sphere(ss) photos?  ','s');


if root == 'bb'
   second_root = input('Are you doing landing strip (ls) or seam (s)?  ','s');
   imagepath = 'C:\Users\Mike\Documents\Marquette Papers\Thesis Documents\Flow
Visualization\Wind Tunnel Flow
Visualization\Baseball\Still\BB_70mph_500fps_C001S0001';
else
   second_root = '1';
   imagepath = uigetdir('C:\Users\Mike\Documents\Marquette Papers\Thesis
Documents\Flow Visualization\Wind Tunnel Flow Visualization\Smooth
Sphere\Still\SS_70mph_500fps_C001S0001');
end

if second_root == 's'
   second_root = '2';
   imagepath = 'C:\Users\Mike\Documents\Marquette Papers\Thesis Documents\Flow
Visualization\Wind Tunnel Flow
Visualization\Baseball\Still\BB_70mph_500fps_C001S0002';
else
   second_root = '1';
end

patternname = '*.tif';

cd(imagepath)

oldimage(1:1024,1:1024) = 0.;

%Loads the image and superimposes them together
```

```
for k=1:trials %image_num

   %Finds image for corresponding trial and angle
   trial =k;
   if (trial < 10)
      variable = [root,'_70mph_500fps_c001s000',second_root,'00000',int2str(trial)];
   elseif (trial < 100)
      variable = [root,'_70mph_500fps_c001s000',second_root,'0000',int2str(trial)];
   elseif (trial < 1000)
      variable = [root,'_70mph_500fps_c001s000',second_root,'000',int2str(trial)];
   else
      variable = [root,'_70mph_500fps_c001s000',second_root,'00',int2str(trial)];
   end

   imagelist = dir(fullfile(imagepath,patternname));

   %Imports image from file
   imdata = imread(variable,'tiff');
   imdata = imrotate(imdata,-0.0,'bilinear','crop');  %change 0.0 to -12.0

   %Finds which element is higher, and replaces with the superimposed image element
   logicalIndex = imdata > oldimage;
   oldimage(logicalIndex) = imdata(logicalIndex);
   progress = 100.*k/trials
end
%Places a protractor on top of the images
% protractor = imread('protractor3.tif');
% logicalIndex = oldimage > protractor;
% oldimage(logicalIndex) = protractor(logicalIndex);
figure(1),imshow(oldimage,[0,256]); colormap('gray'); axis equal;
```

A-2.2. Statistical Analysis

```
clc; clear all;

%************************************************************
%This program find the fluctuation, biased covariance, and power spectra.
%************************************************************

%FINDS DIRECTORY TO LOAD DATA FROM
[filename,pathname,filterindex] = uigetfile('C:\Users\Mike\Desktop','*.txt');
cd(pathname)
signal = load (filename);

x = signal;
[row,col]=size(x);
N=row;     %this is the number of data points collected
NN= N/2;     % this is the number of data points to plot
Hz=2000;     %this is the sample frequency [cycle/s]
%x = signal(1:N,2);
%Not user inputs
deltat=N/Hz; %this is the total time sampled
time(1:N)=(0:N-1)/Hz;
f(1:N/2)=Hz*(1:N/2)/N;  %this is the frequency array
x0=x-mean(x);  %this is the fluctuation
x0=detrend(x);
%PDF
bins = 50.;
binsize= (double(int8(max(x))+1)-double(int8(min(x))-1))/bins;
[NN,ff] = hist(x,double(int8(min(x))-1):binsize:double(int8(max(x))+1));

%PDF time rate of change
delx = 0.;
for i = 1:N-1
   delx(i) = x(i+1) - x(i);
end

binsize1= (double(int8(max(delx))+1)-double(int8(min(delx))-1))/bins;
[Nd,fd] = hist(delx,double(int8(min(delx))-1):binsize1:double(int8(max(delx))+1));

% Autocovariance
R(1:N)=0; %zero out the array for autocovariance
for i = 1:N
   ii = 0;
   for j = 0:N-i
      ii   = ii   + 1;
      R(i) = R(i)+ x0(ii+i-1)*x0(ii);  %*(1/(pi*(amp1^2-x0(ii)^2)^0.5));
```

```
   end
   R(i)  = R(i)/N;      %autocovariance - dividing by ii completes the algrebraic average
   rho(i)= R(i)/var(x0); %autocorrelation - normalized R
end
%
% Spectrum
VarE = 0;  %This is the variance under the spectrum
E(1:N) = 0;
for i=1:N/2    %this is the omega or frequency dimension
   for j=1:N  %this is the s or time lag dimension
      E(i) = E(i) + R(j)*cos( 2*pi*f(i) * deltat*(j-1)/N )*(time(5)-time(4)); %this is
intgration of R(s)cos(ws)ds
   end
   E(i) = (2/pi)*E(i);
   VarE = VarE + (E(i))*(2*pi*(Hz/2)/N); %this is a trapizodial integration
end

FastF=fft(x0);
%
%   The relationship between the DFT and the Fourier coefficients a and b in
%              N/2
%   x(n) = a0 + sum a(k)*cos(2*pi*k*t(n)/(N*dt))+b(k)*sin(2*pi*k*t(n)/(N*dt))
%              k=1
%   is
%      a0 = 2*X(1)/N, a(k) = 2*real(X(k+1))/N, b(k) = 2*imag(X(k+1))/N,
%   where x is a length N discrete signal sampled at times t with spacing dt.
%
a1=sqrt((real(FastF(1:N))/N).^2+(imag(FastF(1:N))/N).^2);
a1(1)=FastF(1)/N;
Mean1=a1(1);
figure(1),plot(time(1:N),x0(1:N),'.-');title('Fluctuation of U');xlabel('time [s]');ylabel('xo');
%figure(2),plot(time(1:N),R,'.-');title('Biased Covariance of U');xlabel('time
[s]');ylabel('R(s)');
figure(3),plot(f,E(1:N/2),'.-');title('Power Spectra');xlabel('Frequency (cycle/s)');ylabel('E
(omega)'); axis tight;
%figure(4),plot(ff,NN./sum(NN),'.-');xlabel('Percentage
(%)');ylabel('Frequency');title('Probability Density Function of EFF'); axis tight;
figure(5),loglog(f,E(1:N/2),'.-');title('Power Spectra');xlabel('Frequency
(cycle/s)');ylabel('E (omega)'); axis tight; grid on;
%figure(9),plot(fd,Nd./sum(Nd),'.-');xlabel('Percentage
(%)');ylabel('Frequency');title('Probability Density Function of \Delta U(t)'); axis tight;

Variance=var(x0)
VarE
```

A-2.3. Non-Spinning Baseball Statistical Analysis

```
clc; clear all;

%************************************************************
%This program computes the average and standard deviations of the
%non-spinning data and converts the voltages to grams.
%************************************************************

 trials = 9;    %max is 9 for now
 angles = 36;    %max is 36

 %Converts Voltage into grams
 % 4-seam non-spinning 46 mph; slope: 151.64, y-int: 1.7092
 % 2-seam spinning and non-spinning 70 mph; slope: 138.84, y-int: -3.4375

 slope = 151.64;
 y_int = 1.7092;

 patternname = '*.txt';
 masterdatapath = uigetdir('C:\Users\Mike\Documents\Marquette Papers\Thesis
Documents\Raw Data\Knuckleball data\MLB Baseball Mod Bar\4Seam46mph','Select
Folder with Trials');

 for angle=0:angles

    %Finds image for corresponding trial and angle
   for trial=1:trials
    %progresstrial = trial
    variable = ['Trial ',int2str(trial)];

    datapath = fullfile(masterdatapath,variable);
    cd(datapath)
    datalist = dir(fullfile(datapath,patternname));

   interval = angle*10;
   dTheta(angle+1) = interval;
   variabledata = [int2str(interval),'degrees.txt'];
   %Loads data from file
   S = load (variabledata);

   all(angle+1,trial) = mean(S(1:5000,2));
   errorbar(angle+1,trial) =  std(S(1:5000,2));

   end
   progress = angle*100/36.
```

```
    average(angle+1,1) =  0.0022046226218*(slope*(mean(all(angle+1,1:trial)))+y_int);
    AveErrorBar(angle+1,1) =
0.0022046226218*(slope*(mean(errorbar(angle+1,1:trial)))+y_int);
 end
%average = detrend(average);
 %shift = mean(average)

 figure(1),plot(dTheta,average-shift,'.-b');ylabel('Force (g)');xlabel('Orientation
(degrees)');axis([0 360 -.15 .15]);
 set(gca,'XTick',0:30:360)
```

A-2.4. Spinning Baseball Statistical Analysis

```
clc; clear all;

%************************************************************
%This program finds the Fourier Transform of any signal, and is
%able to modify the signal to cancel out noise.  It also compares
%other Fourier Transform signals.
%************************************************************

%**********************INPUTS*****************************
load('resonance_frequencyFFX.mat', '-mat')
load('MotorOnlyFFX.mat', '-mat')
%*********************************************************

 %Converts Voltage into grams
 slope_lift = 138.84;
 y_int_lift = -3.4375;
 slope_lateral = 171.01;
 y_int_lateral = -4.4283;

Combineda1 = RSa1;

total = 0.;
N = 1000000.;

%FINDS DIRECTORY TO LOAD DATA FROM
directory_path = uigetdir('C:\Users\Mike\Documents\Marquette Papers\Thesis
Documents\Raw Data\Knuckleball data');
cd(directory_path)

%PROMPTS FOR FREQUENCY INPUT
Hz = input('What is the frequency of the data collected (Hz)?  ');

%READS ALL DATA THAT ENDS WITH .TXT----------------------
%finds number of files that end with .txt
files = dir('*.txt');

rootname = 'KnuckleballData';      % Root filename
extension = '.txt';     % Extension of the files
       for data = 1:length(files)
         variable = [rootname, int2str(data)];
         filename = [variable, extension];
         eval(['load ', filename])
         eval(['data', num2str(data), ' = ', variable, ';'])
         eval(['minN = size(data',num2str(data),');'])
```

```
        eval(['if N>minN(1), N = minN(1);,end'])  %trims down arrays to row minimum
        eval(['clear ', variable])
       end
%-------------------------------------------------------------------------------
%*******************************************************************************
****
%CALCULATES TOTAL OF ALL LIFT DATA
     for data = 1:length(files)
        eval(['total = data', num2str(data),'(1:N,3) + total;'])
     end

     for i = 1:N
        for data = 1:length(files)
          variable = ['data',int2str(data)];
          AngleData(i,data) = eval(['data',num2str(data),'(i,3)']);
        end
        ErrorBar(i) = std(AngleData(i,1:length(files)));
     end


%CALCULATES AVERAGE OF ALL DATA
average = total/(length(files));
%average = detrend(average);
%-----------------------------------
%FOURIER TRANSFORM
FastFx = fft(average);
FastFxEB = fft(ErrorBar);
%-----------------------------------
a1=sqrt((real(FastFx(1:N))/N).^2+(imag(FastFx(1:N))/N).^2);
a1(1)=FastFx(1)/N;
power = FastFx.*conj(FastFx)/N;
f(1:N/2)=Hz*(1:N/2)/N;

%-----------------------------------
%DELETES FREQUENCIES DESIRED
FastFxmod = FastFx;
FastFxEBmod = FastFxEB;
      for i = 13:41%29
         FastFxmod(i) = 0.;
         FastFxEBmod(i) = 0.;
      end

      for i = 32:37
         FastFxmod(i) = 0.;
         FastFxEBmod(i) = 0.;
      end
```

```
    for i = N-41:N-13%29
       FastFxmod(i) = 0.;
       FastFxEBmod(i) = 0.;
    end
    for i = N-37:N-32
       FastFxmod(i) = 0.;
       FastFxEBmod(i) = 0.;
    end
 %-------------------------------------
a1mod=sqrt((real(FastFxmod(1:N))/N).^2+(imag(FastFxmod(1:N))/N).^2);
a1mod(1)=FastFxmod(1)/N;
powermod = FastFxmod.*conj(FastFxmod)/N;

%-------------------------------------
%INVERSE FOURIER TRANSFORM
InvFastFx = ifft(FastFxmod);
InvFastFxEB = ifft(FastFxEBmod);
%-------------------------------------
%**********************************************************************
****
total_lateral = 0.;
%CALCULATES TOTAL OF ALL LATERAL DATA
    for data = 1:length(files)
       eval(['total_lateral = data', num2str(data),'(1:N,2) + total_lateral;'])
    end

    for i = 1:N
       for data = 1:length(files)
          AngleData_lateral(i,data) = eval(['data',num2str(data),'(i,2)']);
       end
       ErrorBar_lateral(i) = std(AngleData_lateral(i,1:length(files)));
    end


%CALCULATES AVERAGE OF ALL DATA
%average_lateral=total_lateral;
average_lateral = total_lateral/(length(files));
%average = detrend(average);
%-------------------------------------
%FOURIER TRANSFORM
FastFx_lateral = fft(average_lateral);
FastFxEB_lateral = fft(ErrorBar_lateral);
%-------------------------------------
a1_lateral=sqrt((real(FastFx_lateral(1:N))/N).^2+(imag(FastFx_lateral(1:N))/N).^2);
a1_lateral(1)=FastFx_lateral(1)/N;
power_lateral = FastFx_lateral.*conj(FastFx_lateral)/N;
```

```
f(1:N/2)=Hz*(1:N/2)/N;

%-------------------------------------
%DELETES FREQUENCIES DESIRED
FastFxmod_lateral = FastFx_lateral;
FastFxEBmod_lateral = FastFxEB_lateral;
      for i = 13:29
         FastFxmod_lateral(i) = 0.;
         FastFxEBmod_lateral(i) = 0.;
      end

      for i = 32:37
         FastFxmod_lateral(i) = 0.;
         FastFxEBmod_lateral(i) = 0.;
      end
      for i = N-29:N-13
         FastFxmod_lateral(i) = 0.;
         FastFxEBmod_lateral(i) = 0.;
      end
      for i = N-37:N-32
         FastFxmod_lateral(i) = 0.;
         FastFxEBmod_lateral(i) = 0.;
      end
 %-------------------------------------
a1mod_lateral=sqrt((real(FastFxmod_lateral(1:N))/N).^2+(imag(FastFxmod_lateral(1:N)
)/N).^2);
a1mod_lateral(1)=FastFxmod_lateral(1)/N;
powermod_lateral = FastFxmod_lateral.*conj(FastFxmod_lateral)/N;

%-------------------------------------
%INVERSE FOURIER TRANSFORM
InvFastFx_lateral = ifft(FastFxmod_lateral);
InvFastFxEB_lateral = ifft(FastFxEBmod_lateral);
%-------------------------------------

%-------------------------------------
%CONVERTS THE VOLTAGE TO GRAMS FROM CALIBRATION
average_lift = (slope_lift*average + y_int_lift);
InvFastFx_lift = (slope_lift*InvFastFx +y_int_lift);
InvFastFxEB_lift = (slope_lift*InvFastFxEB +y_int_lift);
average_lateral = (slope_lateral*average_lateral + y_int_lateral);
InvFastFx_lateral = (slope_lateral*InvFastFx_lateral +y_int_lateral);
InvFastFxEB_lateral = (slope_lateral*InvFastFxEB_lateral +y_int_lateral);
%-------------------------------------
InvFastFxReal_lift = real(InvFastFx_lift);
InvFastFxEBReal_lift = real(InvFastFxEB_lift);
```

```
InvFastFxReal_lateral = real(InvFastFx_lateral);
InvFastFxEBReal_lateral = real(InvFastFxEB_lateral);

corrx_lift = normxcorr2(real(InvFastFx_lift),real(InvFastFx_lift));
corrx_lateral = normxcorr2(real(InvFastFx_lateral),real(InvFastFx_lateral));
NN = (1:N);

Lift_average = mean(InvFastFx_lift);
Lateral_average = mean(InvFastFx_lateral);
InvFastFx_lateral = InvFastFx_lateral-Lateral_average;
InvFastFxReal_lateral = real(InvFastFx_lateral);

FFTx_axis = f(1:N/2);
FFTy_axis = 2*a1(2:N/2+1);
FFTy_axismod = 2*a1mod(2:N/2+1);
FFTx_axismod = RSf(1:1137);
LIFT_ORIGNx_axis = NN/Hz;
LIFT_ORIGNy_axis = average_lift;
LAT_ORIGNx_axis = NN/Hz;
LAT_ORIGNy_axis = average_lateral;

figure(4),semilogy(f(1:N/2),FastFx(1:N/2),'.-b',RSf(1:1137),RSFastFx(1:1137),'.-
r',f(1:N/2),FastFxmod(1:N/2),'.-k');axis([0 1000 -2000 4000]);h = legend('Baseball
Data','Motor and Resonance Freq.','Baseball Data
Mod',1);set(h,'Interpreter','none');title('FFT of Data');xlabel('Frequency
(Hz)');ylabel('Amplitudes');
figure(5),semilogy(f(1:N/2),2*a1(2:N/2+1),'.-b',RSf(1:1137),2*RSa1(2:1137+1),'.-
r',f(1:N/2),2*a1mod(2:N/2+1),'.-k');h = legend('Baseball Data','Motor and Resonance
Freq.','Baseball Data Mod',1);set(h,'Interpreter','none');axis([0 1000 0
1.4]);title('Amplitudes of FFT Data');xlabel('Frequency (Hz)');ylabel('Amplitudes');
figure(6),plot(NN/Hz,average_lift,'.-b',NN/Hz,InvFastFx_lift,'.-r');xlabel('time
(s)');ylabel('Force (g)');h = legend('Baseball Data','Baseball Data
Mod',1);set(h,'Interpreter','none');title('Baseball Data Lift');axis([0 1.2 -90 90]);
figure(7),plot(NN/Hz,average_lateral,'.-b',NN/Hz,InvFastFx_lateral,'.-r');xlabel('time
(s)');ylabel('Force (g)');h = legend('Baseball Data','Baseball Data
Mod',1);set(h,'Interpreter','none');title('Baseball Data Lateral');%axis([0 1.2 -90 90]);
figure(8),plot(NN/Hz,InvFastFx_lift,'.-b',NN/Hz,InvFastFx_lateral,'.-r');xlabel('time
(s)');ylabel('Force (g)');h = legend('Baseball Lift','Baseball
Lateral',1);set(h,'Interpreter','none');title('Baseball Data Lateral');%axis([0 1.2 -90 90]);
```

A-2.5. Movie Compiler

```
clc; clear all;

%************************************************************
%This program superimposes all of the images on a specific angle
%and compiles a movie as well as saves the image of each frame.
%************************************************************

trials = 57;    %max is 57
angles = 600;    %max is 600
minx = 1;
maxx = 1024;
miny = 1;
maxy = 1024;

patternname = '*.tif';

mov = avifile('2SeamSpinningMovie.avi','fps',6);
fig=figure;
set(fig,'DoubleBuffer','on');
set(gca,'xlim',[1 1024],'ylim',[1 1024],'NextPlot','replace','Visible','off');
masterimagepath = uigetdir('C:\Users\Mike\Documents\Marquette Papers\Thesis
Documents\Wind Tunnel Flow Visualization\Baseball\Spinning');
for angle=1:angles
   oldimage(minx:maxx,miny:maxy) = 0;

   %Finds image for corresponding trial and angle
   for trial=1:trials
    if (trial < 10)
       variable = ['BB_70mph_500fps_C001S000',int2str(trial)];
    elseif (trial < 100)
       variable = ['BB_70mph_500fps_C001S00',int2str(trial)];
    else
       variable = ['BB_70mph_500fps_C001S0',int2str(trial)];
    end

    imagepath = fullfile(masterimagepath,variable);
    cd(imagepath)
    imagelist = dir(fullfile(imagepath,patternname));

    %Imports image from file
    imdata = imread(fullfile(imagepath,imagelist(angle).name));

    %Finds which element is higher, and replaces with the superimposed image element
    logicalIndex = imdata > oldimage;
```

```
    oldimage(logicalIndex) = imdata(logicalIndex);
   end
    imagename = ['frame',int2str(angle),'.tif'];
    %Shows image, saves image, and creates movie
    imshow(oldimage,[0,256]); colormap('gray'); axis equal; axis([minx maxx miny
maxy]);
    imwrite(uint8(oldimage),imagename,'tif')
    F = getframe(gca);
    mov = addframe(mov,F);

    progress = angle
 end

mov = close(mov);
```

A-2.6. Tracer Movie Compiler

```
clc; clear all;

%************************************************************
%This program compiles the tracer images into a movie.
%************************************************************

angles = 600;    %max is 600
minx = 1+51;
maxx = 1024-51;
miny = 1+51;
maxy = 1024-51;

patternname = '*.tif';

mov = avifile('2SeamSpinningMovieTracerModProtractor.avi','fps',6);
fig=figure;
set(fig,'DoubleBuffer','on');
set(gca,'xlim',[1 1024],'ylim',[1 1024],'NextPlot','replace','Visible','off');
imagepath = uigetdir('C:\Users\Mike\Documents\Marquette Papers\Thesis
Documents\Flow Visualization\Wind Tunnel Flow Visualization');
cd(imagepath)
imagelist = dir(fullfile(imagepath,patternname));
protractor = imread('protractor3.tif');

for angle=1:angles
   variable = ['frame',int2str(angle)];
   %Imports image from file
   imdata = imread(variable,'tif');
   imdata = imrotate(imdata,-12.0,'bilinear','crop');  %change 4.0 to -6.0

   %Horizontal mirror of image
   %imdata = fliplr(imdata);

   %Places a protractor on top of the images
   logicalIndex = imdata > protractor;
   imdata(logicalIndex) = protractor(logicalIndex);

   if angle <= 571
      imagename = ['TracerProtractorFrame',int2str(angle+29),'.tif'];
   else
      imagename = ['TracerProtractorFrame',int2str(angle-571),'.tif'];
   end
   imwrite(uint8(imdata),imagename,'tif')
```

```
    progress = angle
end

for angle=1:angles
    variable = ['TracerProtractorFrame',int2str(angle)];
    %Imports image from file
    imdata = imread(variable,'tif');
    %Shows image, saves image, and creates movie
    imshow(imdata,[0,256]); colormap('gray'); axis equal; axis([minx maxx miny maxy]);

    F = getframe(gca);
    mov = addframe(mov,F);
end

mov = close(mov);
```

A-2.7. Hot Film Analysis

```
clc; clear all;

%This program analyzes all the data for the hot film

answer = input('Is this for landing strip (ls) or seams (s)? ','s');
cal_input = input('Would you like to apply calibration? (Y/N) ','s');

if cal_input == 'Y'
   y_axis = 'Shear Stress (lbf/ft^2)';
else
   y_axis = 'Voltage (V)';
end

%**********************LANDING STRIP**************************
if answer == 'ls'

   pathname = 'C:\Users\Mike\Documents\Marquette Papers\Thesis
Documents\HotFilm\Hot Film Collected Data\Landing Strip\Modified Landing Strip Hot
Film Collected Data\Gathered Data Landing Strip';
   cd(pathname)

   file_number = 30;
   tau_total(1:2800) = 0.;

   for i = 1:file_number
      %Loads data
      file = ['KnuckleballData',int2str(i),'.txt'];
      data = load (file);
      N = size(data);
      N  = N(1,1);
      tau = data(1:N,3);
      taumod = tau;
      localmin = 1000;
      time = 1:N;

      %Centers stagnation in the middle of the plot
      for t = 1000:1600;
         if abs(taumod(t)-taumod(t+1)) > .03 & abs(taumod(t)-taumod(t-1)) > .03
%Cancels noise
            taumod(t) = 10;
         end
         if taumod(t) < localmin
            localmin = taumod(t);
            localminlocation = t;
```

```
        end
    end

    shift = 1200 - localminlocation;
    time = 1+shift:N+shift;

    if cal_input == 'Y'
        %Converts Voltage into Shear Stress
        for j = 1:N
            tau(j) = (.0316*tau(j)^2-.2421)^3; %14.3 Ohm hot film
        end
    end

    %Ensamble Average of all data
    for j = 1:N
        if (j+shift) > 0
            tau_total(j+shift) = tau(j)+tau_total(j+shift);
        end
    end

    %Plots all of the results on one graph
    figure(1),plot(time/2000., tau);xlabel('Time (s)'),ylabel(y_axis);title('Shear Stress on
Landing Strip of Baseball');%axis([0 1.2 0 2]);

    hold on;
  end
  hold off;

  tau_average = tau_total/file_number;
  time1 = [1:2800]';
  tau_average = tau_average';

  %Finds std of the data
%    for i = 1:2800
%        variance(i) = std(tau(i));
%    end

   cd('C:\Users\Mike\Desktop');
   xlswrite('HotFilmData.xls', tau_average, 'LandingStrip', 'B1');
   xlswrite('HotFilmData.xls', time1/2000., 'LandingStrip', 'A1');
  figure(2),plot(time1/2000.,tau_average);xlabel('Time
(s)'),ylabel(y_axis);title('Ensamble Average of the Shear Stress');%axis([0 1.2 0 2]);

%***************SEAMS*************************************************
******
elseif answer == 's'
```

```
   answer2 = input('Normal Direction (nd) or Reverse Direction (rd)? ','s');
   if answer2 == 'nd'
      pathname = 'C:\Users\Mike\Documents\Marquette Papers\Thesis
Documents\HotFilm\Hot Film Collected Data\Seams\Normal Rotation\Modified Seams
Hot Film Collected Data\Gathered Data Seams Normal Rotation';
      file_number = 30;
   elseif answer2 == 'rd'
      pathname = 'C:\Users\Mike\Documents\Marquette Papers\Thesis
Documents\HotFilm\Hot Film Collected Data\Seams\Reverse\Modified Seams Hot Film
Collected Data\Gathered Data Seams Reverse Direction';
      file_number = 24;
   else
      retry = 'Please enter nd or rd'
   end
count = 0
   cd(pathname)

   tau1_total(1:2800) = 0.;
   tau2_total(1:2800) = 0.;

   for i = 1:file_number
      %Loads data
      file = ['KnuckleballData',int2str(i),'.txt'];
      data = load(file);
      N = size(data);
      N  = N(1,1);
      tau1 = data(1:N,3);
      tau2 = data(1:N,2);
      taumod = tau1;
      localmin = 1000;
      time = 1:N;

      %Centers stagnation in the middle of the plot
      for t = 900:1600;
         if abs(taumod(t)-taumod(t+1)) > .03 & abs(taumod(t)-taumod(t-1)) > .03
%Cancels noise
            taumod(t) = 10;
         end
         if taumod(t) < localmin
            localmin = taumod(t);
            localminlocation = t;
         end
      end

      if answer2 == 'nd'
         shift = 1106 - localminlocation;  %Places second hot film at 166 degrees
```

```
      else
         shift = 1293 - localminlocation;  %Places first hot film at 204 degrees
      end
      time = 1+shift:N+shift;

      if cal_input == 'Y'
         %Converts Voltage into Shear Stress
         for i = 1:N
            tau1(i) = (.0316*tau1(i)^2-.2421)^3;%(.0207*tau1(i)^2+.1982)^3; %14.3 Ohm
Hot Film
            tau2(i) = (.0219*tau2(i)^2+.2059)^3;%(.0316*tau2(i)^2-.2421)^3; %10.3 Ohm
hot Film
         end
      end

      %Ensamble Average of all data
      for j = 1:N
         if (j+shift) > 0
            tau1_total(j+shift) = tau1(j)+tau1_total(j+shift);
            tau2_total(j+shift) = tau2(j)+tau2_total(j+shift);
         end
      end

      logic = 0;
      for j = 1:N
         if tau2(j) > 3 & logic == 0
            count = count + 1
            logic = 1;
         end
      end
      %Plots all of the results on one graph
      figure(1),plot(time/2000., tau1,'-b',time/2000.,tau2,'-r');xlabel('Time
(s)');ylabel(y_axis);title('Shear Stress Before and after a Seam on Baseball');%axis([0 1.2
0 2]);
      hold on;
   end
   if answer2 == 'nd'
      legend('Second Hot Film','First Hot Film','Location','Northwest');
   elseif answer2 == 'rd'
      legend('First Hot Film','Second Hot Film','Location','Northwest');
   else
      retry = 'Please enter nd or rd'
   end
   hold off;
    tau1_average = (tau1_total/file_number)';
    tau2_average = (tau2_total/file_number)';
```

```
    time1 = [1:2800]';
    cd('C:\Users\Mike\Desktop');
     xlswrite('HotFilmData.xls', tau2_average, 'Seam', 'C1');
     xlswrite('HotFilmData.xls', tau1_average, 'Seam', 'B1');
     xlswrite('HotFilmData.xls', time1/2000., 'Seam', 'A1');
    figure(2),plot(time1/2000.,tau1_average,'-b',time1/2000.,tau2_average,'-
r');xlabel('Time (s)'),ylabel(y_axis);title('Ensamble Average of the Shear
Stress');%axis([0 1.2 0 2]);

    if answer2 == 'nd'
       legend('Second Hot Film','First Hot Film','Location','Northwest');
    elseif answer2 == 'rd'
       legend('First Hot Film','Second Hot Film','Location','Northwest');
    else
       retry = 'Please enter nd or rd'
    end

    %INCORRECT
RESPONSE**************************************************
else
    retry = 'Please enter ls or s'
end
```

A-2.8. Blasius Profile

```
clc; clear all;

%PROMPTS FOR VELOCITY INPUT
Umph = input('What is the velocity? (mph)  ');

ReKnuckleball = 1.6E5;
nu = 1.61E-4;
U = 1.46666666*Umph; %(ft/s)
mu = 3.82E-7;
f = 0.4696;

%Length on plate where Re = 1.6e5
x = ReKnuckleball*nu/U;
maxi = x/.0001;
L = x*12;

%Shear stress at all Re numbers
for i = 1:15001  %maxi+1
   y = (i-1)*.0001;
   l(i) = y*12.;
   test(i) = mu*U*f*inv(sqrt(2.*nu*(y)/U));
   Re_local(i) = y*U/nu;
end


xfront = 3/12.;
xback = 12/12.;
Rexfront = xfront*U/nu
%Shear Stress at local Re Number
twfront = mu*U*f*inv(sqrt(2.*nu*(xfront)/U))
twback = mu*U*f*inv(sqrt(2.*nu*(xback)/U))

figure(1),plot(l,test,'b');ylabel('Shear Stress (lb/ft^2)');xlabel('Distance on Plate
(inches)');axis([0 12 0 1]);
figure(2),plot(l,Re_local);xlabel('Distance on Plate (inches)');ylabel('Local Reynolds
Number');

for U = 1:110
   tw3in(U) = mu*U*f*inv(sqrt(2.*nu*(3/12.)/U));
   i(U) = U*.68181818181;
end

figure(3),plot(i,tw3in,'-b');axis([0 75 0 .1]);
```

A-3. UNCERTAINTY CALCULATIONS

A-3.1. Uncertainty Constants

$$\Delta\theta_{AZIMUTHAL,SPINNING} = \frac{360\ degrees}{2400\ points\ per\ rotation} = 0.15\ degrees$$

$$\Delta\theta_{AZIMUTHAL,STATIC} = 5\ degrees$$

$$\Delta\theta_{SEPARATION} = 5\ degrees$$

A-3.2. Uncertainty of Lift

$$m = ME + B \text{ (Lift Calibration)}$$

$$\Delta m = \left[\left(\frac{\partial m}{\partial M}\Delta M\right)^2 + \left(\frac{\partial m}{\partial E}\Delta E\right)^2 + \left(\frac{\partial m}{\partial B}\Delta B\right)^2\right]^{1/2}$$

$$M = 138.84\ grams$$

$$B = -3.4375\ grams$$

$$\Delta E = .0001\ Volts \quad \text{(Uncertainty of voltage from NI box)}$$

$$\Delta m = [0 + (M\Delta E)^2 + 0]^{1/2}$$

$$\Delta m = 0.01388\ grams = 3.06x10^{-5}\ lbs$$

A-3.3. Uncertainty of Shear Stress

$$\tau_w = (E^2 * C_1 + C_2)^3 \text{ (King's Law)}$$

$$\Delta\tau = \left[\left(\frac{\partial\tau}{\partial E}\Delta E\right)^2 + \left(\frac{\partial\tau}{\partial C_1}\Delta C_1\right)^2 + \left(\frac{\partial\tau}{\partial C_2}\Delta C_2\right)^2\right]^{1/2}$$

$$C_1 = 0.0316$$

$$C_2 = -0.2421$$

$\Delta E = .0001\ Volts$ (Uncertainty from voltage from NI box)

$$\Delta\tau_w = [(6C_1E(E^2C_1 + C_2)^2\Delta E)^2 + 0 + 0]^{1/2}$$

$$\Delta\tau_w = 1.0\text{x}10^{-6}\ \frac{lbs}{ft^2}$$

A-4. LIST OF PARTS

Part Number	Part	Manufacturer/Supplier	Pack	Quantity/Pack	Total Quantity	Price/Pack	Total Price
GEN.1	Rawlings Official Major League	Sports Authority	4	1	4	$15.99	$63.96
GEN.2	Hardwood Ball (3" Diameter)	McMaster	1	2	2	$14.27	$14.27
GEN.3	Wind Tunnel	Engineering Laboratory Design, Inc.	1	1	1 Marquette Supplied		-
GEN.4	LabVIEW Computer	Hewlett-Packard	1	1	1 Marquette Supplied		-
FB.1	1018 Steel Bar (17"x1"x1/4")	Speedy Metals	2	1	2	$3.80	$7.60
FB.2	Miniature 303 Stainless Steel Drive Shaft (3/16" OD, 18" Length)	McMaster	1	1	1	$8.21	$8.21
FB.3	18-8 Stainless Steel Threaded Rod (10-24 Thread, 2' Length)	McMaster	1	1	1	$3.17	$3.17
FB.4	18-8 Stainless Steel Fully Threaded Stud (10-24 Thread, 5" Length)	McMaster	1	5	5	$4.51	$4.51
FB.5	Ultra-Precision Mini Stainless Steel Ball Bearing (ABEC-7, Open for .1875" Shaft Diameter, .5" OD, .1562")	McMaster	2	1	2	$11.57	$23.14
FB.6	Plastic Gear Set	American Science & Surplus	1	4	4	$1.95	$1.95
FB.7	Electric Gear Motor, 24-12 VDC, 120-60 rpm	American Science & Surplus	1	1	1	$14.50	$14.50
FB.8	650 nm wavelength visible red lasers	Lasermate Group	1	1	1 Marquette Supplied		-
FB.9	Silicon Photodiode	Thor Labs	1	1	1 Marquette Supplied		-
FB.10	Omnical 2001 Power Supply	WP Instraments, Inc.	1	1	1 Marquette Supplied		-
FB.11	Lift/Drag Force Balance and Model Set	Engineering Laboratory Design, Inc.	1	1	1 Marquette Supplied		-
FB.12	Travel Mirror (5" Diamter)	Walgreens	1	1	1	$4.99	$4.99
FB.13	Plastic for Chopper Plate	Midland Plastics	1	1	1 Marquette Supplied		-
FB.14	12 Volt DC 100 mA Power Supply	American Science & Surplus	1	1	1	$4.95	$4.95
FB.15	Mylar	Marquette University	1	1	1 Marquette Supplied		-
FB.16	Worm Drive Tube Clamp	Ace Hardware	1	1	1		$0.00
FB.17	Oscilloscope	Hewlett-Packard	1	1	1 Marquette Supplied		-
FV.1	"M" Female Coupler Plug	Ace Hardware	1	1	1	$1.99	$1.99
FV.2	"M" Female Coupler Body	Ace Hardware	1	1	1	$5.99	$5.99
FV.3	1/4X1-1/2 Galvinized Nipple	Ace Hardware	1	1	1	$1.49	$1.49
FV.4	Helim Tank, Size E Cylinder	Aero Compressed Gases, Inc.	1	1	1	$30.00	$30.00
FV.5	Nylon 6/6 Tube, Tight Tolerance (3/8" OD, 5/16" ID, 5' Length)	McMaster	1	1	1	$2.46	$2.46
FV.6	Helium Bubble Generator	Sage Action, Inc.	1	1	1 Notre Dame Supplied		-
FV.7	High Speed Camera (Fastcam-APX RS)	Photron	1	1	1 Marquette Supplied		-
FV.8	Computer for Photron	MPC	1	1	1 Marquette Supplied		-
FV.9	Fournelle Lens (8.5" x 10"Sheet)	Marquette University	1	2	2 Marquette Supplied		-
FV.10	Gimp 2.6	GNU Image Manipulation Program	1	1	1	$0.00	$0.00
HF.1	Basic Aluminum Tube (9/32" OD, .2533" ID, 1' Length)	McMaster-Carr	1	8	8	$8.87	$8.87
HF.2	Acrylic Rod (1/4" Diameter)	Midland Plastics	1	1	1	$0.25	$0.25
HF.3	Tungsten Wire (5 micron diameter)	California Fine Wire Company	1	50 feet	1	$265.00	$265.00
HF.4	Hot Wire Probe Type 55P16	Dantec Dynamics	1	1	1 Marquette Supplied		-
HF.5	Right Circular Cylinder (2.5" diameter)	Discovery Learning Center	1	1	1 Marquette Supplied		-
HF.6	Distilled Water	Nursery Purified Water	1	1 gallon	1 Marquette Supplied		-
HF.7	5760 Acid Flux Neutralizer	Kester	1	1 gallon	1 Marquette Supplied		-
HF.8	Soldering Flux	Kester	1	1	1 Marquette Supplied		-
HF.9	Loctite Quick Set Epoxy	Locttie	1	1	1 Marquette Supplied		-
HF.10	Solid Copper Wire, 18 gauge	Radioshack	1	1	1	$6.59	$6.59
HF.11	Copper Sulfate	Marquette University	1	100 mL	1 Marquette Supplied		-
FP.1	Alloy Steel Shoulder Screw (1/2" Shoulder Diameter, 7/8" L Shoulder, 3/8"-16 Thread)	McMaster-Carr	2	1	2	$4.11	$8.22
FP.2	Polycarbonate Sheet (0.5" x 18" x 18") and Acrylic Sheet (0.25" x 20" 24")	Midland Plastics	1	1	1	$25.00	$25.00
FP.3	Aluminum (2" x 0.5" x 18")	Marquette University	1	1	1 Marquette Supplied		-